$\overline{8}$-89 JT ①

Spent Fuel Assembly Hardware: Characterization and 10 CFR 61 Classification for Waste Disposal

Volume 1—Activation Measurements and Comparison with Calculations for Spent Fuel Assembly Hardware

A. Luksic

June 1989

PNL-6906 Vol. 1

DO NOT MICROFILM
COVER

MASTER

DISCLAIMER

DISCLAIMER

Portions of this document may be illegible in electronic image products. Images are produced from the best available original document.

DISCLAIMER

This program was prepared as an account of work sponsored by an agency of the United States Government. Neither the United States Government nor any agency thereof, nor Battelle Memorial Institute, nor any of their employees, makes **any warranty, express or implied, or assumes any legal liability or responsibility for the accuracy, completeness, or usefulness of any information, apparatus, product, or process disclosed, or represents that its use would not infringe privately owned rights.** Reference herein to any specific commerical product, process, or service by trade name, trademark, manufacturer, or otherwise, does not necessarily constitute or imply its endorsement, recommendation, or favoring by the United States Government or any agency thereof, or Battelle Memorial Institute. The views and opinions of authors expressed herein do not necessarily state or reflect those of the United States Government or any agency thereof.

SPENT FUEL ASSEMBLY HARDWARE:
CHARACTERIZATION AND 10 CFR 61
CLASSIFICATION FOR WASTE DISPOSAL

Volume 1

Activation Measurements and
Comparison With Calculations for
Spent Fuel Assembly Hardware

A. Luksic

June 1989

Pacific Northwest Laboratory
Richland, Washington 99352

MASTER

ABSTRACT

Consolidation of spent fuel is under active consideration as the U.S. Department of Energy plans to dispose of spent fuel as required by the Nuclear Waste Policy Act of 1982. During consolidation, the fuel pins are removed from an intact fuel assembly and repackaged into a more compact configuration. After repackaging, approximately 30 kg of residual spent fuel assembly hardware per assembly remains that is also radioactive and requires disposal. Understanding the nature of this secondary waste stream is critical to designing a system that will properly handle, package, store, and dispose of the waste.

This report presents a methodology for estimating the radionuclide inventory in irradiated spent fuel hardware. Ratios are developed that allow the use of ORIGEN2 computer code calculations to be applied to regions that are outside the fueled region. The ratios are based on the analysis of samples of irradiated hardware from spent fuel assemblies.

The results of this research are presented in three volumes. In Volume 1, the development of scaling factors that can be used with ORIGEN2 calculations to estimate activation of spent fuel assembly hardware is documented. The results from laboratory analysis of irradiated spent-fuel hardware samples are also presented in Volume 1. In Volumes 2 and 3, the calculated flux profiles of spent nuclear fuel assemblies are presented for pressurized water reactors and boiling water reactors, respectively. The results presented in Volumes 2 and 3 were used to develop the scaling factors documented in Volume 1.

SUMMARY

Under the NWPA, the DOE will be accepting spent nuclear fuel for disposal. Included with the fuel will be a significant quantity of activated metal in the form of fuel assembly end fittings, grid spacers, guide tubes, etc. that must be characterized for disposal. If spent fuel assemblies are proposed for disposal by consolidation, spent fuel hardware will then represent a separate waste form. This report presents a method for characterizing these activated metal components for classification within the Federal Waste Management System.

The radionuclide inventory in materials irradiated in a reactor is dependent upon several parameters. The major variables are initial material composition, irradiation history, and location in the reactor. In the case of spent fuel assembly hardware, the structural materials are composed of various alloys of stainless steel, Inconel, and Zircaloy. The irradiation history is a function of the burnup of the fuel assembly; the location is governed by the fuel assembly structure.

For a specific fuel assembly, the ORIGEN2 computer code (Croff 1980) can be used to estimate the radionuclide inventory of materials irradiated in the fueled region of the reactor. Input parameters include the composition of the material to be irradiated and the irradiation history. The results of the calculation are applicable to materials irradiated in the core's fueled region. Outside the fueled region, the results are not applicable due to changes in the absolute magnitude of the neutron flux and shifts in the neutron spectrum. For spent fuel assembly hardware, much of the material of interest is located at the end fittings, outside of the fueled region. To estimate the radionuclide inventory in these components. Scaling factors are applied to ORIGEN2 calculations to compensate for the changed neutron flux outside the fueled region.

A total of 38 samples was obtained from three spent fuel assemblies. Each sample was individually analyzed for both elemental composition and for radionuclide content. Based on the results of the analysis, scaling factors were developed that relate the activation rate in the reactor's fueled region

to those outside. These factors are presented in Table S.1. These factors are applied to ORIGEN2 results by multiplying the fueled-region radionuclide inventories, as calculated in ORIGEN2, by the appropriate scaling factor for the region in which the material is located.

These global factors are only useful for average radionuclide inventory estimates, and should not be applied to small sections due to significant variations in the neutron flux with respect to position. Based on the sample analysis described in this report, it was found that the activation rate of small regions within the top end fitting of a PWR fuel assembly can vary by an order of magnitude. For example, a sample taken from the lower portion of the top end fitting will have 10 times more radioactivity than an identical sample at the upper portion of the top end fitting. The bottom end fitting showed much less variation. It is therefore important to note that these are average scaling factors to be applied to general regions.

The scaling factor for the top end fitting of the Combustion Engineering assembly is one-half that for a Westinghouse assembly. This is a result of the longer gas plenum in the Combustion Engineering fuel rods compared with

TABLE S.1. ORIGEN2 Scaling Factors

Region	Westinghouse	Combustion Engineering	General Electric	Average
Top End Fitting	0.1	0.05	0.1	0.1
Gas Plenum	0.2	0.2	0.2	0.2
Fueled Region	1.0	1.0	1.0	1.0
Bottom End Fitting	0.2	0.2	0.15	0.2

Notes:
1. The values given above have an uncertainty of ±50%.
2. For a Babcock and Wilcox assembly, use the scaling factors for a Westinghouse assembly.
3. Values apply to activation fraction of the initial amount present.

the Westinghouse fuel rods. This difference places the Combustion Engineering top end fitting further away from the fueled region. Hence, it is in a lower flux region than the Westinghouse top fitting. However, once the flux reaches the top end fitting, the flux has an order of magnitude reduction over the end fittings length for both assembly types. The General Electric bottom end fitting has a lower scaling factor than either of the pressurized water reactors. This is apparently due to the greater length of the end fitting and a greater reduction of flux over its length.

Calculations were also done in order to estimate these scaling factors. The calculations included using the one-dimensional neutronics code, ANISN. The fuel assemblies were individually modeled, in order to produce assembly-specific scaling factors. The calculated scaling factors were compared against those that were empirically derived.

Results of a comparison of calculations to laboratory analysis indicated that the analyzed samples had higher radionuclide inventories than predicted. the indications ar that the use of one-dimensional neutronics calculations may not be appropriate to determine scaling factors, and as a result, the recommended scaling factors are empirically derived from the sample analyses rather than calculations. The calculations, as shown in Volume 2, indicate that the neutron flux changes significantly outside the fueled region. This is true both in the magnitude of the flux (which decreases rapidly) and its spectrum (as seen in the rapidly changing one-group spectrum averaged cross sections). The presence of a significantly changing flux is shown by the order-of-magnitude reduction in the radionuclide inventory in the pressurized water reactor (PWR) top end fittings from the results of the laboratory analysis. The discrepancies between measured and calculated end fitting results are probably due to the one-dimensional representation of the assembly geometry in the calculations. Calculations with more accurate geometric representation should lessen the discrepancy.

It was found that even in the fueled region, where the ORIGEN2 calculations apply directly, comparing calculational results with laboratory analysis indicated higher concentrations than the calculation predicted, while for others the concentrations were lower. For ^{60}Co, there was evidence

of both underprediction and overprediction from different sets of samples. More detailed analysis is needed to resolve the discrepancies. In the interim, there are discernable patterns in how activation rates vary in spent fuel hardware. these patterns, within appropriate uncertainty bounds, can be used to estimate radionuclide inventories for activated hardware and are the basis for the scaling factors presented in Table 1.1.

An interesting fact that was noted in the laboratory measurements was the variation in the minor constituents of the base metals. The level of cobalt and niobium impurity varied significantly in samples of the same alloy. The uncertainty in the values in Table 1.1 does not allow for any uncertainty in the initial composition of the material being irradiated. For cobalt, the level of impurity was found to vary by a factor of two between different samples of Inconel 718. In the stainless steel samples, the same variation was observed. Several of the samples had cobalt levels in excess of 0.1%, an upper limit for many specifications. This would lead to an underestimation of the amount of ^{60}Co, even if the correct scaling factors were used. For niobium, the variation range was much larger. In Zircaloy, elemental analyses reflected niobium values from below detectable limits up to several hundred ppm. Curiously, ^{94}Nb was detectable in most of the samples. This is an important result since most items made of Zircaloy are disposed of as low-level waste with no consideration of ^{94}Nb content. Our analyses showed that levels of ^{94}Nb were a significant fraction of 10 CFR 61 limits (17% - 97%).

CONTENTS

FIGURES

TABLES

1.0 INTRODUCTION

1.1 BACKGROUND

When the Department of Energy (DOE) begins accepting spent nuclear fuel as directed by the Nuclear Waste Policy Act of 1982 (NWPA), it will be accepting complete assemblies, including end fittings, grid spacers, guide tubes, and other structural hardware. To accurately assess the options and impact of handling and disposal of this hardware on the Federal Waste Management System, it is necessary that hardware be adequately characterized. This report is part of that characterization study.

The first part of the study identified the types and quantities of hardware that must be handled. Those results are documented in a Pacific Northwest Laboratory (PNL) report entitled, Spent Fuel Disassembly Hardware and Other Non-Fuel Bearing Components: Characterization, Disposal Cost Estimates, and Proposed Repository Acceptance Requirements (Luksic et al. 1986, PNL-6046). The report contains descriptions, the material compositions, and weights of the nonfuel hardware components. This information was used by the Oak Ridge National Laboratory (ORNL) and documented in a DOE report entitled, Characteristics of Spent Fuel, High-Level Waste, and Other Radioactive Wastes Which May Require Long-Term Isolation (DOE 1987).

A key issue discussed in PNL-6046 was the characterization of the radionuclide inventory of the hardware. Section 4.3 of that report described how the radionuclide content of the hardware was estimated using the ORIGEN2 computer code, coupled with a methodology described in a report published by ORNL (Croff et al. 1978, ORNL/TM-6051). The ORIGEN2 code can be used to predict the activity of the hardware irradiated in the reactor's fueled region based on the reactor power history; however, the fueled region of the reactor core is the only region were ORIGEN2 results are directly applicable. Scaling factors (given in ORNL/TM-6051) can be used to adjust for changes in the neutron flux, and the energy spectrum outside the fueled region. It was noted in PNL-6046 that the authors had some reservations regarding the adequacy of the factors used at that time. It was thought that radionuclide inventories might be higher in the end fittings (particularly the bottom)

than predicted. The bottom end fitting is considerably closer to the fueled region than the top one, and it was postulated that the flux in that region would more closely resemble the flux in the gas plenum region. The scaling factors in ORNL/TM-6051 were limited to only a few of the radionuclides of interest. Thus, there were significant incentives to further investigate these scaling factors.

Of specific concern were the concentrations of ^{94}Nb, ^{14}C, ^{59}Ni, and ^{63}Ni. The parent isotopes for these radionuclides are found primarily in stainless steel and Inconel, and these materials are primarily located outside the core region where the scaling factors had to be applied. These nuclides affect the waste classification of the activated hardware under 10 CFR Part 61. Classification in turn has an impact on the disposal options available for the waste, its treatment, and its packaging. Another important consideration was whether or not the ^{60}Co inventory was being underestimated. This could have an impact on the shielding design of the cask and hardware handling facilities.

A critical aspect of the activation calculations is the initial composition of the parent material. The impurity level of the parent isotope has a one-to-one effect on the amount of activation product produced. Of particular interest was the level of trace elements such as cobalt and niobium. Specifications were available that provided maximum values for cobalt, but there was little information on niobium. In particular, there is no specification for the amount of niobium in Zircaloy-4, the primary metal used within the fueled core region itself. This has led some analysts to overlook ^{94}Nb in classifying waste hardware per 10 CFR 61. There was little information on the actual levels of these elements, or how they varied in different materials.

To resolve these issues, a methodology was needed that would accurately predict the radionuclide concentrations of all spent fuel assembly hardware components. Also, the methodology should be validated against sample measurements. The work reported here describes the results of the research

undertaken to resolve these issues and to develop a methodology for calculating activation product concentrations in the fuel assembly hardware and to validate the results with actual sample measurements.

1.2 APPROACH

Detailed neutronic calculations were performed to predict the neutron flux as a function of position from the bottom to the top of the fuel assembly. These calculations, which are described in Volumes 2 and 3 of this report, were used to develop preliminary scaling factors that were applied to ORIGEN2 calculations. These factors accounted for both the reduction in the magnitude of the flux and the change in the neutron spectrum. Both of these changes affect reaction rates, which in turn affect the production rate of the various radionuclides.

To validate these calculated factors, samples of irradiated hardware were obtained from actual spent fuel assemblies and were analyzed. The samples are described in Section 2.0 and the results of the laboratory analyses are described in Section 3.0. Both radionuclide concentrations and elemental compositions were measured. The calculational methodology and results are described in Section 4.0. ORIGEN2 calculations were performed for the specific irradiation history of the fuel assemblies that were sampled. The calculated preliminary factors for the specific sample locations were then applied to the ORIGEN2 results. Comparisons of the ORIGEN2 calculations with the experimental measurements are presented in Section 5.0.

Calculations were performed to predict and understand what the rates of activation in different parts of the fuel assembly would be. These calculations included both the one-dimensional neutron transport code, ANISN, and ORIGEN2. ORIGEN2 was used to predict core average radionuclide concentrations, taking into account irradiation histories and material compositions. ANISN predicted how the neutron flux (and spectrum) changed as a function of distance from the fueled region. Together, ORIGEN2 and ANISN were used to predict the radionuclide concentrations at the specific locations where the samples were taken.

2.0 SAMPLE DESCRIPTION

2.1 FUEL ASSEMBLIES

A number of assemblies were considered before deciding which fuel assemblies to sample. Seven assemblies were available at PNL. These assemblies included three from boiling water reactors (BWR assemblies (Cooper Nuclear Station) and four from PWRs (two from Calvert Cliffs and two from Point Beach 1). Idaho National Engineering Laboratory (INEL) was initiating a program to consolidate 48 fuel PWR assemblies from Surry and Turkey Point, and Battelle Columbus Laboratory (BCL) had consolidated five PWR assemblies from Ginna.

Each of the sources was contacted to ascertain the availability of the fuel assemblies for hardware sampling and to obtain cost estimates for obtaining the samples. Given the variety of assemblies at PNL and the fact that cost considerations would limit the sampling to be done at one site only, it was decided to perform the sampling at PNL. The overriding consideration was that samples from several different types of fuel assemblies. Table 2.1 lists the general properties of the spent fuel that was chosen for sampling.

All of the assemblies at INEL were Westinghouse 15x15s from Surry 1 and 2. Initial consideration was given to these because they represented several different enrichments and a variety of burnups. The assemblies at BCL were Westinghouse 14x14s from Ginna. The assemblies at PNL consisted of three General Electric 7x7s from Cooper, two Combustion Engineering 14x14s from Calvert Cliffs, and two Westinghouse 14x14s from Point Beach 1. BCL was involved in its own characterization study for Rochester Gas and Electric, and was not interested in expanding their program. INEL was planning to do

TABLE 2.1. PNL Spent Fuel

Fuel Assembly Type	Burnup (MWD/MTU)	Discharge
Westinghouse 14x14	32,700	October 1981
Combustion Engineering 14x14	41,800	April 1982
General Electric 8x8	27,500	May 1982

some characterization of their hardware after completing rod consolidation. Information will be available from both of these sites eventually.

2.2 SAMPLES

The assembly samples were taken so that each of the construction materials in each possible location and each of the fuel assembly's main structural components were represented. Samples were taken from the grid spacers in each of the fuel assemblies, and from the main casting of both the bottom and top end fittings. Additionally, samples of the spring material in each of the top end fittings were also obtained.

Thirty-eight samples of activated metals were obtained from three spent fuel assemblies (Table 2.1). The samples were obtained by mechanical means (i.e., by cutting and snipping). These were latter subsampled into sample sizes on the order of 0.1 to 5.0 mg, as described in Section 3.4. The remainder of each sample was reserved for further analysis, if required.

The sample locations are shown on Figures 2.1, 2.2, and 2.3. These locations were selected to represent all the different materials available on each fuel assembly in as many different regions as practicable. Samples were taken from each grid spacer to provide as much data as possible regarding the neutron flux through the core region. The grid spacer sample also provided a good indication of the variance due to the elemental composition, particularly for the trace elements.

2.3 FUEL ASSEMBLY IRRADIATION HISTORY

The irradiation history for each of the fuel assemblies sampled was obtained from information supplied by the utilities to the DOE in the Annual Spent Fuel Data Survey, Form RW-859. Tables 2.2, 2.3, and 2.4 provide a detailed irradiation history of each fuel assembly sampled.

W-10 Hold-down Spring [Inc]

W-12 Upper Nozzle [SS]

W-9   Upper Nozzle [SS]

W-8   Grid Spacer [Inc]

W-7   Grid Spacer [Inc]

W-6   Grid Spacer [Inc]

W-5   Grid Spacer [Inc]

W-4   Grid Spacer [Inc]

W-3   Grid Spacer [Inc]

W-2   Grid Spacer [Inc]

W-11 Lower Nozzle [SS]

W-1   Lower Nozzle [SS]
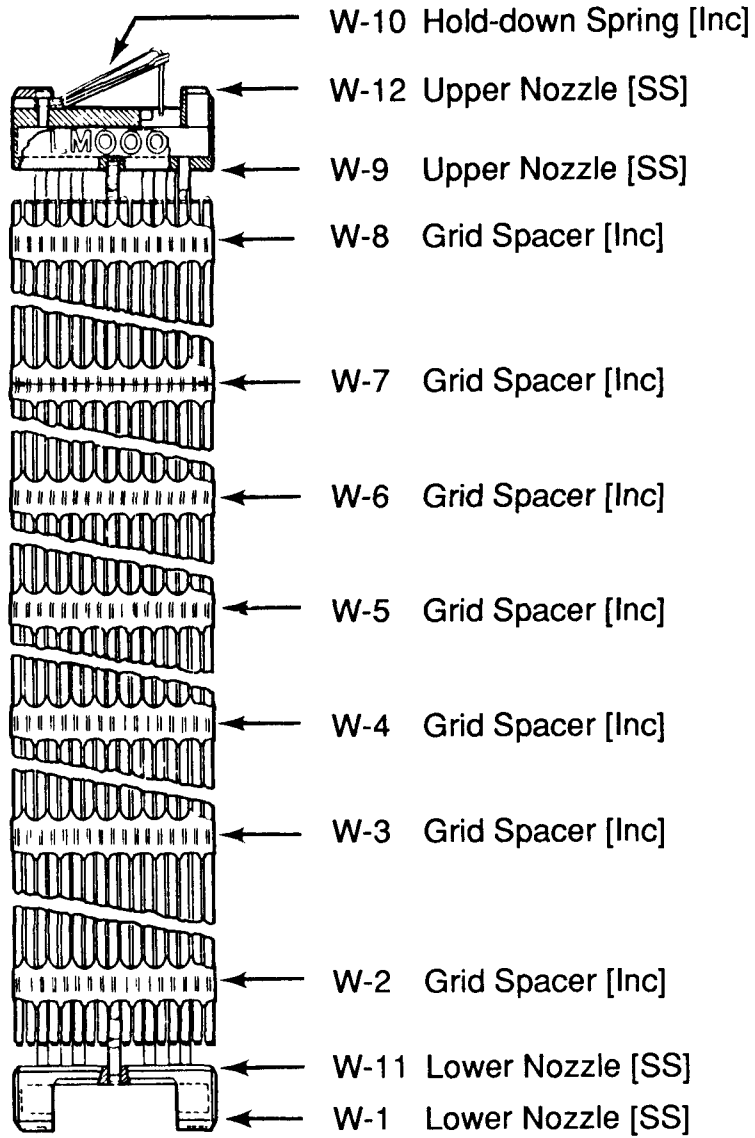
FIGURE 2.1. Sample Locations for the Westinghouse 14x14 Fuel Assembly

CE-12 Hold-down Spring [SS]
CE-13 Hold-down Spring [Inc]

CE-11 Flow Plate [SS]

CE-10 Grid Spacer [Zirc]

CE-9 Grid Spacer [Zirc]

CE-8 Grid Spacer [Zirc]

CE-7 Grid Spacer [Zirc]

CE-6 Grid Spacer [Zirc]

CE-5 Grid Spacer [Zirc]

CE-4 Grid Spacer [Zirc]

CE-3 Grid Spacer [Zirc]

CE-2 Grid Spacer [Inc]

CE-14 Lower Nozzle [SS]

CE-1 Lower Nozzle [SS]
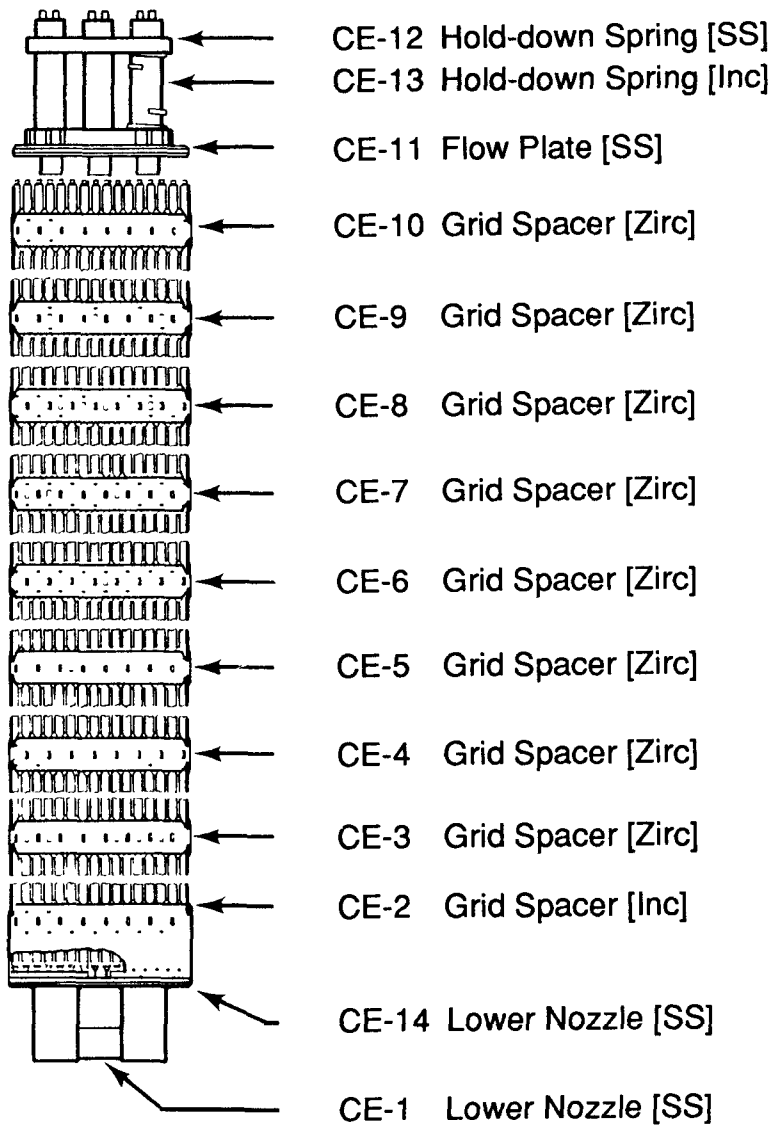
FIGURE 2.2. Sample Locations for the Combustion Engineering 14x14 Fuel Assembly

2.4

GE-19   Handle [SS]

GE-18   Flow Plate {SS]
GE-17   Expansion Spring [Inc]

GE-15   Grid Spacer [Zirc]

GE-13   Grid Spacer [Zirc]

GE-11   Grid Spacer [Zirc]

GE-9   Grid Spacer [Zirc]

GE-7   Grid Spacer [Zirc]

GE-5   Grid Spacer [Zirc]

GE-3   Grid Spacer [Zirc]

GE-1   Lower Nozzle [SS]

GE-2   Lower Nozzle [SS]
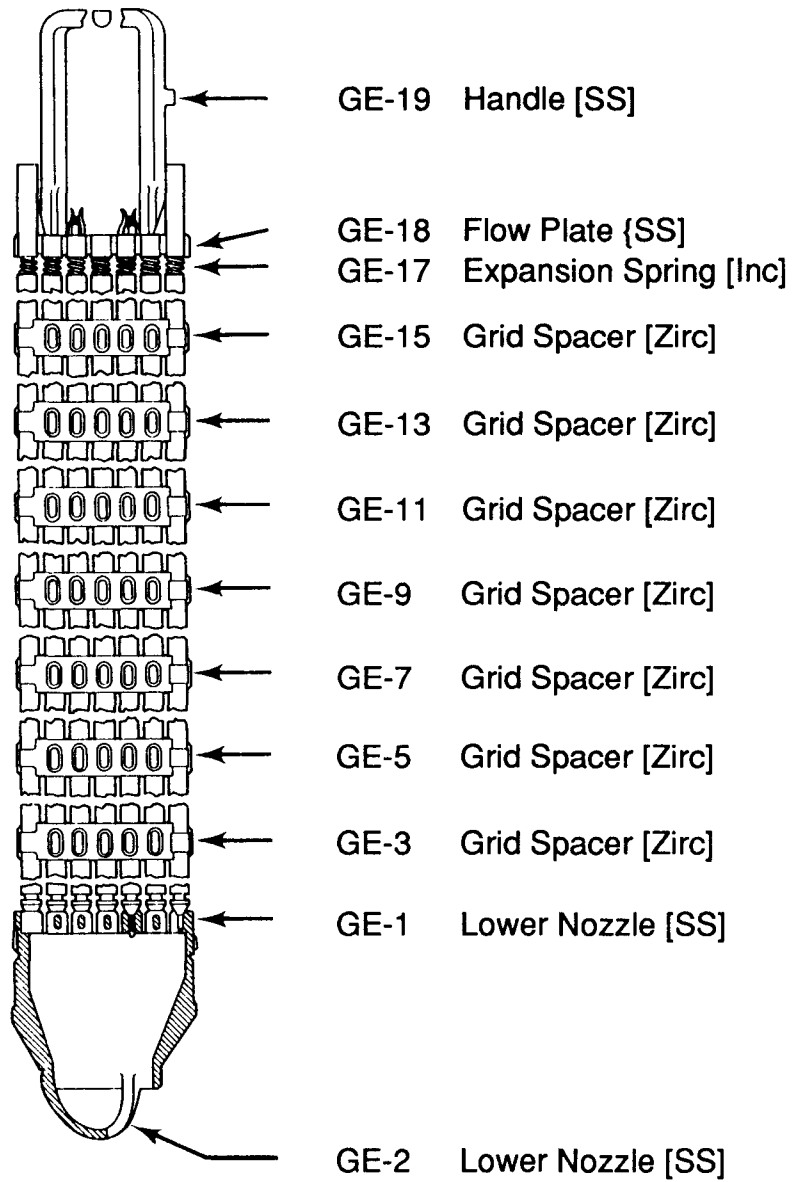
FIGURE 2.3. Sample Locations for the General Electric 7x7 Fuel Assembly

2.5

TABLE 2.2. Westinghouse 14x14 (LM 036F)

Point Beach 1: 400.7 kg U, 3.192 ^{W}/o ^{235}U

Cycle Number	End of Cycle	Burnup at End of Cycle (MWD/MTU)
4 (out)	October 1, 1976	0
5	October 10, 1977	6,147
6	September 20, 1978	16,784
7	October 5, 1979	26,195
8	November 26, 1980	29,621
9	October 8, 1981	32,729

TABLE 2.3. Combustion Engineering 14x14 (D 047)

Calvert Cliffs: 388.6 kg U, 3.068 ^{W}/o ^{235}U

Cycle Number	End of Cycle	Burnup at End of Cycle (MWD/MTU)
1 (out)	January 1, 1977	0
2	January 23, 1978	9,466
3	April 21, 1979	20,895
4	October 18, 1980	32,317
5	April 17, 1982	41,781

TABLE 2.4. General Electric 7x7 (CZ 348)

Cooper Nuclear Station: 190.4 kg U, 2.506 $^w/o$ ^{235}U

Cycle Number	End of Cycle	Burnup at End of Cycle (MWD/MTU)
Begin Commercial Operation	July 1974	0
1	September 1976	13,046
2	September 1977	18,910
3	April 1978	22,098
4 (out)	April 1979	22,098
5 (out)	March 1980	22,098
6	April 1981	24,974
7	May 1982	27,480

3.0 LABORATORY ANALYSIS

3.1 SAMPLE PREPARATION

The 0.1 to 5.0 gram specimens of neutron activated stainless steel, Inconel, and Zircaloy, that were cut from the fuel assemblies were transferred from the original hot cell to a sample-preparation hot cell where the metal specimens were initially surface-decontaminated by acid etching. This cleaning consisted of immersing each specimen in hot (80 to 90°C) 6N hydrochloric acid for 60 seconds. The specimens were then rinsed with fresh 6N hydrochloric acid. This etching was repeated three times, and was followed by a final acid etching by immersing each specimen for 60 seconds in hot (80 to 90°C) 8N nitric acid. The specimens were then immediately rinsed with distilled water, dried on a paper towel, and placed in clean polyethylene vials. The vials were then transported to a radiochemistry laboratory for final decontamination of the metal specimens prior to initiating the radiochemical analyses.

The final acid etching process was conducted in a clean, shielded laboratory fume hood and consisted of repeating the immersion and rinsing steps conducted in the hot cell. Repeated acid etching and rinsing was necessary to completely remove traces of fission product and transuranic radionuclide contamination deposited during the cutting operations in the hot cell and to remove remnants of corrosion films that formed on the metal surface during its exposure to the reactor coolant.

Following the cleaning operation, the metal specimens were initially weighed and then partially dissolved in high purity acid (Ultrex) for radiochemical analyses. The stainless steel samples were immersed in hot (80 to 90°C), 6N Ultrex hydrochloric acid for 10 to 20 minutes. The samples were then rinsed with doubly-distilled-deionized water, dried, and reweighed to determine the amount of metal dissolved in the acid solution. The acid was then diluted with high purity water to give a final stock solution of exactly 100 ml in 3N hydrochloric acid, and the samples were stored in cleaned polyethylene bottles. Aliquots of this solution were taken for gamma spectrometric analysis and destructive radiochemical analyses.

The process used to partially dissolve the Inconel specimens was identical to that for the stainless steel, except that several drops of hydrofluoric acid were added during the acid leaching to aid in the dissolution of niobium constituents and for preservation of these solutions during storage. The Zircaloy specimens were partially dissolved as described for the stainless steel samples, except that a total of 3 to 5 ml of hydrofluoric acid was gradually added during the acid leaching to aid in the sample dissolution and preservation of the zirconium solutions. The hydrochloric/hydrofluoric acid dissolution of the Inconel and Zircaloy specimens was conducted in cleaned teflon beakers to avoid etching of glass containers by the hydrofluoric acid.

3.2 RADIONUCLIDE ANALYSIS

Appropriate aliquots of the stock solutions were taken, diluted to appropriate levels, and 10 ml volumes placed in a standard calibrated counting geometry. The samples were then counted from 10 to 100 minutes on a Ge(Li) or IG gamma ray spectrometer to measure all detectible gamma emitting radionuclides. Cobalt-60 was detectable in all samples, with ^{54}Mn being measurable in most specimens. Niobium-94 was detectible in Inconel samples containing niobium additives, and ^{125}Sb was a major gamma-emitter in the Zircaloy samples. The ^{125}Sb (2.73y) was produced by an (n,g) reaction on ^{124}Sn to form ^{125}Sn, (9.65d) followed by beta decay to ^{125}Sb. Zircaloy typically contains percent levels of tin.

Several of the radionuclides involved nonstandard counting techniques. Chemical separation was required for these radionuclides and are described below.

3.2.1 Nickel-59 and Nickel-63

The nickel separation entails initial precipitation of the hydroxide and additional purification using dimethyloglyoxime. After destruction of the nickel dimethyloglyoxime precipitate, the nickel is electroplated onto a stainless steel disc from a basic sulfate solution. Nickel-59 is quantified, via the cobalt x-ray emitted during decay using a thin window intrinsic germanium diode. Nickel-63 is determined using a NaI(Tl) anticoincidence

shielded windowless beta proportional counter. Absorption curves are determined for all samples to confirm the ^{63}Ni. Nickel-65 is utilized as an internal tracer for quality assurance and yield determination.

3.2.2 Iron-55

The analytical procedure utilized for ^{55}Fe entails initial separation by precipitation as the hydroxide in the presence of stable iron carrier and a ^{59}Fe yield tracer. The hydroxide is then dissolved with strong hydrochloric acid and the solution passed through an anion exchange column, where the iron chloride complex is retained. Iron is eluted from the exchange media using strong nitric acid. This solution is evaporated to dryness, the residue is dissolved in acid, and the iron is electroplated from an oxalate-sulfate media onto a copper disc. The ^{55}Fe is quantified using a thin window intrinsic germanium diode via the ^{54}Mn x-ray. Analytical yields are determined simultaneously using a ^{59}Fe gamma-ray.

3.2.3 Niobium-94

When ^{94}Nb concentrations are too low to measure by direct gamma spectrometry, the niobium is radiochemically separated from other radionuclides by precipitation of niobic oxide from an acid medium after dissolution of the metal sample. Both niobium carrier and ^{95}Nb tracer were added during the separation. Niobium-94 was measured by gamma-ray spectrometric techniques and radiochemical yield determined by tracing with ^{95}Nb.

3.3 ELEMENTAL ANALYSIS

Elemental analyses of the 3N hydrochloric acid stock solution of activated metals was accomplished by inductively coupled argon plasma atomic emission spectrometry (ICAP/AES). Appropriate dilutions (10 or 100-fold) of the original stock solutions and reagent blanks were analyzed in a shielded ICAP system.

The ICP is an argon plasma formed by the interaction of an RF field and an inert argon gas stream. This spatially stable plasma is reported to reach a temperature as high as 10,000°K. This high temperature and inert argon

atmosphere minimize chemical interferences such as refractory oxide forma-
tions with aluminum and rare earths that are encountered in flame emission
methods. The argon carrier gas nebulizes the liquid sample into the spray
chamber. It also transports the smaller sample droplets into the center of
the plasma. The high temperature in the plasma desolvates the droplets and
dissociates the sample material into individual atoms and ions that are
excited to emit light at wavelengths characteristic of the elements in the
sample. An atomic emission spectrometer (AES) sorts the various wavelengths
and measures the intensity of specific spectral lines. Photomultiplier tubes
convert the emitted light to an electrical signal that is proportional to the
intensity of the spectral lines. The digitized signals are converted by the
computer into concentration units (i.e., mg/L) that are printed directly on
the input/output terminal.

Three ICP/AES systems are used for various analyses. A Jarrell-Ash
Model 95-965 direct reader spectrometer with the capability of determining up
to 40 elements simultaneously has the source stand isolated in a hood, and
thus allows the analysis of samples containing low levels of radioactivity.
An ARL Model 35000 vacuum system for the simultaneous determination of
37 elements is also utilized. A third ARL Model 35800 instrument has the
source mounted inside a lead-shielded glovebox. This ICP/AES is used for the
analysis of samples containing high levels of radioactive isotopes.

In ICP/AES analyses, spectral interferences from the major elements in
the samples (e.g., Fe, Cr, and Ni in stainless steel) is a potential source
of error in the determination of trace elements. Correction on the trace
elements are performed by analyzing different concentrations of single ele-
ment standards of the major constituents in the sample at the time of sample
analysis and these values are used for spectral corrections of the trace
elements.

A fourth plasma system was used to measure niobium at extremely low con-
centrations in highly diluted samples. This instrument, a VG Plasmaquad
inductively coupled plasma mass spectrometer (ICP/MS), is capable of measur-
ing part-per-billion concentrations of niobium, as well as many other
elements.

3.4 RESULTS OF PNL RADIONUCLIDE AND ELEMENTAL ANALYSIS

The combined results of the radionuclide concentrations and the elemental analysis of each sample is given in Figures 3.1 through 3.19. Also given is the concentration of each radionuclide divided by the weight percent of the parent element. This normalized value can be used to compare the relative production rate of radionuclides at different locations throughout the assembly. These values were used to generate the scaling factors.

Tables 3.1 through 3.9 present a tabulation of the same data. Included in those tables are the one-sigma uncertainties, as determined by the laboratories. These are an extremely important consideration when making use of the nominal values seen in the figures.

Curies per g sample	Parent element w/o Cobalt	Curies Co-60 per g Cobalt
7.34E−4	7.09E−2	1.04E0
1.63E−3	1.50E−1	1.09E0
1.30E−2	1.47E−1	8.72E0
1.31E−2	1.48E−1	8.85E0
4.07E−2	8.90E−2	4.57E1
7.47E−2	1.15E−1	6.49E1
8.82E−2	1.31E−1	6.73E1
8.01E−2	1.19E−1	6.73E1
8.03E−2	1.30E−1	6.18E1
3.05E−2	1.11E−1	2.75E1
1.28E−2	1.15E−1	1.11E1
1.83E−2	1.47E−1	1.24E1
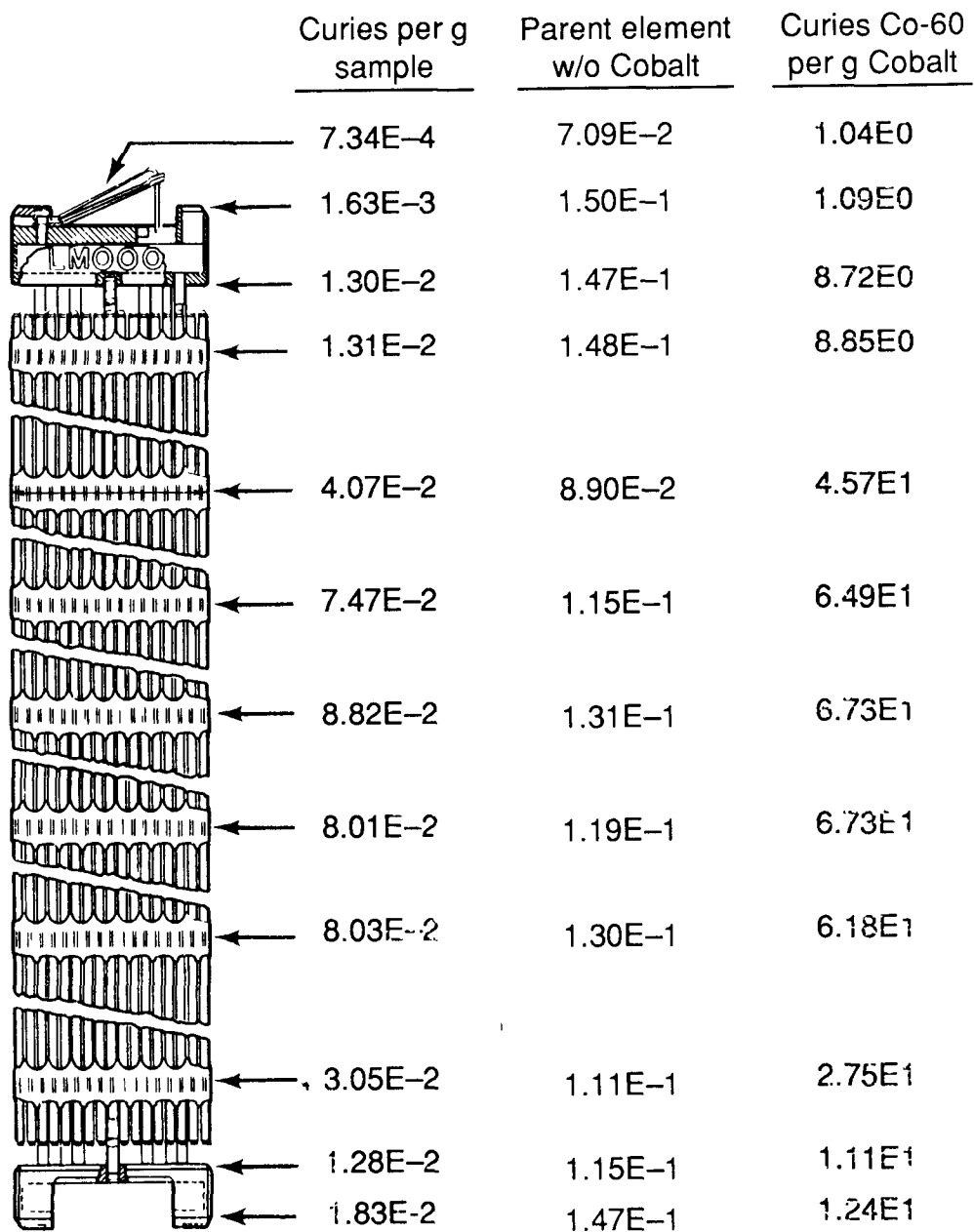
FIGURE 3.1. Results of Laboratory Analysis (Westinghouse 14x14, ^{60}Co)

Curies per g sample	Parent element w/o Nickel	Curies Ni-59 per g Nickel
1.18E-5	5.08E1	2.32E-5
1.66E-6	8.27E0	2.01E-5
1.31E-5	9.10E0	1.44E-4
7.52E-5	5.30E1	1.42E-4
2.55E-4	4.65E1	5.48E-4
3.50E-4	4.80E1	7.29E-4
3.27E-4	5.08E1	6.44E-4
2.76E-4	4.71E1	5.86E-4
3.35E-4	4.92E1	6.81E-4
1.35E-4	4.93E1	2.74E-4
1.48E-5	9.36E0	1.58E-4
1.00E-5	7.96E0	1.26E-4
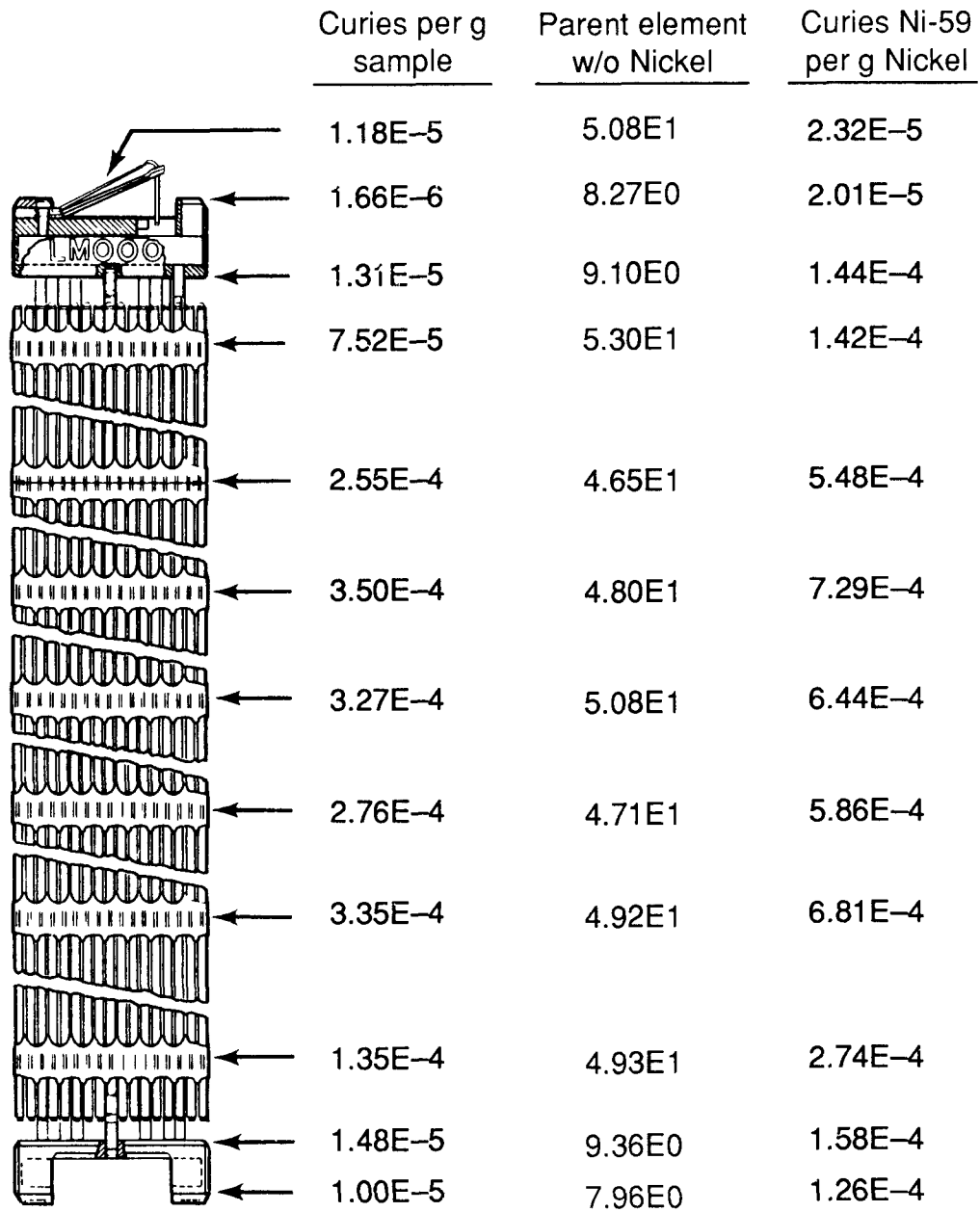
FIGURE 3.2. Results of Laboratory Analysis (Westinghouse 14x14, ^{59}Ni)

Curies per g sample	Parent element w/o Nickel	Curies Ni-63 per g Nickel
2.70E-3	5.08E1	5.30E-3
3.51E-4	8.27E0	4.25E-3
3.05E-3	9.10E0	3.35E-2
1.96E-2	5.30E1	3.70E-2
6.51E-2	4.65E1	1.40E-1
8.49E-2	4.80E1	1.77E-1
8.80E-2	5.08E1	1.73E-1
7.99E-2	4.71E1	1.70E-1
8.89E-2	4.92E1	1.81E-1
3.74E-2	4.93E1	7.59E-2
3.75E-3	9.36E0	4.01E-2
2.86E-3	7.96E0	3.59E-2
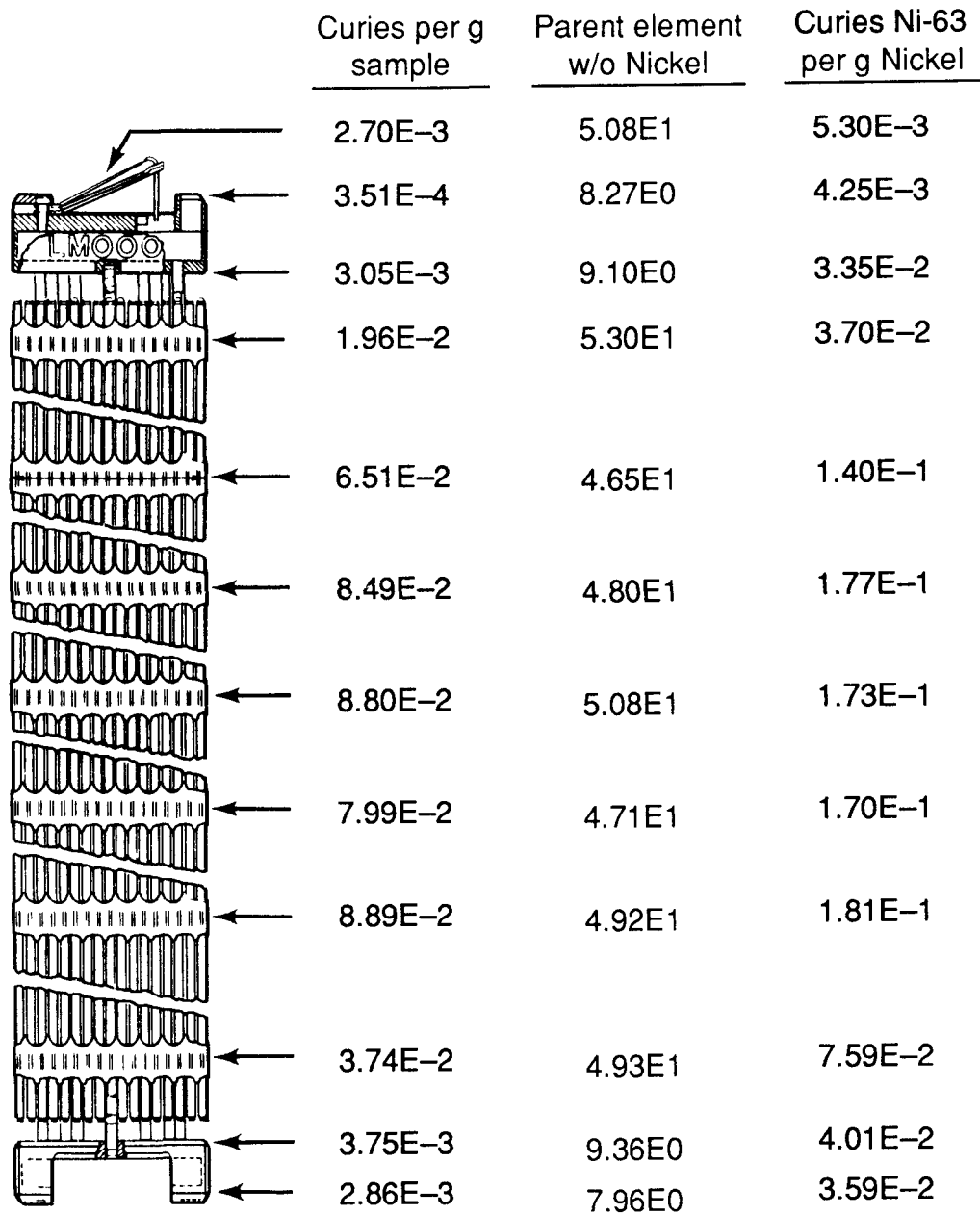
FIGURE 3.3. Results of Laboratory Analysis (Westinghouse 14x14, ^{63}Ni)

Curies per g sample	Parent element w/o Iron	Curies Fe-55 per g Iron
1.84E–3	1.72E1	1.07E–2
3.67E–3	6.75E1	5.43E–3
2.87E–2	6.50E1	4.41E–2
1.29E–2	1.60E1	8.06E–2
5.31E–2	1.52E1	3.49E–1
5.53E–2	1.60E1	3.46E–1
6.27E–2	1.70E1	3.69E–1
6.45E–2	1.62E1	3.98E–1
6.92E–2	1.65E1	4.19E–1
3.14E–2	1.58E1	1.99E–1
4.75E–2	6.55E1	7.25E–2
4.21E–2	6.50E1	6.48E–2
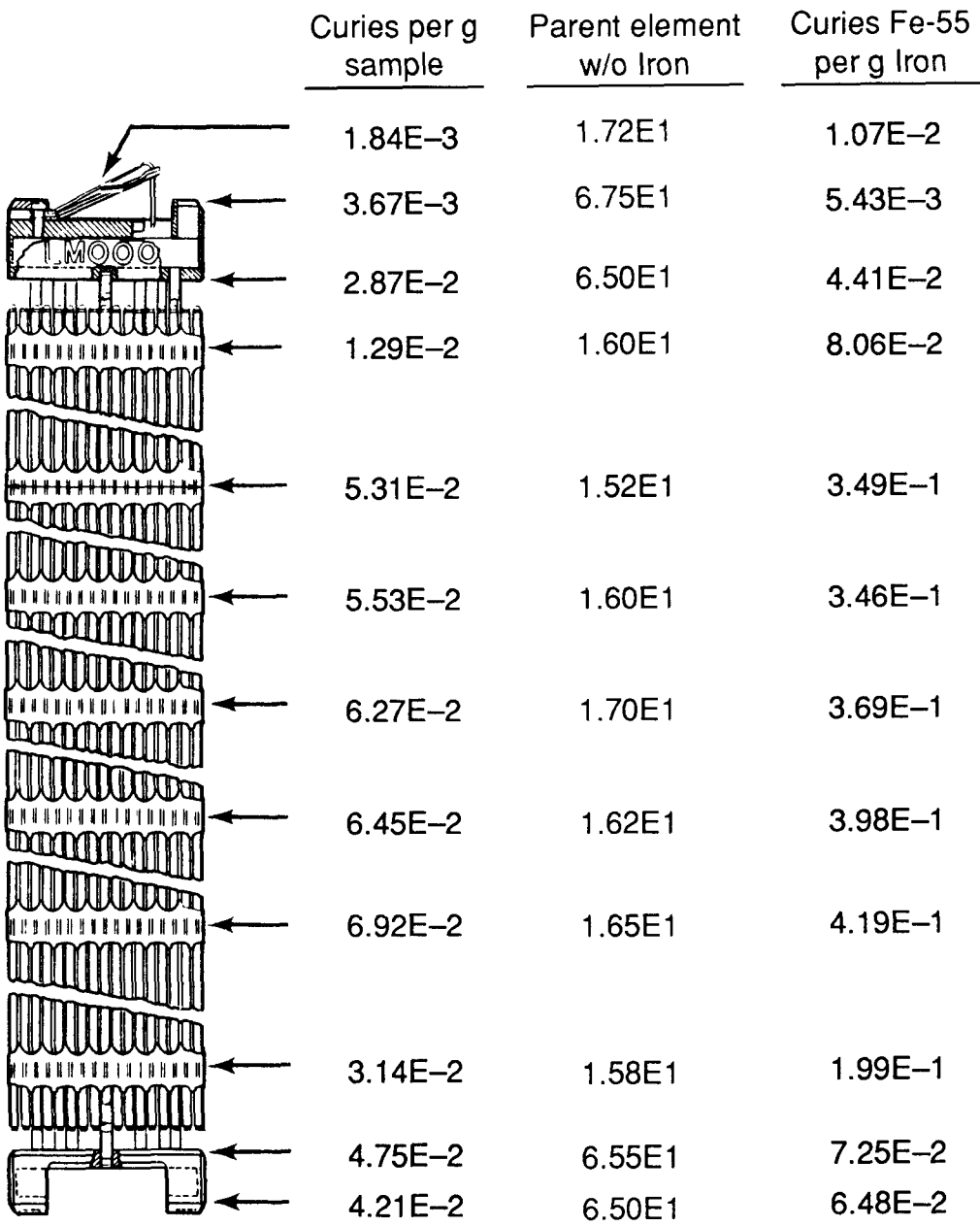
FIGURE 3.4. Results of Laboratory Analysis (Westinghouse 14x14, ^{55}Fe)

Curies per g sample	Parent element w/o Niobium	Curies Nb-94 per g Niobium
7.39E–7	4.50E0	1.64E–5
4.09E–10	3.30E–3	1.24E–5
1.79E–9	2.40E–3	7.20E–5
6.98E–6	4.40E0	1.59E–4
---	---	---
---	---	---
1.20E–4	4.60E0	2.61E–3
---	---	---
---	---	---
4.14E–5	4.60E0	9.01E–4
6.40E–9	3.00E–2	2.20E–5
2.07E–8	1.56E–2	1.32E–4
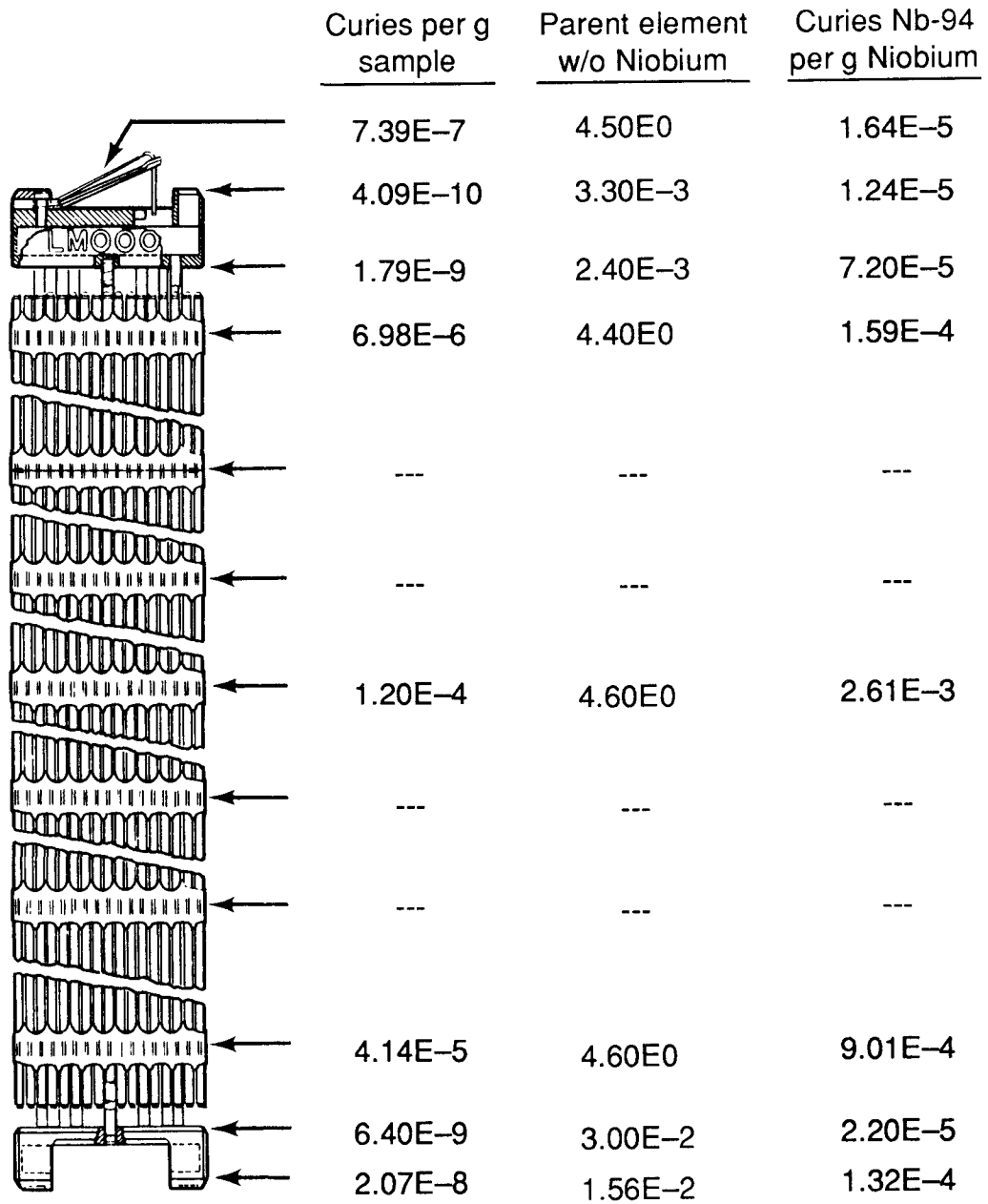
FIGURE 3.5. Results of Laboratory Analysis (Westinghouse 14x14, ^{94}Nb)

Curies per g sample	Parent element w/o Iron	Curies Mn-54 per g Iron
5.73E–5	1.72E1	3.33E–4
1.79E–4	6.75E1	2.65E–4
6.39E–4	6.50E1	9.83E–4
<3.5E–4	1.60E1	<2.2E–3
5.50E–3	1.52E1	3.62E–2
8.52E–3	1.60E1	5.33E–2
3.76E–3	1.70E1	2.21E–2
3.90E–3	1.62E1	2.41E–2
3.52E–3	1.65E1	2.13E–2
<1.1E–3	1.58E1	<6.9E–3
3.52E–3	6.55E1	5.37E–3
2.26E–3	6.50E1	3.48E–3
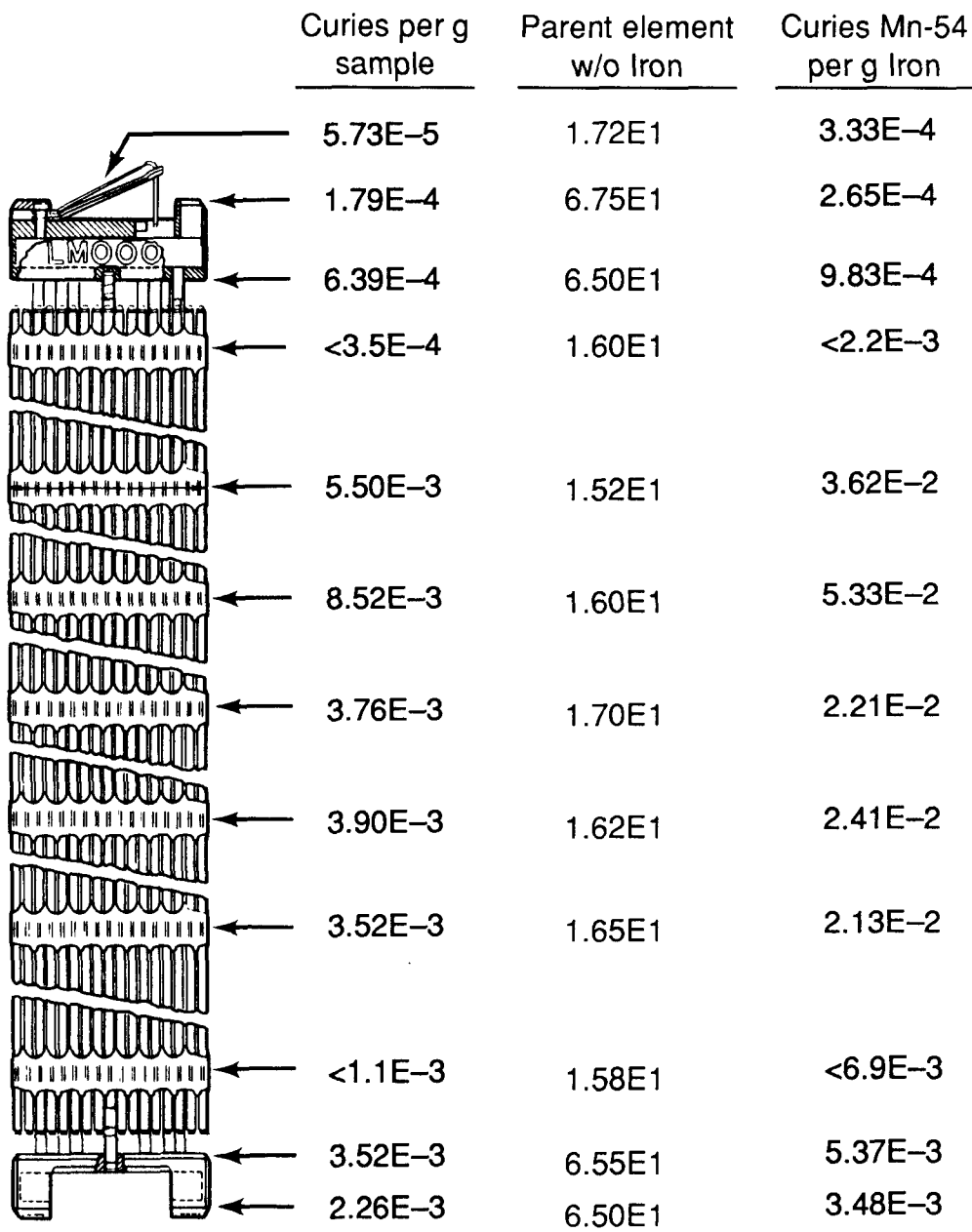
FIGURE 3.6. Results of Laboratory Analysis (Westinghouse 14x14, [54]Mn)

	Curies per g of sample	Parent element w/o Tin	Curies Sb-125 per g Tin
	<1.23E−6		
	<1.88E−6		
	2.82E−5		
	<1.37E−5		
	<4.44E−5		
	<8.34E−5		
	<9.15E−5		
	<9.40E−5		
	8.72E−5		
	4.48E−5		
	1.41E−5		
	<2.73E−3		
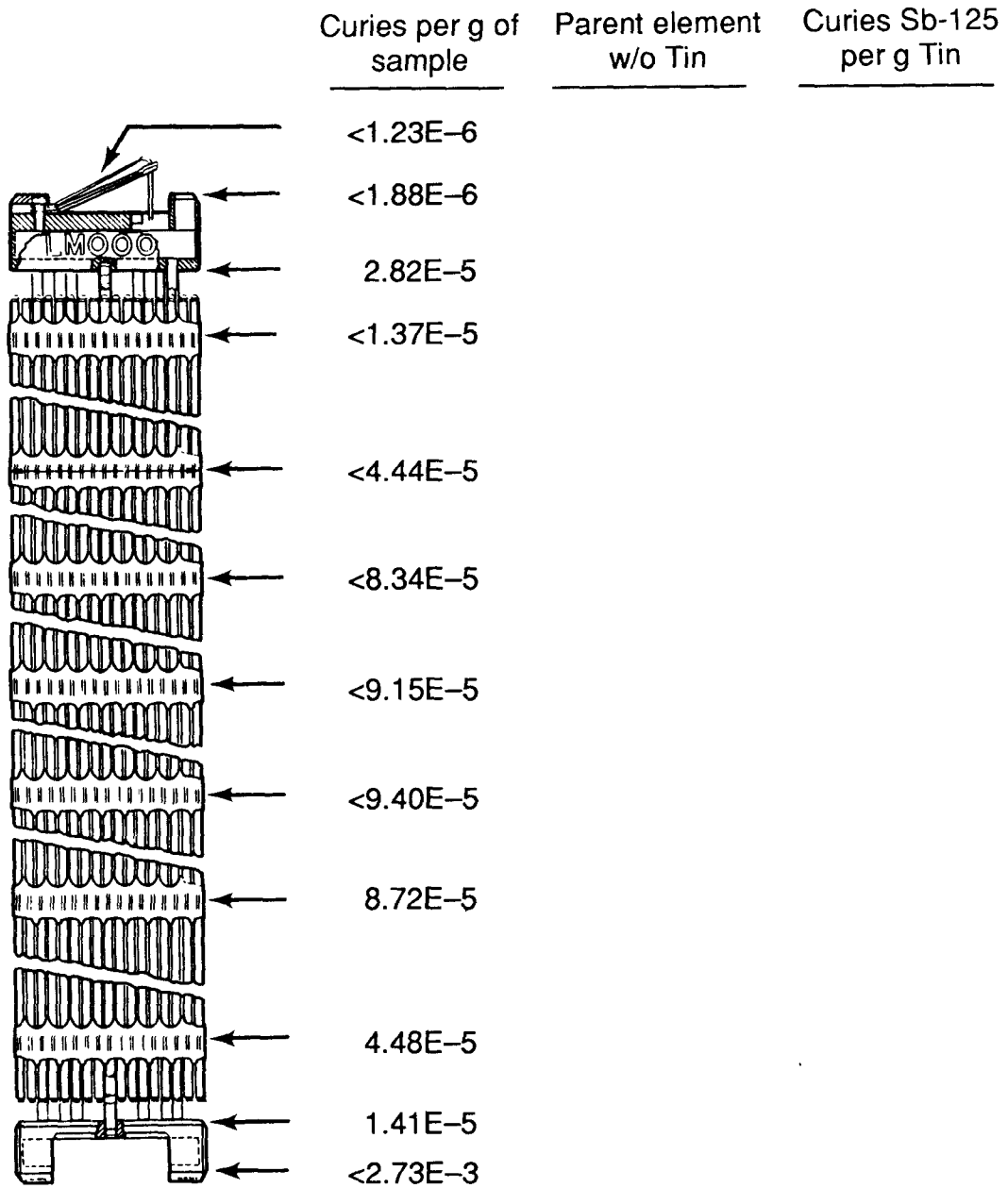
FIGURE 3.7. Results of Laboratory Analysis (Westinghouse 14x14, ^{125}Sb)

3.12
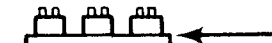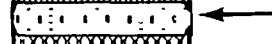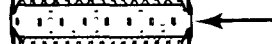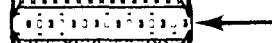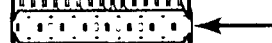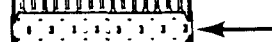
	Curies per g of sample	Parent element w/o Cobalt	Curies Co-60 per g Cobalt
	6.53E–4	5.10E–2	1.27E0
	8.79E–4	3.20E–2	2.78E0
	7.98E–3	9.30E–2	8.61E0
	1.32E–4	<2.70E–3	>4.9E0
	9.03E–5	<2.70E–3	>3.3E0
	1.04E–4	<2.70E–3	>3.9E0
	1.40E–4	<2.70E–3	>5.2E0
	1.09E–4	<2.70E–3	>4.0E0
	1.67E–4	<2.70E–3	>6.2E0
	1.19E–4	<2.70E–3	>4.4E0
	8.65E–5	<2.70E–3	>3.2E0
	4.23E–2	1.14E–1	3.71E1
	6.18E–2	1.28E–1	4.83E1
	3.10E–2	1.48E–1	2.09E1

FIGURE 3.8. Results of Laboratory Analysis (Combustion Engineering 14x14, ^{60}Co)

3.13

	Curies per g of sample	Parent element w/o Iron	Curies Fe-55 per g Iron
	3.25E–3	6.97E1	4.66E–3
	1.71E–3	8.00E0	2.14E–2
	3.29E–2	6.05E1	5.44E–2
	2.83E–4	2.12E–1	1.33E–1
	1.17E–3	2.13E–1	5.49E–1
	1.77E–3	2.11E–1	8.39E–1
	1.81E–3	2.29E–1	7.90E–1
	1.45E–3	2.20E–1	6.56E–1
	3.63E–3	2.00E–1	1.82E–0
	2.17E–3	2.60E–1	8.35E–1
	1.16E–3	1.82E–1	6.37E–1
	1.04E–2	2.49E0	4.18E–1
	1.18E–1	6.08E1	2.97E–1
	1.03E–1	6.71E1	1.52E–1
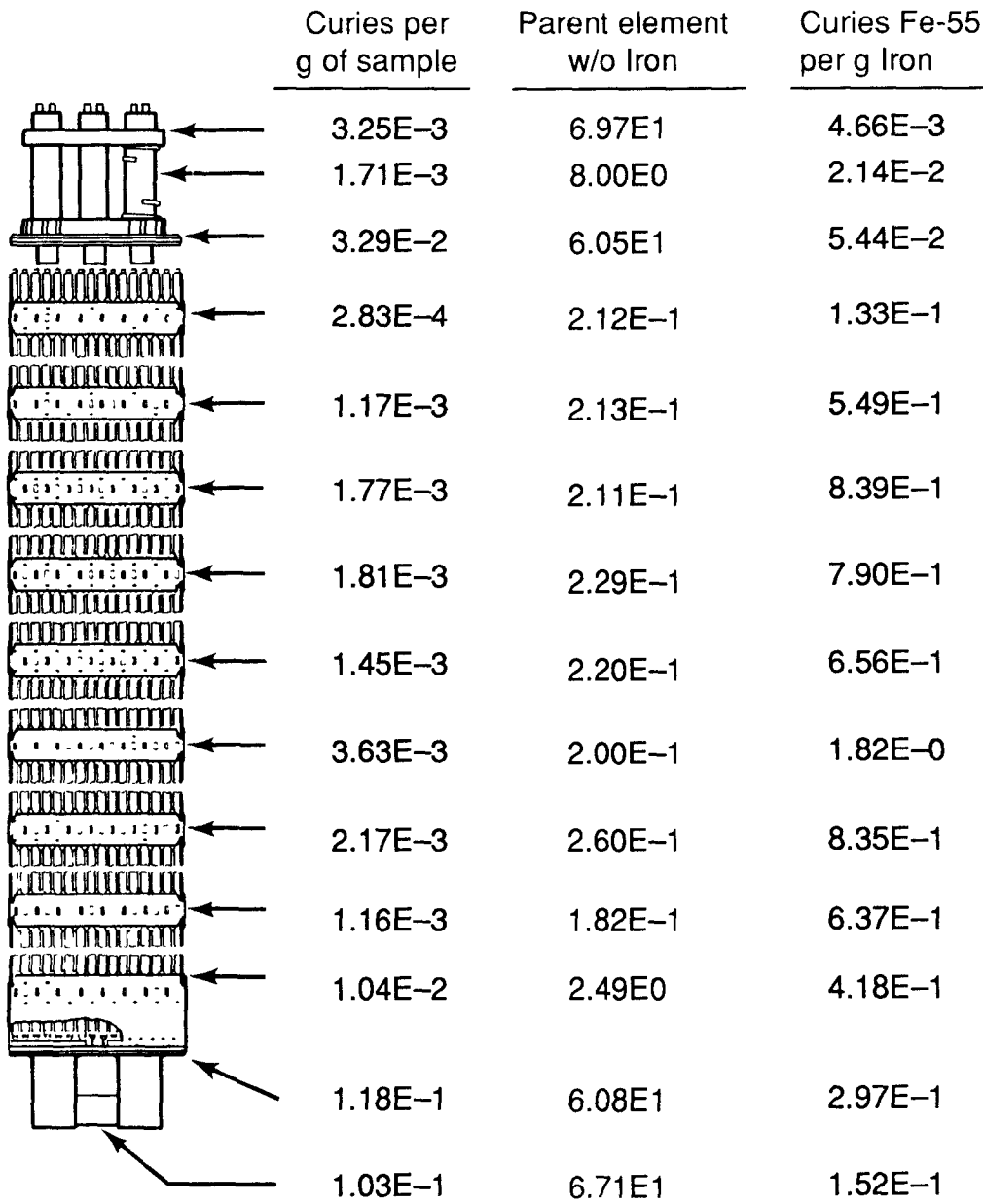
FIGURE 3.9. Results of Laboratory Analysis (Combustion Engineering 14x14, ^{55}Fe)

	Curies per g of sample	Parent element w/o Niobium	Curies Nb-94 per g Niobium
	4.77E–10	<1.50E–3	>3.2E–5
	2.85E–7	2.25E0	1.27E–5
	4.35E–9	<1.5E–3	>2.9E–4
	---	---	---
	1.68E–8	1.56E–2	1.09E–4
	---	---	---
	---	---	---
	---	---	---
	2.97E–8	2.59E–2	1.19E–4
	---	---	---
	2.09E–8	1.47E–2	1.42E–4
	2.26E–5	2.25E0	1.00E–3
	1.59E–8	<9.10E–3	>1.8E–4
	4.68E–9	<2.00E–2	>2.3E–5
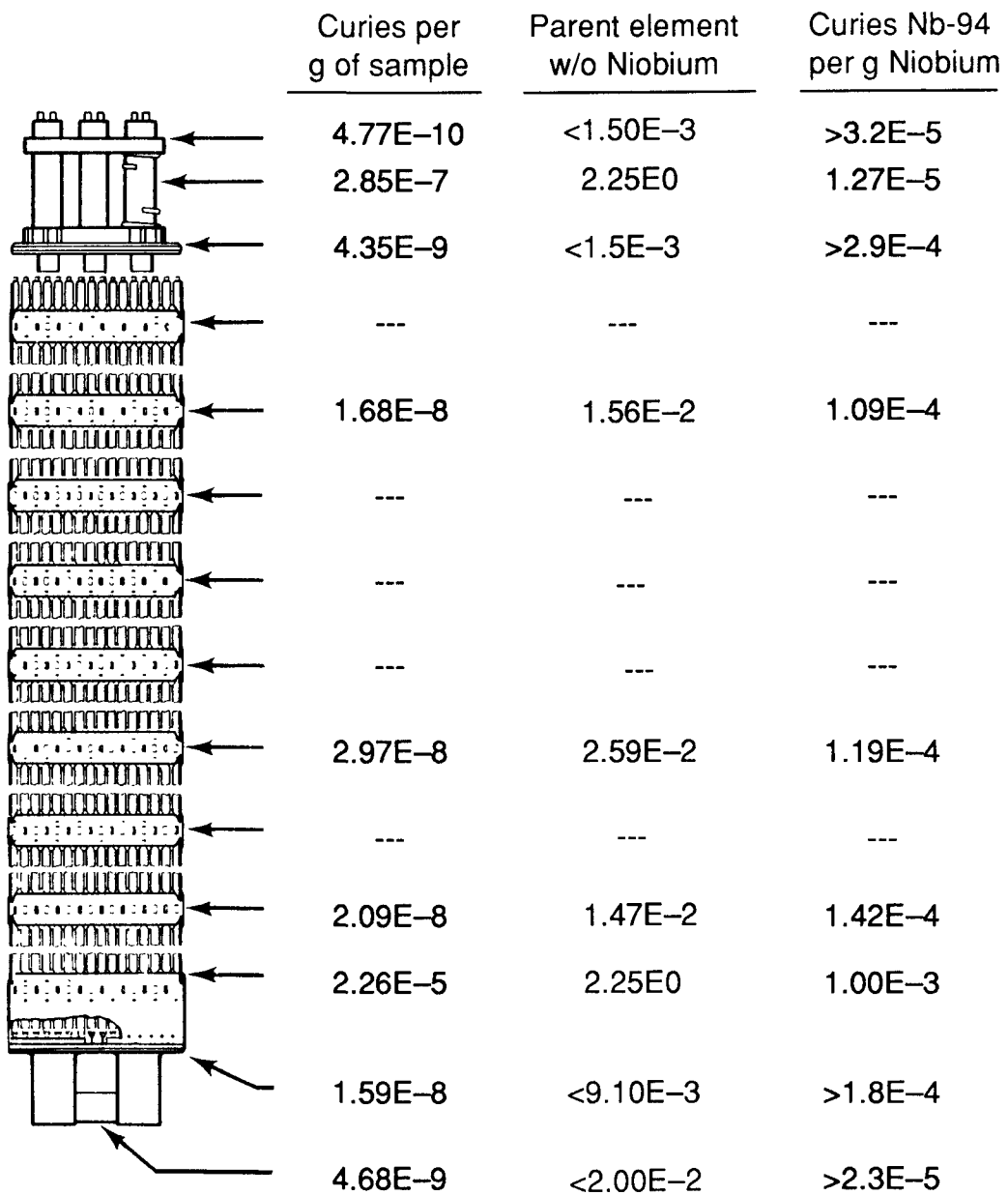
FIGURE 3.10. Results of Laboratory Analysis (Combustion Engineering 14x14, ^{94}Nb)
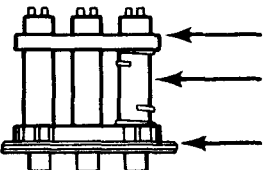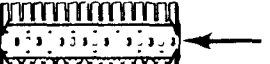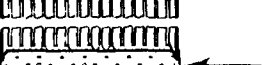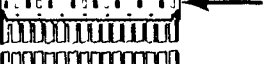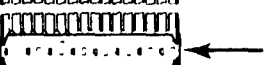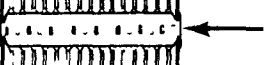
	Curies per g of sample	Parent element w/o Nickel	Curies Ni-59 per g Nickel
	1.09E–6	9.72E0	1.12E–5
	1.38E–5	7.29E1	1.89E–5
	7.12E–6	8.52E0	8.36E–5
	2.40E–9	<5.00E–3	>4.80E–5
	1.75E–8	<5.00E–3	>3.56E–4
	1.35E–8	<5.00E–3	>2.70E–4
	3.89E–8	<5.00E–3	>7.78E–4
	1.23E–8	<5.00E–3	>2.46E–4
	3.54E–8	<5.00E–3	>7.08E–4
	1.77E–8	<5.00E–3	>3.54E–4
	1.08E–8	<5.00E–3	>2.16E–4
	1.63E–4	3.266E1	4.45E–4
	5.54E–5	9.60E0	5.77E–4
	2.28E–5	9.84E0	2.32E–4

FIGURE 3.11. Results of Laboratory Analysis (Combustion Engineering 14x14, ^{59}Ni)
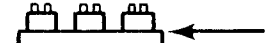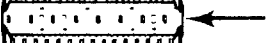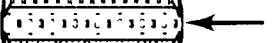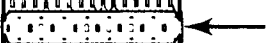
	Curies per g of sample	Parent element w/o Nickel	Curies Ni-63 per g Nickel
	1.64E–4	9.72E0	1.68E–3
	4.00E–3	7.29E1	5.49E–3
	1.63E–3	8.52E0	1.91E–2
	6.97E–7	<5.00E–3	>1.4E–2
	5.94E–6	<5.00E–3	>1.2E–1
	4.50E–6	<5.00E–3	>9.0E–2
	8.80E–6	<5.00E–3	>1.8E–1
	3.59E–6	<5.00E–3	>7.2E–2
	8.38E–6	<5.00E–3	>1.7E–1
	3.00E–6	<5.00E–3	>6.0E–2
	2.23E–6	<5.00E–3	>4.5E–2
	4.50E–2	3.66E1	1.35E–1
	1.59E–2	9.60E0	1.66E–1
	6.34E–3	9.84E0	6.44E–2

FIGURE 3.12. Results of Laboratory Analysis (Combustion Engineering 14x14, ^{63}Ni)

	Curies/g of sample	Parent element w/o Cobalt	Curies Co-60 per g Cobalt
	5.95E–4	2.60E–2	2.39E0
	5.41E–4	2.50E–2	2.16E0
	1.88E–3	5.00E–2	3.77E0
	2.42E–4	<6.00E–3	>3.4E0
	1.68E–3	<7.00E–3	>1.8E1
	9.20E–3	<6.00E–3	>1.3E1
	1.68E–3	<7.00E–3	>2.4E1
	7.32E–4	<6.00E–3	>1.0E1
	4.68E–4	<7.00E–3	>6.7E0
	2.28E–4	<7.00E–3	>3.3E0
	6.24E–2	2.10E–1	2.97E1
	7.03E–3	2.07E–1	3.50E0
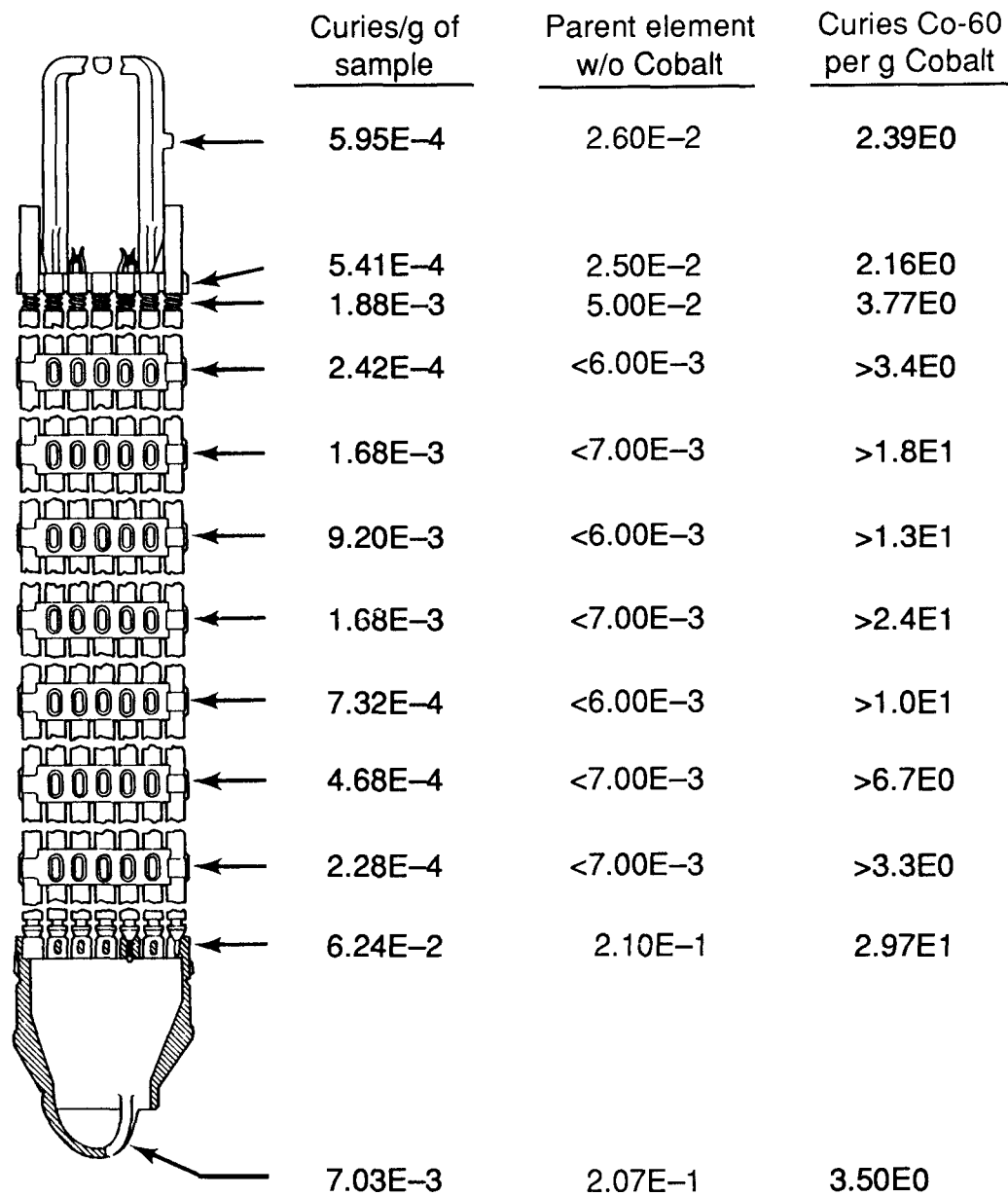
FIGURE 3.13. Results of Laboratory Analysis (General Electric 7x7, ^{60}Co)

	Curies/g of sample	Parent element w/o Iron	Curies Fe-55 per g Iron
	1.43E-2	6.83E1	2.08E-2
	8.79E-3	6.76E1	1.30E-2
	2.42E-3	6.04E1	4.00E-2
	8.41E-4	4.70E-1	1.79E-1
	2.59E-3	4.30E-1	6.03E-1
	1.87E-3	4.50E-1	4.16E-1
	3.31E-3	6.20E-1	5.34E-1
	3.52E-3	4.70E-1	7.50E-1
	2.46E-3	5.50E-1	4.48E-1
	2.55E-3	5.60E-1	4.55E-1
	1.35E-1	6.99E1	1.92E-1
	1.27E-2	6.91E1	1.83E-2
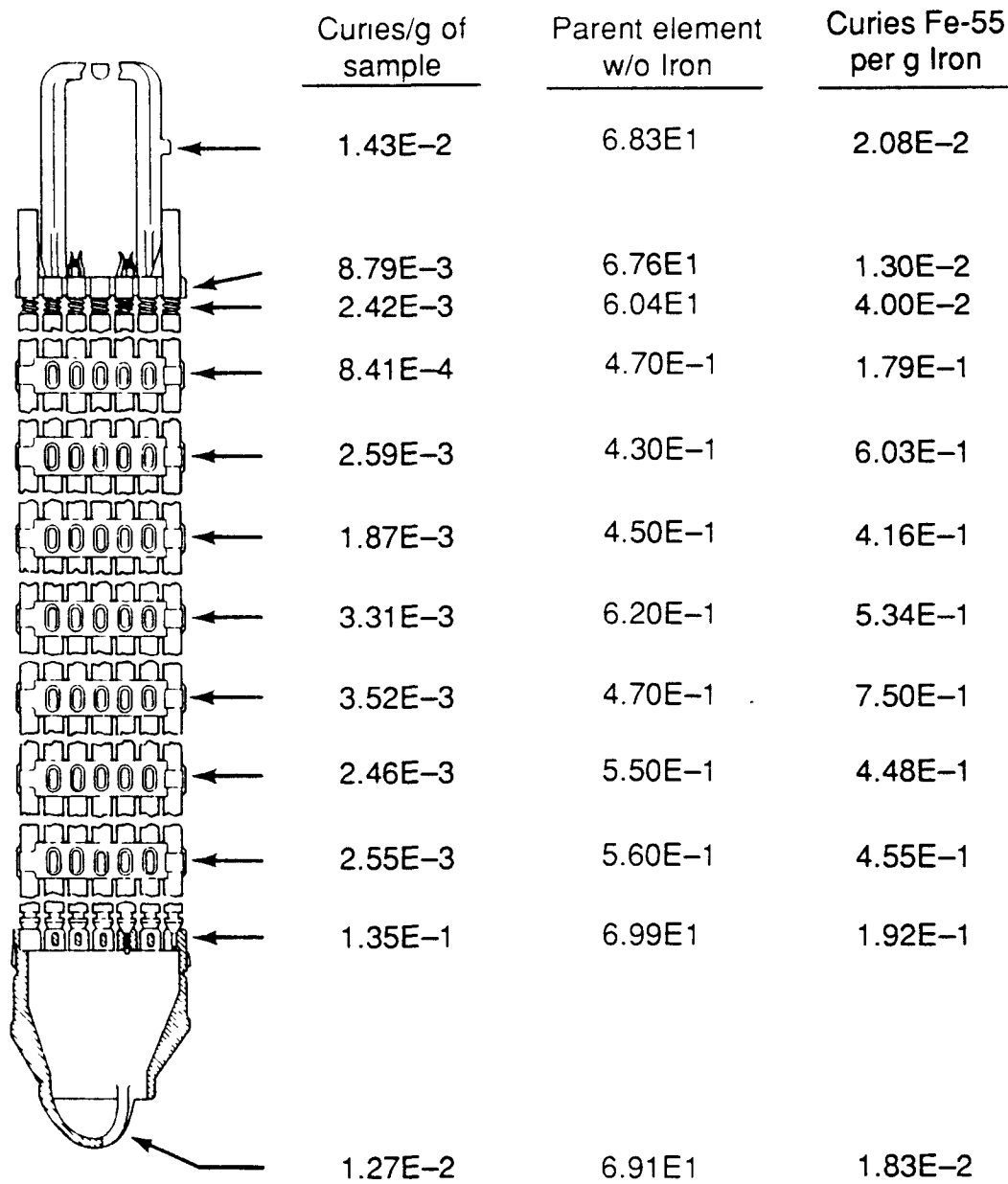
FIGURE 3.14. Results of Laboratory Analysis (General Electric 7x7, ^{55}Fe)

3.19

	Curies/g of sample	Parent element w/o Nickel	Curies Ni-59 per g Nickel
	3.68E–6	8.38E0	4.39E–5
	5.00E–6	8.26E0	6.04E–5
	4.73E–5	6.82E1	6.94E–5
	2.77E–7	7.20E–2	3.85E–4
	1.07E–6	8.30E–2	1.29E–3
	8.56E–7	6.60E–2	1.30E–3
	9.41E–7	8.80E–2	1.07E–3
	1.35E–6	4.40E–2	3.38E–3
	5.45E–7	4.30E–2	1.27E–3
	2.16E–7	3.00E–2	7.20E–4
	8.15E–5	8.68E0	9.39E–4
	1.14E–5	8.75E0	1.30E–4
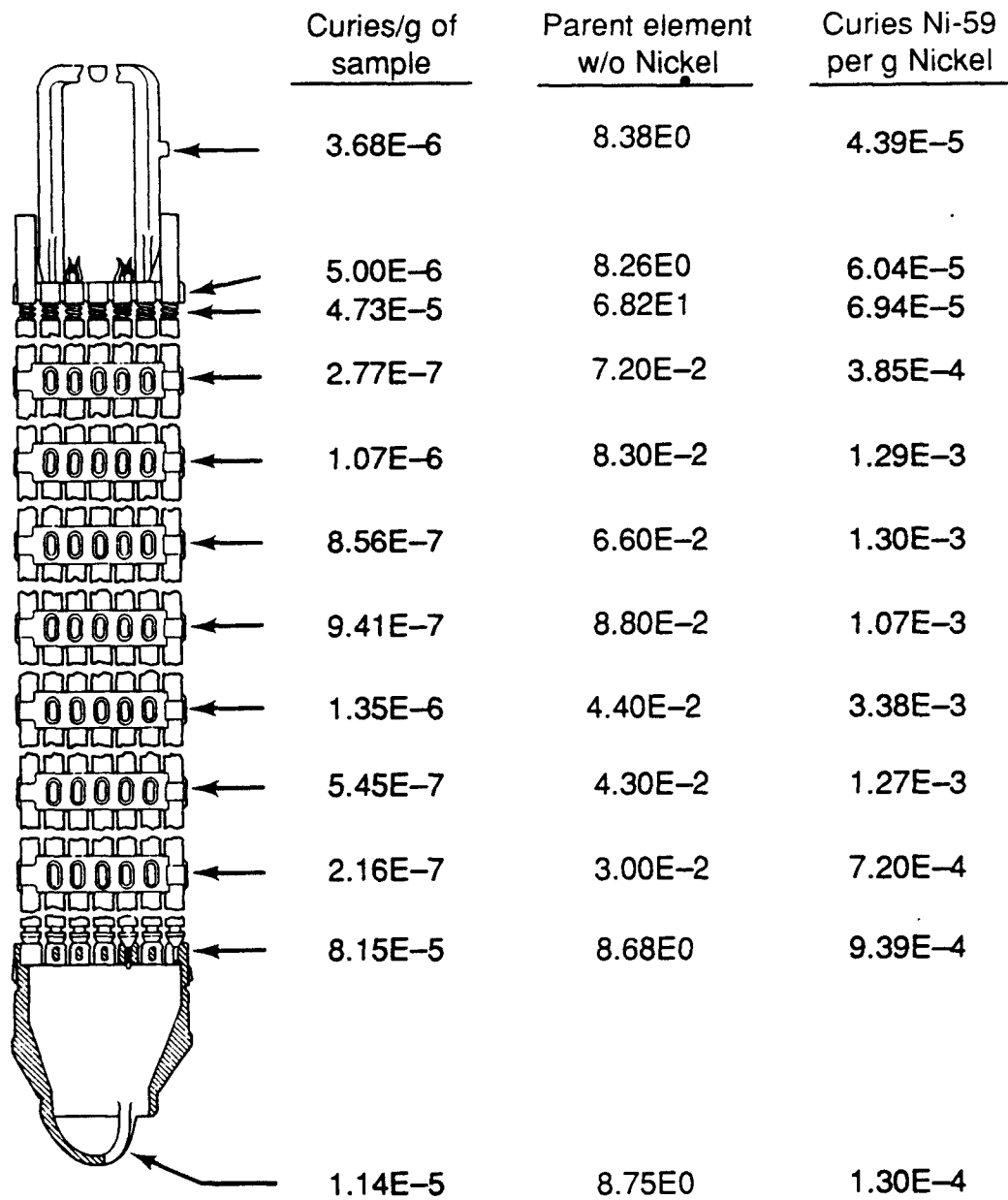
FIGURE 3.15. Results of Laboratory Analysis (General Electric 7x7, ^{59}Ni)

	Curies/g of sample	Parent element w/o Nickel	Curies Ni-63 per g Nickel
	8.01E–4	8.38E0	9.55E–3
	8.86E–4	8.26E0	1.07E–2
	9.48E–3	6.82E1	1.39E–2
	3.10E–5	7.20E–2	4.31E–2
	1.07E–4	8.30E–2	1.29E–1
	8.10E–5	6.60E–2	1.23E–1
	1.39E–4	8.80E–2	1.58E–1
	1.91E–4	4.40E–2	4.78E–1
	7.06E–5	4.30E–2	1.64E–1
	2.63E–5	3.00E–2	8.77E–2
	7.54E–3	8.68E0	8.69E–2
	1.28E–3	8.75E0	1.46E–2
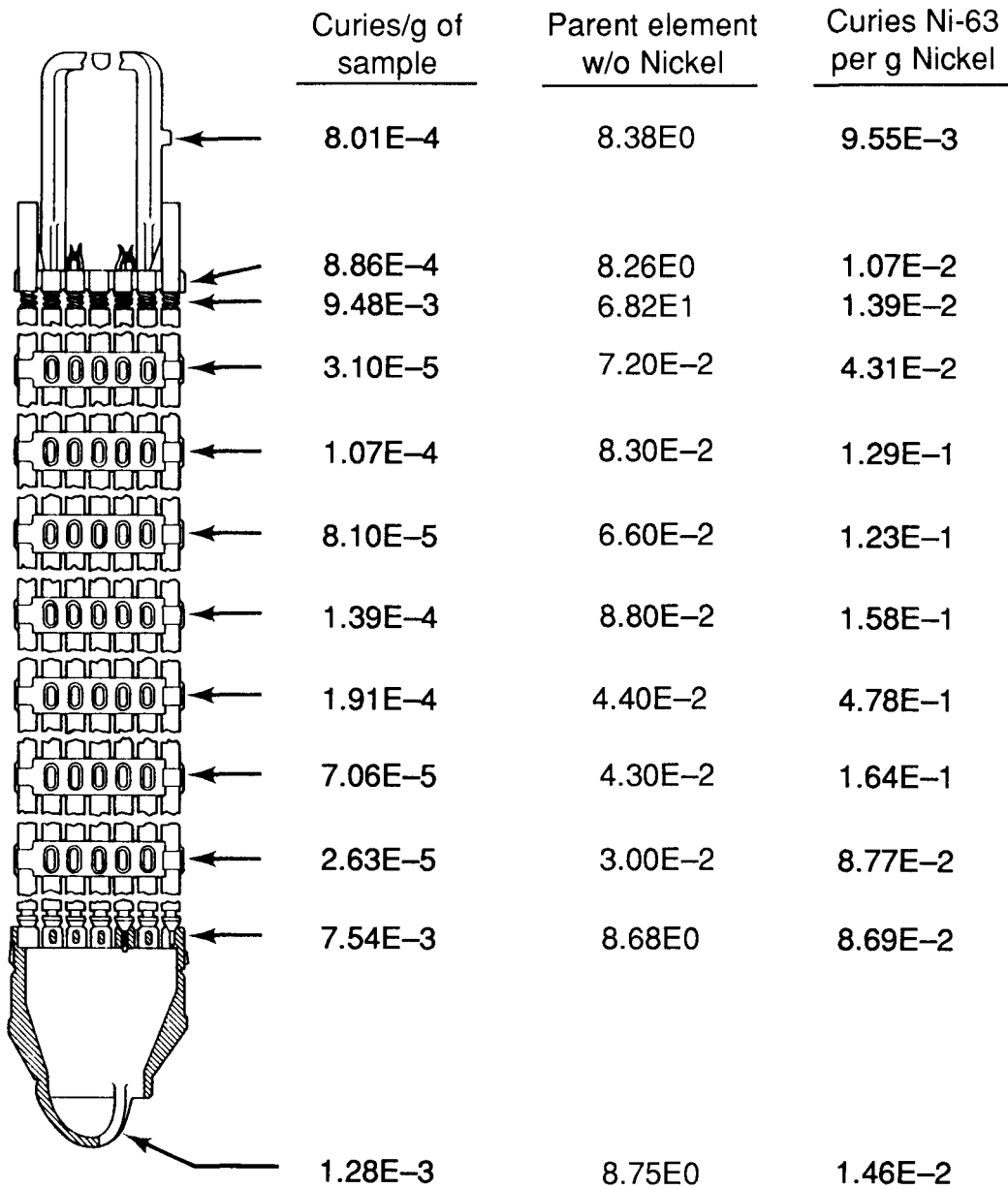
FIGURE 3.16.   Results of Laboratory Analysis (General Electric 7x7, ^{63}Ni)

	Curies/g of sample	Parent element w/o Niobium	Curies Nb-94 per g Niobium
	7.61E–10	1.00E–3	7.61E–5
	3.89E–9	7.40E–4	5.27E–4
	5.95E–7	8.10E–1	7.34E–5
	5.09E–9	5.10E–3	1.00E–4
	---	---	---
	---	---	---
	---	---	---
	9.14E–9	2.00E–2	4.59E–5
	---	---	---
	9.86E–7	1.80E–2	5.45E–5
	7.97E–8	3.70E–2	2.15E–4
	6.04E–9	1.80E–2	3.35E–5
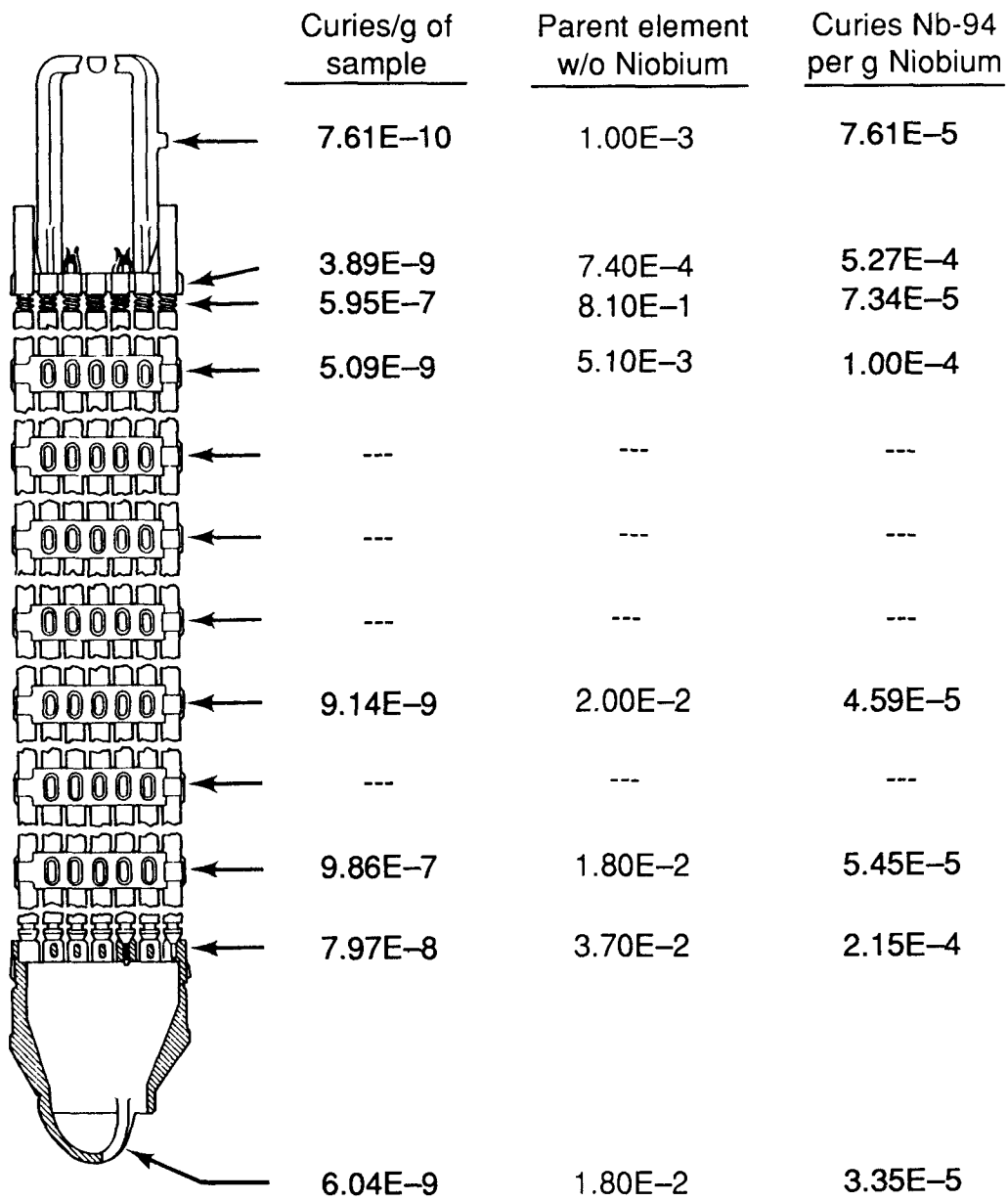
FIGURE 3.17. Results of Laboratory Analysis (General Electric 7x7, ^{94}Nb)

	Curies/g of sample	Parent element w/o Iron	Curies Mn-54 per g Manganese
	1.10E-4	6.83E1	1.61E-4
	1.15E-4	6.76E1	1.70E-4
	<9.5E-5	6.04E1	<1.6E-3
	3.53E-5	4.70E-1	7.51E-3
	1.58E-4	4.30E-1	3.67E-2
	1.49E-4	4.50E-1	3.31E-2
	2.14E-4	6.20E-1	3.45E-2
	1.61E-4	4.70E-1	3.43E-2
	2.02E-4	5.50E-1	3.67E-2
	1.01E-4	5.60E-1	1.80E-2
	<4.3E-3	6.99E1	<6.2E-3
	<5.8E-4	6.91E1	<8.4E-4
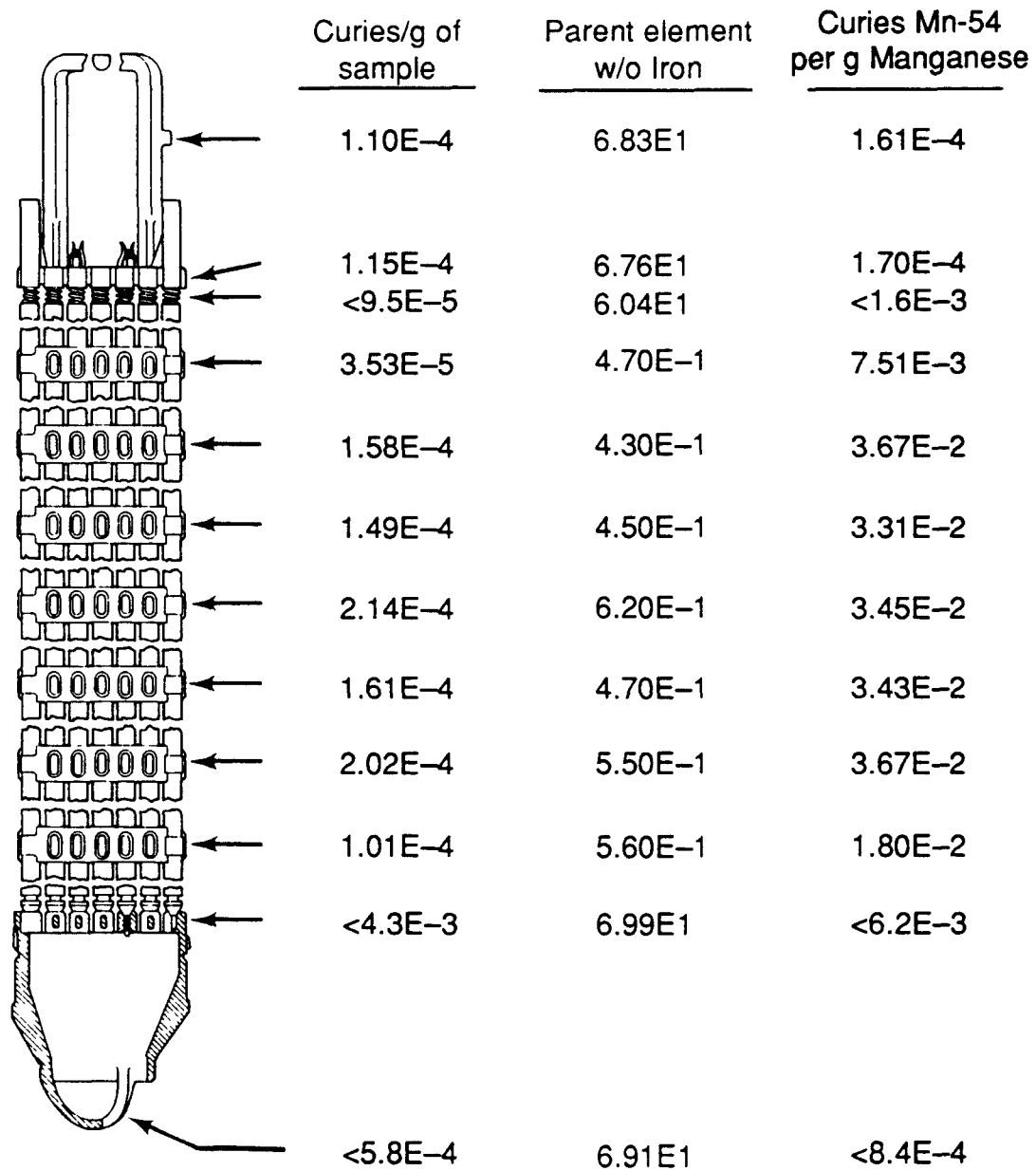
FIGURE 3.18. Results of Laboratory Analysis (General Electric 7x7, ^{54}Mn)

	Curies/g of sample	Parent element w/o Tin	Curies Sb-125 per g Tin
	4.23E–6	<2.20E–1	---
	<1.9E–6	<2.10E–1	---
	1.44E–5	<2.60E–1	>5.5E–5
	4.16E–3	1.09E0	3.81E–1
	1.41E–3	1.13E0	1.24E–1
	1.02E–3	8.60E–1	1.18E–1
	1.81E–3	1.09E0	1.65E–1
	1.72E–3	1.10E0	1.56E–1
	1.33E–3	1.06E0	1.26E–1
	1.22E–3	1.10E0	1.11E–1
	<1.7E–4	<3.00E–1	<5.8E–2
	<2.3E–5	<2.00E–1	<1.1E–2
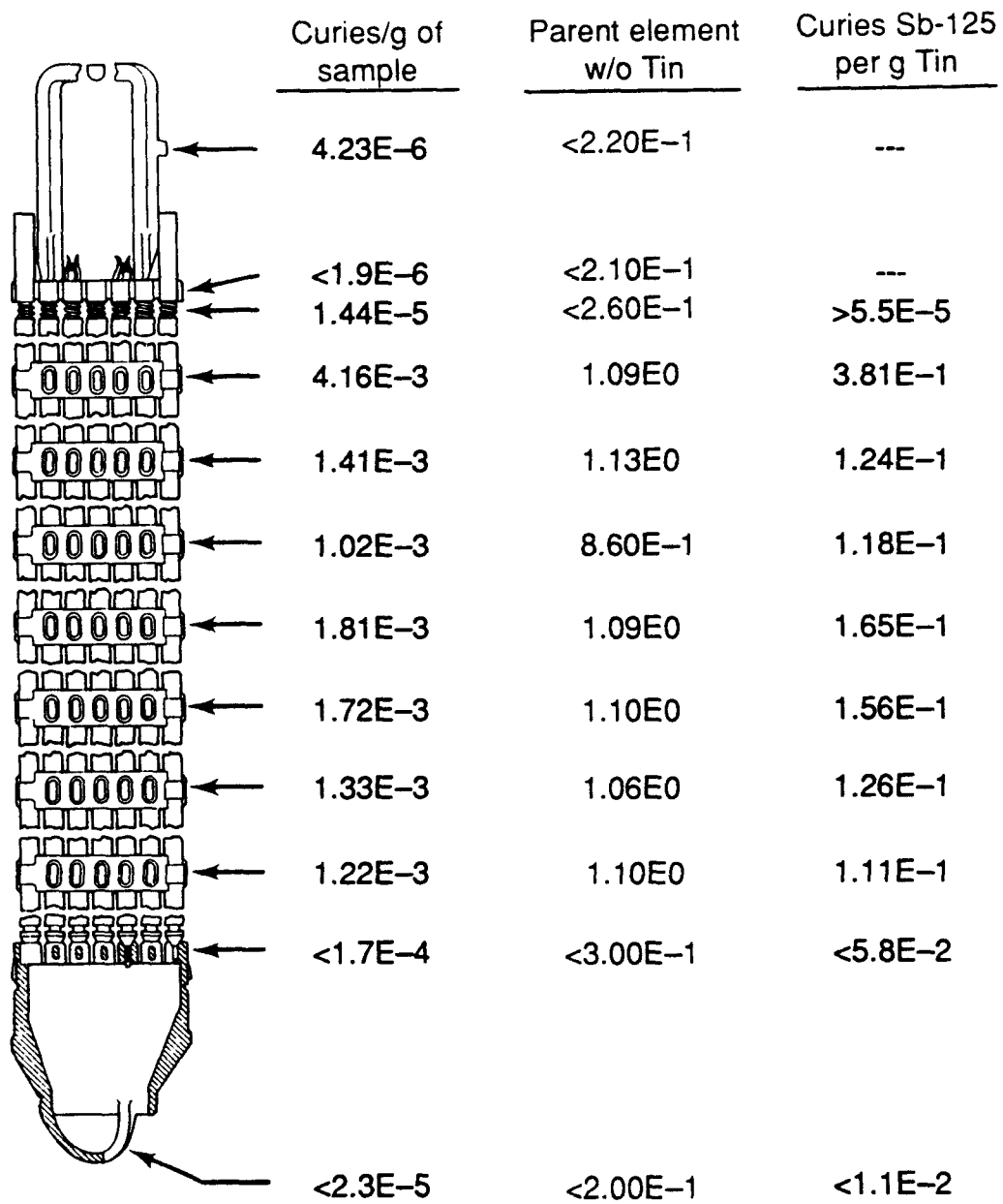
FIGURE 3.19. Results of Laboratory Analysis (General Electric 7x7, ^{125}Sb)

TABLE 3.1. Radionuclide Concentrations in Westinghouse Spent Fuel Assembly Hardware Alloys (Point Beach Station)

Sample Number	Alloy	Location	Concentration (Ci/g alloy)[a]						
			^{54}Mn [b]	^{55}Fe	^{59}Ni	^{63}Ni	^{60}Co	^{94}Nb	^{93m}Nb [c]
W-10	Inconel	Holddown spring at top end	(5.73±3.08)E-5	(1.84±0.02)E-3	(1.18±0.01)E-5	(2.7±0.03)E-3	(7.34±0.07)E-4	(7.39±1.17)E-7	(5.48±0.55)E-5
W-12	SS	Upper end fitting (top)	(1.79±0.48)E-4	(3.67±0.04)E-3	(1.66±0.01)E-6	(3.51±0.04)E-4	(1.63±0.02)E-3	(4.09±0.69)E-10	(7.36±0.74)E-8
W-9	SS	Upper end fitting casting (bottom)	(6.39±3/89)E-4	(2.87±0.02)E-2	(1.31±0.01)E-5	(3.05±0.04)E-3	(1.30±0.01)E-2	(1.79±0.37)E-9	(2.39±0.24)E-7
W-8	Inconel	Spacer grid #7	<3.5E-4	(1.29±0.01)E-2	(7.52±0.01)E-5	(1.96±0.02)E-2	(1.31±0.01)E-2	(6.98±1.17)E-6	(6.06±0.61)E-4
W-7	Inconel	Spacer grid #6	(5.50±1.14)E-3	(5.31±0.05)E-2	(2.55±0.03)E-4	(6.51±0.04)E-2	(4.07±0.04)E-2	--	--
W-6	Inconel	Spacer grid #5	(8.52±0.21)E-3	(5.53±0.05)E-2	(3.50±0.04)E-4	(8.49±0.08)E-2	(7.47±0.07)E-2	--	--
W-5	Inconel	Spacer grid #4	(3.76±2.33)E-3	(6.27±0.05)E-2	(3.27±0.04)E-4	(8.80±0.08)E-2	(8.82±0.09)E-2	(1.20±0.32)E-4	(2.81±0.28)E-2
W-4	Inconel	Spacer grid #3	(3.90±2.36)E-3	(6.45±0.05)E-2	(2.76±0.03)E-4	(7.99±0.08)E-2	(8.01±0.08)E-2	--	--
W-3	Inconel	Spacer grid #2	(3.52±1.68)E-3	(6.92±0.05)E-2	(3.35±0.03)E-4	(8.89±0.08)E-2	(8.03±0.08)E-2	--	--
W-2	Inconel	Spacer grid #1	<1.1E-3	(3.14±0.02)E-2	(1.35±0.01)E-4	(3.74±0.04)E-2	(3.05±0.03)E-2	(4.14±0.77)E-5	(8.45±0.85)E-3
W-11	SS	Bottom end fitting (top)	(3.52±0.33)E-3	(4.75±0.04)E-2	(1.48±0.01)E-5	(3.75±0.04)E-3	(1.28±0.01)E-2	(6.40±0.81)E-9	(8.07±0.81)E-7
W-1	SS	Bottom end fitting (bottom)	(2.26±0.69)E-3	(4.21±0.04)E-2	(1.00±0.01)E-5	(2.86±0.03)E-3	(1.83±0.02)E-2	(2.07±0.36)E-8	(2.67±0.27)E-6

(a) Decay corrected to discharge data of 10/8/81.
(b) Parent element is iron (Fe). ^{54}Mn is formed by the fast neutron reaction ^{54}Fe(n,p)^{54}Nm.
(c) Parent element is Nb. ^{93m}Nb is predominantly produced by the raction ^{93}Nb(n,N')^{93m}Nb.

TABLE 3.2. Elemental Concentrations in Westinghouse Spent Fuel Assembly Hardware Alloys (Point Beach Station)

Sample Number	Alloy	Location	Concentration--Weight Percent							
			Mn	Fe	Cr	Ni	Co	Nb	Cu	Mo
W-10	Inconel	Holddown spring at top end	0.0629±0.004	17.2±0.5	17.6±0.5	50.8±1.5	0.0709±0.009	4.50±0.05	0.062±0.006	2.86±0.08
W-12	SS	Upper end fitting (top)	1.52±0.05	67.5±2.0	18.3±0.5	8.27±0.25	0.150±0.015	0.0033±0.0007	0.10±0.010	0.41±0.01
W-9	SS	Upper end fitting casting (bottom)	1.44±0.04	65.0±2.0	18.0±0.5	9.10±0.25	0.149±0.015	0.0024±0.0024	0.095±0.009	0.12±0.01
W-8	Inconel	Spacer grid #7	0.133±0.008	16.0±0.5	16.6±0.5	53.0±1.6	0.148±0.015	4.40±0.05	0.18±0.02	2.79±0.08
W-7	Inconel	Spacer grid #6	0.133±0.008	15.2±0.5	15.7±0.5	46.5±1.4	0.089±0.009	--	0.18±0.02	2.66±0.08
W-6	Inconel	Spacer grid #5	0.069±0.002	16.0±0.5	17.0±0.5	48.0±1.4	0.115±0.012	--	0.078±0.008	2.83±0.08
W-5	Inconel	Spacer grid #4	0.073±0.002	17.0±0.5	17.8±0.5	50.8±1.5	0.131±0.013	4.60±0.05	0.085±0.008	2.98±0.08
W-4	Inconel	Spacer grid #3	0.062±0.002	16.2±0.5	16.2±0.5	47.1±1.4	0.119±0.012	--	0.075±0.008	2.65±0.08
W-3	Inconel	Spacer grid #2	0.068±0.006	16.5±0.5	17.4±0.5	49.2±1.5	0.130±0.017	--	0.091±0.009	2.87±0.08
W-2	Inconel	Spacer grid #1	0.113±0.006	15.8±0.5	17.4±0.5	49.3±1.5	0.111±0.011	4.60±0.05	0.172±0.017	2.67±0.08
W-11	SS	Bottom end fitting (top)	1.71±0.05	65.5±2.0	18.7±0.5	9.36±0.25	0.115±0.035	0.03±0.03	0.094±0.009	0.23±0.01
W-1	SS	Bottom end fitting (bottom)	1.54±0.05	65.0±2.0	17.6±0.5	7.96±0.25	0.147±0.015	0.0156±0.0022	0.125±0.013	0.25±0.01

TABLE 3.3. Specific Activities of Long-Lived Radionuclides in Westinghouse Spent Fuel Assembly Hardware Alloys (Point Beach Station)

Sample Number	Alloy	Location	Concentration (Ci/g parent element) [a]						
			^{54}Mn [b]	^{55}Fe	^{59}Ni	^{63}Ni	^{60}Co	^{94}Nb	^{93m}Nb [c]
W-10	Inconel	Holddown spring at top end	(3.33±1.79)E-4	(1.07±0.03)E-2	(2.32±0.07)E-5	(5.30±0.16)E-3	(1.04±0.13)E0	(1.64±0.26)E-5	(1.22±0.12)E-3
W-12	SS	Upper end fitting (top)	(2.65±0.71)E-4	(5.43±0.16)E-3	(2.01±0.06)E-5	(4.25±0.13)E-3	(1.09±0.11)E0	(1.24±0.26)E-5	(2.21±0.47)E-3
W-9	SS	Upper end fitting casting (bottom)	(9.83±5.98)E-4	(4.41±0.13)E-2	(1.44±0.04)E-4	(3.35±0.10)E-2	(8.72±0.87)E0	(7.20±7.20)E-5	(9.9±9.9)E-3
W-8	Inconel	Spacer grid #7	<2.2E-3	(8.06±0.24)E-2	(1.42±0.04)E-4	(3.70±0.11)E-2	(8.85±0.89)E0	(1.59±0.27)E-4	(1.37±0.14)E-2
W-7	Inconel	Spacer grid #6	(3.62±0.75)E-2	(3.49±0.10)E-1	(5.48±0.16)E-4	(1.40±0.04)E-1	(4.57±0.46)E1	--	--
W-6	Inconel	Spacer grid #5	(5.33±0.13)E-2	(3.46±0.10)E-1	(7.29±0.22)E-4	(1.77±0.05)E-1	(6.49±0.65)E1	--	--
W-5	Inconel	Spacer grid #4	(2.21±0.62)E-2	(3.69±0.19)E-4	(6.44±0.19)E-4	(1.73±0.05)E-1	(6.73±0.67)E1	(2.61±0.70)E-3	(6.12±0.61)E-1
W-4	Inconel	Spacer grid #3	(2.41±1.46)E-2	(3.98±0.11)E-1	(5.86±0.18)E-4	(1.70±0.05)E-1	(6.73±0.67)E1	--	--
W-3	Inconel	Spacer grid #2	(2.13±1.02)E-2	(4.19±0.12)E-1	(6.81±0.20)E-4	(1.81±0.05)E-1	(6.18±0.62)E1	--	--
W-2	Inconel	Spacer grid #1	<6.9E-3	(1.99±0.06)E-1	(2.74±0.08)E-4	(7.59±0.22)E-2	(2.75±0.28)E1	(9.01±1.67)E-4	(1.83±0.18)E-1
W-11	SS	Bottom end fitting (top)	(3.57±0.50)E-3	(7.25±0.22)E-2	(1.58±0.05)E-4	(4.01±0.12)E-2	(1.11±0.34)E1	(2.20±2.20)E-5	(2.7±2.7)E-3
W-1	SS	Bottom end fitting (bottom)	(3.48±1.06)E-3	(6.48±0.19)E-2	(1.26±0.04)E-4	(3.59±0.11)E-2	(1.24±0.12)E1	(1.32±0.23)E-4	(1.72±0.24)E-2

(a) Decay corrected to discharge data of 10/8/81.
(b) Parent element is iron (Fe). ^{54}Mn is formed by the fast neutron reaction $^{54}Fe(n,p)^{54}Nm$.
(c) Parent element is Nb. ^{93m}Nb is predominantly produced by the raction $^{93}Nb(n,n')^{93m}Nb$.

TABLE 3.4. Radionuclide Concentrations in Combustion Engineering Spent Fuel Assembly Hardware Alloys (Calvert Cliffs Station)

Sample Number	Alloy	Location	Concentration (Ci/g alloy)[a]							
			^{54}Mn[b]	^{55}Fe	^{59}Ni	^{63}Ni	^{60}Co	^{94}Nb	^{93m}Nb[c]	^{125}Sb[d]
CE-25	SS	Upper holddown plate	(2.92±0.15)E-4	(3.25±0.08)E-3	(1.09±0.02)E-6	(1.64±0.03)E-4	(6.53±0.13)E-4	(4.77±0.81)E-10	(7.70±0.77)E-8	(1.99±0.82)E-6
CE-26	Inconell	Upper holddown spring	(4.27±2.37)E-5	(1.71±0.03)E-3	(1.38±0.03)E-5	(4.00±0.08)E-3	(8.79±0.18)E-4	(2.85±0.50)E-7	(3.18±0.32)E-5	(3.70±1.38)E-6
CE-24	SS	Upper flow plate	(7.70±1.35)E-4	(3.29±0.08)E-2	(7.12±0.18)E-6	(1.63±0.03)E-3	(7.98±0.33)E-3	(4.35±0.73)E-9	(9.20±0.92)E-7	<7.4E-6
CE-10	Zircaloy	Top spacer grid	(6.77±0.89)E-6	(2.83±0.06)E-4	(2.40±0.24)E-9	(6.97±1.10)E-7	(1.32±0.3)E-4	--	--	(1.36±0.14)E-4
CE-9	Zircaloy	Spacer grid #7	(1.79±0.06)E-4	(1.17±0.02)E-3	(1.75±0.10)E-8	(5.94±0.49)E-6	(9.03±0.18)E-5	(1.68±0.26)E-8	(1.95±0.20)E-5	(2.46±0.25)E-3
CE-8	Zircaloy	Spacer grid #6	(1.80±0.07)E-4	(1.77±0.04)E-3	(1.35±0.12)E-8	(4.50±0.50)E-6	(1.04±0.03)E-4	--	--	(2.49±0.25)E-3
CE-7	Zircaloy	Spacer grid #5	(2.02±0.10)E-4	(1.81±0.04)E-3	(3.89±0.18)E-8	(8.80±0.70)E-6	(1.40±0.03)E-4	--	--	(2.68±0.27)E-3
CE-6	Zircaloy	Spacer grid #4	(2.06±0.08)E-4	(1.45±0.03)E-3	(1.23±0.10)E-8	(3.59±0.43)E-6	(1.09±0.03)E-4	--	--	(2.29±0.23)E-3
CE-5	Zircaloy	Spacer grid #3	(2.65±0.14)E-4	(3.63±0.06)E-3	(3.54±0.22)E-8	(8.38±1.17)E-6	(1.67±0.04)E-4	(2.97±0.58)E-8	(3.64±0.36)E-5	(3.50±0.24)E-3
CE-4	Zircaloy	Spacer grid #2	(2.19±0.11)E-4	(2.17±0.06)E-3	(1.77±0.21)E-8	(3.00±0.69)E-6	(1.19±0.03)E-4	--	--	(1.68±0.17)E-3
CE-3	Zircaloy	Spacer grid #2	(1.54±0.05)E-4	(1.16±0.02)E-3	(1.08±0.14)E-8	(2.23±0.32)E-6	(8.65±0.19)E-5	(2.09±0.45)E-8	(1.63±0.16)E-5	(1.56±0.16)E-3
CE-2	Inconel	Bottom spacer grid	(9.70±0.75)E-4	(1.04±0.03)E-2	(1.63±0.05)E-4	(4.50±0.14)E-2	(4.23±1.07)E-2	(2.26±0.39)E-5	(4.46±0.45)E-3	<4.6E-5
CD-14	SS	Bottom retention plate	(8.69±0.12)E-3	(1.18±0.05)E-1	(5.54±0.17)E-5	(1.59±0.05)E-2	(6.18±0.49)E-2	(1.59±0.27)E-8	(2.17±0.22)E-6	<7.0E-5
CE-1	SS	Bottom end fitting near axial middle	(2.98±0.48)E-3	(1.03±0.03)E-1	(2.28±0.68)E-5	(6.34±1.83)E-3	(3.10±0.46)E-2	(4.68±0.81)E-9	(1.21±0.12)E-6	<2.9E-5

(a) Decay corrected to discharge data of 4/17/82.
(b) Parent element is iron (Fe). ^{54}Mn is formed by the fast neutron reaction ^{54}Fe(n,p)^{54}Mn.
(c) Parent element is Nb. ^{93m}Nb is predominantly produced by the reaction ^{93}Nb(n,n)^{93m}Nb.
(d) Parent element of ^{125}Sb is Sn. ^{125}Sb is formed by the thermal neutron reaction ^{124}Sn(n,γ)^{125}Sn followed by beta decay to ^{125}Sb.

TABLE 3.5. Elemental Concentrations in Combustion Engineering Spent Fuel Assembly Hardware Alloys (Calvert Cliffs Station)

Sample Number	Alloy	Location	Concentration--Weight Percent								
			Mn	Fe	Cr	Ni	Co	Nb	Sn	Mo	Zr
CE-25	SS	Upper holddown plate	1.22±0.01	69.7±2.1	21.2±0.8	9.72±0.39	0.0513±0.004	<0.0015	<0.018	0.007±0.001	
CE-26	Inconel	Upper holddown spring	0.200±0.002	8.00±0.33	15.5±0.6	72.9±2.2	0.0316±0.003	2.25±0.03	0.27±0.09	0.039±0.002	
CE-24	SS	Upper flow plate	0.95±0.01	60.5±1.8	16.2±0.7	8.52±0.33	0.0927±0.008	<0.0015	<0.018	0.004±0.002	<0.8
CE-10	Zircaloy	Top spacer grid	<0.002	0.212±0.009	0.11±0.01	<0.005	<0.0027	--	2.2±0.2	<0.005	91.8±2.9
CE-9	Zircaloy	Spacer grid #7	<0.002	0.213±0.008	0.11±0.01	<0.005	<0.0027	0.0156±0.0009	2.3±0.2	0.018±0.002	89.0±2.8
CE-8	Zircaloy	Spacer grid #6	<0.002	0.211±0.006	0.11±0.01	<0.005	<0.0027	--	2.4±0.2	0.022±0.001	91.7±2.7
CE-7	Zircaloy	Spacer grid #5	<0.002	0.229±0.011	0.11±0.01	<0.005	<0.0027	--	2.6±0.3	0.012±0.002	92.0±2.8
CE-6	Zircaloy	Spacer grid #4	<0.006	0.220±0.018	0.11±0.01	<0.005	<0.0027	--	3.0±0.5	<0.02	92.5±3.0
CE-5	Zircaloy	Spacer grid #3	<0.013	0.200±0.020	0.13±0.01	<0.005	<0.0027	0.0259±0.0017	3.9±1.0	<0.04	115±3.5
CE-4	Zircaloy	Spacer grid #2	<0.012	0.260±0.028	0.10±0.004	<0.005	<0.0027	--	3.4±1.0	<0.04	106±3.9
CE-3	Zircaloy	Spacer grid #1	<0.005	0.182±0.017	0.078±0.023	<0.005	<0.0027	0.0147±0.0009	2.0±0.4	<0.017	73.5±2.5
CE-2	Inconel	Bottom spacer grid	0.093±0.009	2.49±0.07	13.8±0.4	36.6±1.1	0.114±0.029	2.25±0.03	--	14.5±0.4	--
CE-14	SS	Bottom retention plate	1.08±0.03	60.8±1.8	18.2±0.5	9.60±0.3	0.128±0.010	<0.0091	--	0.032±0.005	--
CE-1	SS	Bottom end fitting near axial middle	1.10±0.03	67.1±2.0	18.8±0.5	9.84±2.95	0.148±0.022	<0.02	--	0.050±	--

TABLE 3.6. Specific Activities of Long-Lived Radionuclides in Combustion Engineering Spent Fuel Assembly Hardware Alloys (Calvert Cliffs Station)

Sample Number	Alloy	Location	Concentration (Ci/g parent element)[a]						
			^{54}Mn[b]	^{55}Fe	^{59}Ni	^{63}Ni	^{60}Co	^{94}Nb	^{93m}Nb[c]
CE-25	SS	Upper holddown plate	(4.19 ± 0.22)E-4	(4.66 ± 0.14)E-3	(1.12 ± 0.02)E-5	(1.68 ± 0.07)E-3	(1.27 ± 0.09)E0	>3.2E-5	<5.1E-3
CE-26	Inconel	Upper holddown spring	(5.34 ± 3.40)E-4	(2.14 ± 0.09)E-2	(1.89 ± 0.05)E-5	(5.49 ± 0.16)E-3	(2.78 ± 0.26)E0	(1.27 ± 0.22)E-5	(1.42 ± 0.14)E-3
CE-24	SS	Upper flow plate	(1.27 ± 0.23)E-3	(5.44 ± 0.16)E-2	(8.36 ± 0.32)E-5	(1.91 ± 0.06)E-2	(8.61 ± 0.74)E0	>2.9E-4	>6.1E-2
CE-10	Zircaloy	Top spacer grid	$(3.19\pm0.42($E-3	(1.33 ± 0.06)E-1	>4.8E-5	>1.4E-2	>4.9E0	--	--
CE-9	Zircaloy	Spacer grid #7	(8.40 ± 0.28)E-2	(5.49 ± 0.21)E-1	>3.5E-4	>1.2E-1	>3.3E0	(1.09 ± 0.17)E-4	(1.24 ± 0.04)E-1
CE-8	Zircaloy	Spacer grid #6	(8.53 ± 0.33)E-2	(8.39 ± 0.33)E-1	>2.7E-4	>9.0E-2	>3.9E0	--	--
CE-7	Zircaloy	Spacer grid #5	(8.82 ± 0.44)E-2	(7.90 ± 0.32)E-1	>7.8E-4	>1.8E-1	>5.2E0	--	--
CE-6	Zircaloy	Spacer grid #4	(9.36 ± 0.36)E-2	(6.59 ± 0.26)E-1	>2.5E-4	>7.2E-2	>4.0E0	--	--
CE-5	Zircaloy	Spacer grid #3	(1.33 ± 0.07)E-1	(1.82 ± 0.07)E0	>7.1E-4	>1.7E-1	>6.2E0	(1.19 ± 0.23)E-4	(1.40 ± 0.09)E-1
CE-4	Zricaloy	Spacer grid #2	(8.42 ± 0.42)E-2	(8.35 ± 0.33)E-1	>3.5E-4	>6.0E-2	>4.4E0	--	--
CE-3	Zricaloy	Spacer grid #1	(8.46 ± 0.27)E-2	(6.37 ± 0.25)E-1	>2.2E-4	>4.5E-2	>3.2E0	(1.42 ± 0.30)E-4	(1.11 ± 0.68)E-1
CE-2	Inconel	Bottom spacer grid	(3.90 ± 3.02)E-2	(4.18 ± 0.24)E-1	(4.45 ± 0.13)E-4	(1.35 ± 0.04)E-1	(3.71 ± 0.94)E1	(1.00 ± 0.17)E-3	(1.98 ± 0.19)E-1
CE-14	SS	Bottom retention plate	(1.43 ± 0.19)E-2	(2.97 ± 0.08)E-1	(5.77 ± 0.17)E-4	(1.66 ± 0.05)E-1	(4.83 ± 0.38)E1	>1.8E-4	>2.4E-2
CE-1	SS	Bottom end fitting near axial middle	(4.44 ± 0.72)E-3	(1.52 ± 0.06)E-1	(2.32 ± 0.07)E-4	(6.44 ± 0.19)E-2	(2.09 ± 0.31)E1	>2.3E-5	>2.8E-3

(a) Decay corrected to discharge data of 4/17/82.
(b) Parent element is iron (Fe). ^{54}Mn is formed by the fast neutron reaction ^{54}Fe(n,p)^{54}Nm.
(c) Parent element is Nb. ^{93m}Nb is predominantly produced by the reaction ^{03}Nb(n,N')^{93m}Nb.

TABLE 3.7. Radionuclide Concentrations in General Electric Spent Fuel Assembly Hardware Alloys (Cooper Station)

Sample Number	Alloy	Location	Concentration (Ci/g alloy)[a]							
			^{54}Mn[b]	^{55}Fe	^{59}Ni	^{63}Ni	^{60}Co	^{94}Nb	^{93m}Nb[c]	^{125}Sb[d]
GE-19	SS	Tab on handle	(1.10±0.30)E-4	(1.43±0.08)E-2	(3.68±0.55)E-6	(8.01±0.95)E-4	(5.95±0.06)E-4	(7.61±1.26)E-10	(2.49±0.26)E-7	(4.23±1.34)E-6
GE-18	SS	Upper tie plate	(1.15±0.32)E-4	(8.79±0.30)E-3	(5.00±0.68)E-6	(8.86±0.90)E-4	(5.41±0.05)E-4	(3.89±0.63)E-9	(9.04±0.95)E-7	<1.9E-6
GE-17	Inconel	Expansion spring at top of fuel pin)	<9.5E-5	(2.42±0.08)E-3	(4.73±0.68)E-5	(9.48±1.04)E-3	(1.88±0.01)E-3	(5.95±0.99)E-7	(3.98±0.42)E-5	(1.44±0.37)E-5
GE-15	Zircaloy	Spacer grid #7	(3.53±0.95)E-5	(4.41±0.53)E-4	(2.77±0.34)E-7	(3.10±0.27)E-5	(2.42±0.01)E-4	(5.09±1.13)E-9	(2.36±0.25)E-5	(4.16±0.02)E-3
GE-13	Zircaloy	Spacer grid #6	(1.58±0.53)E-4	(2.59±0.08)E-3	(1.07±0.16)E-6	(1.07±0.12)E-4	(1.68±0.01)E-3	--	--	(1.41±0.01)E-3
GE-11	Zircaloy	Spacer grid #5	(1.49±0.49)E-4	(1.87±0.03)E-3	(8.56±1.31)E-7	(8.10±0.19)E-5	(9.20±0.87)E-3	--	--	(1.02±0.01)E-3
GE-9	Zircaloy	Spacer grid #4	(2.14±0.73)E-4	(3.31±0.15)E-3	(9.41±1.31)E-7	(1.39±0.10)E-4	(1.68±0.02)E-3	--	--	(1.81±0.02)E-3
GE-7	Zircaloy	Spacer grid #3	(1.61±0.33)E-4	(3.52±0.21)E-3	(1.35±0.16)E-6	(1.91±0.20)E-4	(7.32±0.07)E-4	(9.14±4.28)E-9	--	(1.72±0.02)E-3
GE-5	Zircaloy	Spacer grid #2	(2.02±0.27)E-4	(2.46±0.08)E-3	(5.45±0.81)E-7	(7.06±1.52)E-5	(4.68±0.02)E-4	--	--	(1.33±0.01)E-3
GE-3	Zircaloy	Spacer grid #1 (starting at bottom)	(1.01±0.20)E-4	(2.55±0.06)E-3	(2.16±0.28)E-7	(2.63±0.31)E-5	(2.28±0.03)E-4	(9.86±1.89)E-9	(1.50±0.16)E-5	(1.22±0.02)E-3
GE-1	SS	Bottom end fitting (near top of casting)	<4.3E-3	(1.35±0.07)E-1	(8.15±1.13)E-5	(7.54±0.76)E-3	(6.24±0.07)E-2	(7.97±1.35)E-8	(6.86±0.72)E-6	<1.7E-4
GE-2	SS	Bottom end fitting (near nozzle end)	<5.8E-4	(1.27±0.09)E-2	(1.14±0.13)E-5	(1.28±0.13)E-3	(7.03±0.07)E-3	(6.04±0.99)E-9	(4.84±0.51)E-7	<2.3E-5

(a) Decay corrected to discharge data of 5/1/82.
(b) Parent element is Fe. ^{54}Mn is produced by the fast neutron reaction ^{54}Fe(n,p)^{54}Mn.
(c) Parent element is Nb. ^{93m}Nb is produced by the reaction ^{93}Nb(n,n')^{93m}Nb.
(d) Parent element is Sn. ^{125}Sb is produced by the reaction ^{124}Sn(n,γ)^{125}Sn, followed by beta decay to ^{125}Sb.

3.31

TABLE 3.8. Elemental Concentrations in General Electric Spent Fuel Assembly Hardware Alloys (Cooper Station)

Sample Number	Alloy	Location	Concentration--Weight Percent									
			Mn	Fe	Cr	Ni	Co	Nb	Sn	Cu	Mo	Zr
GE-19	SS	Tab on handle	0.058±0.02	68.3±2.1	19.3±0.1	8.38±0.25	0.026±0.004	0.001±0.00067	<0.22	0.013±0.002	<0.007	<0.004
GE-18	SS	Upper tie plate (at base where fuel pin touches)	0.56±0.02	67.6±2.0	19.0±0.1	8.26±0.25	0.025±0.005	0.00074±0.00016	<0.21	0.009±0.002	<0.006	<0.003
GE-17	Inconel	Expansion spring (at top of fuel pin)	0.070±0.003	6.04±0.18	13.2±0.4	68.2±2.0	0.050±0.008	0.81±0.001	<0.26	0.027±0.003	0.049±0.007	0.094±0.009
GE-15	Zircaloy	Spacer grid #7	0.011±0.005	0.47±0.01	0.14±0.02	0.072±0.011	<0.006	0.0051±0.0032	1.09±0.18	<0.004	0.072±0.011	93.1±2.8
GE-13	Zircaloy	Spacer grid #6	0.02±0.006	0.43±0.02	0.14±0.02	0.083±0.012	<0.007	--	1.13±0.20	<0.005	0.083±0.012	96.5±2.9
GE-11	Zircaloy	Spacer grid #5	0.013±0.005	0.45±0.01	0.10±0.02	0.066±0.010	<0.006	--	0.86±0.17	<0.004	<0.02	72.3±2.2
GE-9	Zircaloy	Spacer grid #4	0.02±0.005	0.62±0.02	0.14±0.02	0.088±0.013	<0.007	--	1.09±0.20	<0.005	0.03±0.02	94.9±2.8
GE-7	Zircaloy	Spacer grid #3	0.009±0.005	0.47±0.02	0.13±0.02	0.040±0.009	<0.006	0.020±0.003	1.10±0.20	<0.005	<0.02	95.6±2.9
GE-5	Zircaloy	Spacer grid #2	0.01±0.005	0.55±0.02	0.13±0.02	0.043±0.009	<0.007	--	1.06±0.20	<0.004	<0.02	94.3±2.8
GE-3	Zircaloy	Spacer grid #1 (starting at bottom)	0.008±0.004	0.56±0.02	0.12±0.01	0.030±0.010	<0.007	0.018±0.003	1.10±0.22	<0.003	0.02±0.02	92.4±2.8
GE-1	SS	Bottom end fitting (near top of casting)	1.01±0.03	69.2±2.0	17.5±0.5	8.68±0.26	0.21±0.02	0.037±0.011	<0.3	0.28±0.01	0.37±0.03	0.006±0.003
GE-2	SS	Bottom end fitting (near nozzle end)	1.03±0.03	69.1±2.0	17.4±0.5	8.75±0.26	0.207±0.02	0.018±0.003	<0.2	0.29±0.01	0.87±0.004	<0.003

TABLE 3.9. Specific Activities of Long-Lived Radionuclides in General Electric Spent Fuel Assembly Hardware Alloys (Cooper Station)

Sample Number	Alloy	Location	Concentration (Ci/g parent element)[a]							
			^{54}Mn[b]	^{55}Fe	^{59}Ni	^{63}Ni	^{60}Co	^{94}Nb	^{93m}Nb[c]	^{125}Sb[d]
GE-19	SS	Tab on handle	(1.61±0.44)E-4	(2.08±0.11)E-2	(4.39±0.66)E-5	(9.55±1.13)E-3	(2.39±0.36)E0	(7.61±5.09)E-5	(2.49±1.66)E-2	--
GE-18	SS	Upper tie plate	(1.70±0.47)E-4	(1.30±0.05)E-2	(6.04±0.82)E-5	(1.07±0.11)E-2	(2.16±0.43)E0	(5.27±1.13)E-4	(1.23±0.27)E-1	--
GE-17	Inconel	Expansion spring	<1.6E-3	(4.00±0.14)E-2	(6.94±0.99)E-5	(1.39±0.15)E-2	(3.77±0.60)E0	(3.77±0.60)E-5	(4.92±0.49)E-3	<5.5E-3
GE-15	Zircaloy	Spacer grid #7	(7.51±2.02)E-3	(1.79±0.04)E-1	(3.85±0.59)E-4	(4.31±0.66)E-2	<3.4E0	(1.00±0.63)E-4	(4.62±2.90)E-1	(3.81±0.63)E-1
GE-13	Zircaloy	Spacer grid #6	(3.67±1.23)E-2	(6.03±0.28)E-1	(1.29±0.19)E-3	(1.29±0.19)E-1	<1.8E1	--	--	(1.24±0.22)E-1
GE-11	Zircaloy	Spacer grid #5	(3.31±1.04)E-2	(4.16±0.09)E-1	(1.30±0.20)E-3	(1.23±0.19)E-1	<1.3E1	--	--	(1.18±0.24)E-1
GE-9	Zircaloy	Spacer grid #4	(3.45±1.18)E-2	(5.34±0.17)E-1	(1.07±0.16)E-3	(1.58±0.23)E-1	<2.4E1	--	--	(1.65±0.30)E-1
GE-7	Zircaloy	Spacer grid #3	(3.43±0.70)E-2	(7.50±0.32)E-1	(3.38±0.71)E-3	(4.78±1.08)E-1	<1.0E1	(4.59±2.16)E-5	--	(1.56±0.28)E-1
GE-5	Zircaloy	Spacer grid #2	(3.67±0.49)E-2	(4.48±0.16)E-1	(1.27±0.27)E-3	(1.64±0.34)E-1	<6.7E0	--	--	(1.26±0.24)E-1
GE-3	Zircaloy	Spacer grid #1	(1.80±0.36)E-2	(4.55±0.16)E-1	(7.20±2.38)E-4	(8.77±2.89)E-2	<3.3E0	(5.45±1.04)E-5	(8.32±1.39)E-2	(1.11±0.22)E-1
GE-1	SS	Bottom end fitting	<6.2E-3	(1.92±0.10)E-1	(9.39±1.30)E-4	(8.69±0.87)E-2	(2.97±0.30)E1	(2.15±0.64)E-4	(1.85±0.55)E-2	<5.8E-2
GE-2	SS	Bottom end fitting	<8.4E-4	(1.83±0.12)E-2	(1.30±0.15)E-4	(1.46±0.15(#-2	(3.50±0.35)E0	(3.35±0.56)E-5	(2.69±0.45)E-3	<1.1E-2

(a) Decay corrected to discharge data of 5/1/82.
(b) Parent element is Fe. ^{54}Mn is produced by the fast neutron reaction ^{54}Fe(n,p)^{54}Mn.
(c) Parent element is Nb. ^{93m}Nb is produced by the raction ^{93}Nb(n,n')^{93m}Nb.
(d) Parent element is Sn. ^{125}Sb is produced by the reaction ^{124}Sn(n,γ)^{125}Sn, followed by beta decay to ^{125}Sb.

3.33

4.0 CALCULATIONS

4.1 INTRODUCTION

The process of calculating the radionuclide concentration in the activated metal is two-fold. The first step is to calculate a core average inventory based on the irradiation history of the samples using the ORIGEN2 code. Since the results of the ORIGEN2 calculations are valid for an average over the cores' fueled region only, adjustments need to be made if the results are to be applied to metals that are activated outside the fueled region. In the core, the flux varies depending upon location. The flux is near its peak in the center of the fueled region, and drops off closer to the edge of the fueled region. Axially up a single assembly, the flux can vary ±20% from the average. This means that the activation in a sample from the fueled region can vary ±20% from the core average, based on the flux level alone. If the samples are activated outside the fueled region, the change from the core average will be greater. Adjustment factors are calculated using ANISN. These factors are then applied to the core average values from ORIGEN2 to produce the calculated radionuclide concentrations.

4.2 ACTIVATION CALCULATION

4.2.1 Description

The ORIGEN2 computer code is a widely used tool for estimating the radionuclide inventory of irradiated materials. The code is an extremely useful tool due to its capability to track a large number of isotopes through user-specified irradiation and decay time steps. It calculates the depletion and creation of isotopes as a function of time.

ORIGEN2 requires the user to describe the initial composition of the materials to be irradiated, the irradiation history, and to specify the nuclear data libraries that the code uses to perform calculations. These libraries are supplied with the code by the Radiation Shielding Information Center (RSIC). The list of available libraries consists of many reactor

types, including PWRs and BWRs. These libraries contain, in addition to half-lives and decay data, one-group cross sections.

For the ORIGEN2 calculations, the standard PWR and BWR libraries were used. The irradiation histories specified in Tables 3.2 to 3.4 with appropriate decay times were modeled. For each of the radionuclides of interest, the irradiation of 1 gram of the parent element was modeled. ORIGEN2 outputs a table of radionuclides resulting from the irradiation of that gram of material, in units of curies. An example is the irradiation of 1 gram of cobalt, and the resultant number of curies of ^{60}Co. ORIGEN2 calculates the production of ^{60}Co due to activation of the initial elemental cobalt, and accounts for the depletion of the initial ^{59}Co due to its transformation to ^{60}Co, as well as the removal due to decay and burnup after its creation. The curies of ^{60}Co after irradiation per initial gram of elemental cobalt can then be compared with the sample data, and is independent of the amount of cobalt initially in each sample, which varies from sample to sample. ORIGEN2 calculations were done for each of the PNL fuel assemblies, as well as the INEL and BCL fuel assemblies. The latter assemblies are discussed in Section 5.0.

4.2.2 Results

The results of the ORIGEN2 calculations are presented in Table 4.1. The radionuclide concentrations per gram of parent element calculated are the concentrations that would be expected if the parent material was uniformly mixed throughout the fueled region. In order to be useful for comparison with the samples, sample specific values had to be calculated, based on the core average value and the samples location with respect to the core.

4.3 FLUX CALCULATION

4.3.1 Description

The spectrum-averaged, cross section values in the ORIGEN2 libraries were computed using detailed reactor core models used in calculating activation in the fueled region of similar reactor cores. Cross section sets are available for a variety of reactor types, but all are applicable only to

TABLE 4.1. ORIGEN2 Results at Time of Discharge
(curies per gm parent)

Radionuclide	PNL W(a) 14x14	PNL CE(b) 14x14	PNL GE(c) 7x7	INEL W 15x15	BCL W 15x15
^{14}C/gm N	1.959E-2	2.40E-2	1.776E-2	2.52E-2	1.38E-2
^{59}Ni/gm Ni	5.32E-4	5.40E-4	4.345E-4	6.56E-4	3.91E-4
^{63}Ni/gm Ni	7.18E-2	8.61E-2	6.474E-2	9.18E-2	5.18E-2
^{94}Nb/gm Nb	1.79E-3	2.51E-3	1.679E-3	2.26E-3	1.28E-3
^{60}Co/gm Co	9.00E+1	1.15E+2	6.391E+1	1.28E+2	7.9E+1
^{55}Fe/gm Fe	4.039E-1	5.209E-1	2.343E-1	6.514E-1	4.155E-1
^{99}Tc/gm Mo	2.72E-6	3.87E-6	1.138E-5	3.38E-6	1.97E-6
^{54}Mn/gm Fe	4.05E-2	7.09E-2	1.621E-2	9.114E-2	6.814E-2

(a) Westinghouse.
(b) Combustion Engineering.
(c) General Electric.

the fueled region of the specified reactor core. When the neutron spectrum
varies significantly from that used in the reactor model, either a new one-
group cross section is required or an adjustment must be made to the ORIGEN2
results. Much of the hardware that is of interest in this study is in the
region of the end fittings, which is outside the cores active fuel region.
The neutron spectrum in the end fitting region is changed quite a bit from
the fueled region. No fissions are occurring in this region, so as the fast
neutrons are thermalized (reduced in energy), the average neutron energy
decreases. From Figure 4.1(a), it can be seen that the ^{59}Co (n,γ) cross
section generally increases with decreasing neutron energy. Therefore, it
would be expected that the one-group, spectrum-averaged cross section in the
end fitting region would increase compared to its value in the core region.
This change must be calculated accurately to estimate the amount of ^{60}Co
present in the end fittings. This effect is also seen in all of the isotopes
of interest.

The one-group cross sections used in the data libraries are developed
from rigorous multigroup calculations for the individual reactor models. In
multigroup calculations, the neutron spectrum is divided into energy groups
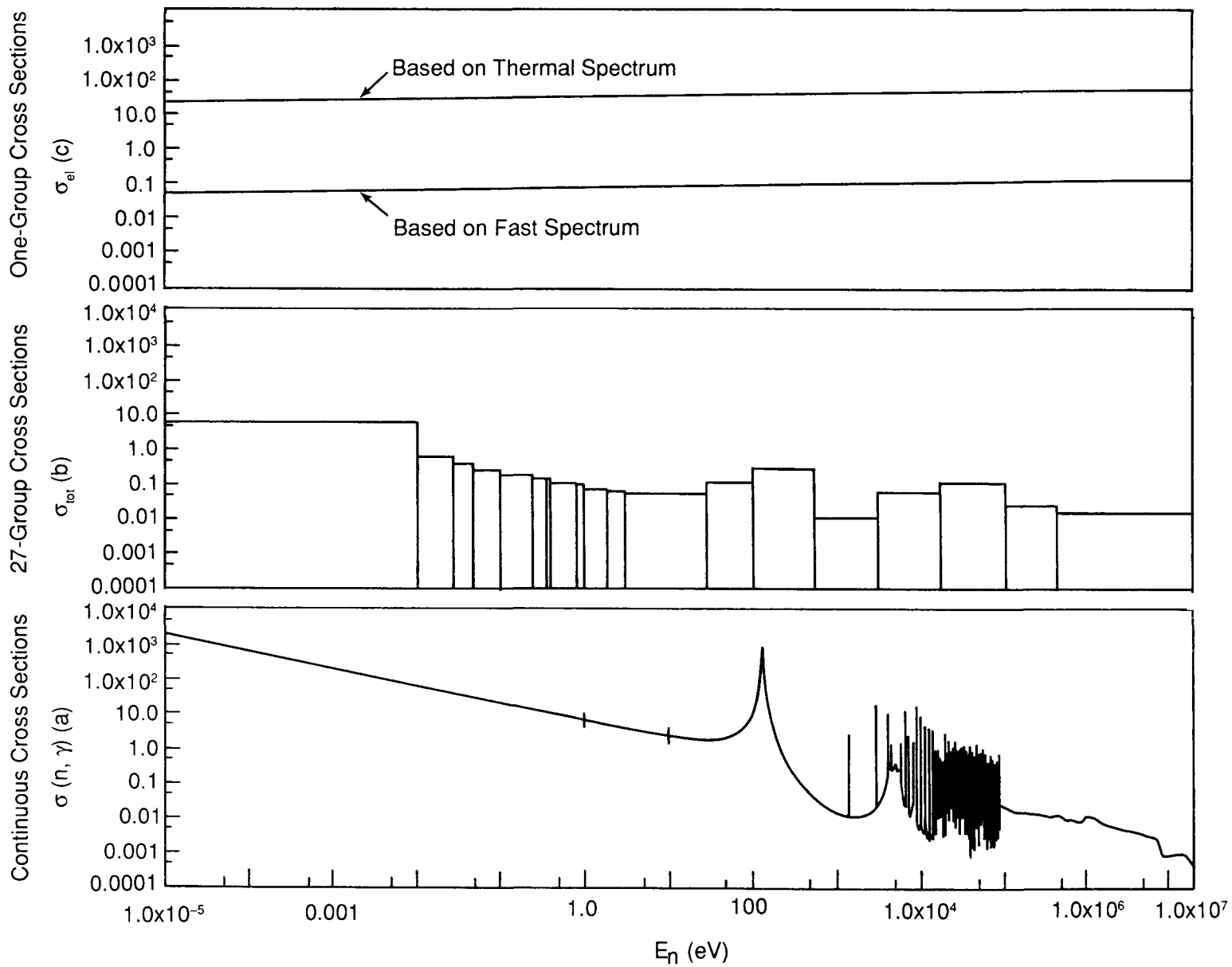
FIGURE 4.1. $^{59}Co(n,\gamma)$ ^{60}Co Cross Sections

and the calculations are performed on a group basis. The scattering between the groups is taken into account within the calculation. The multigroup method is necessary for many problems, such as in the reactor core, because the cross sections (which are a measure of the probability of reaction occurring) vary considerably with neutron energy.

As an example, the continuous cross section for the activation of natural cobalt to ^{60}Co [^{59}Co (n,γ) ^{60}Co] [Figure 4.1(a)] has a value of ~37 barns for thermal neutrons (0.0253 eV). For fission neutrons, which are in the range of 1-10 MeV, the cross section is less than 0.01 barns, four orders of magnitude less than the thermal cross section (~37 barns at 0.0253 thermal). For neutrons with energies just over 100.0 eV, the cross section has a resonance of nearly 1000.0 barns. It should be apparent that in order to correctly estimate the total ^{59}Co(n,γ) reaction rate over the entire neutron spectrum (i.e., the total ^{60}Co production rate) the energy dependence of the neutrons must be taken into account.

One approach is to perform a multigroup transport calculation (other techniques exist as well). The continuous cross section is divided into a finite number of groups, and a single value for the cross section is determined for each group. The specific energy group divisions are based on how the cross sections vary with neutron energy. Figure 4.1(b) a 27-group structure for the ^{59}Co (n,γ) cross section. With a large enough number of groups the average value of the cross section within an energy group is a reasonable representation of the continuous cross section value.

Another consideration is that the neutron energy distribution affects the choice of the energy group structure for determination of the cross section values. For example, if all the neutrons are above 1.0 MeV (fast spectrum), then a single value representing the one-group cross section would be determined by the continuous cross section above 1.0 MeV. Alternately, if all the neutrons were less than 1.0 eV (thermal spectrum), the single value representing the cross section would be determined by the continuous cross section below 1.0 eV. This would result in significantly different values. The values are referred to as the one-group cross sections. Figure 4.1(c) illustrates what the one-group cross sections might look like for the two

examples given. In most applications however, the neutrons have a wide range of energies, and the one-group cross sections would not vary as much as in the two examples given. However, the cross sections must be appropriately weighted in order to account for differences in the neutron spectrum, that affect the one-group cross section.

To calculate a one-group cross section, it is first necessary to perform a multigroup calculation. A neutronic model is developed that represents the reactor core of interest and an appropriate multigroup cross section library is selected. Once a group structure is defined, all the cross sections used in that calculation must have the same energy group structure. Then the multigroup calculation is performed, and the multi-group reaction rate and flux can be summed over all energy groups to provide the total reaction rate and total flux. The total flux can then be divided into the total reaction rate, resulting in a one-group cross section. By definition, the resultant one-group cross section is the number, which when multiplied by the total flux, gives the correct total reaction rate. This one-group cross section can now be used in subsequent calculations to multiply by the total flux, in order to estimate the total reaction rate, if the neutron spectrum does not change significantly. However, as discussed before, the spectrum does change upon leaving the fueled region, and in fact, changes within the fueled region itself. The changes within the fuel region are not significant from an activation perspective, but are significant outside the core.

The neutronics calculations described in Volumes 2 and 3 of this report estimate the relative change for a variety of one-group cross sections in both PWRs and BWRs. Three PWR models were generated to determine the change in the one-group cross sections for various fuel designs. A representative model was generated for each of the major PWR vendors: Westinghouse, Babcock and Wilcox, and Combustion Engineering. A single BWR model for General Electric was generated.

The fuel assembly models used for each of the three sets of PWR calculations are detailed in Volume 2. Each reactor was modeled from below the fuel assembly to above it. The model extended beyond the ends of the fuel to account for backscatter from the fuel assembly regions. The fueled regions

4.6

were modeled in great detail. Volumes 2 and 3 describe these models in detail, and provide a great deal of information about the fuel assemblies.

These fuel assemblies are representative of the types of the spent fuel that must be accommodated by the Federal Waste Management System and many utilities. They are representative both in their irradiation history and material composition. Other fuel configurations by the same manufacturers are neutronically similar to those sampled. There is little difference, neutronically, between the three reactor vendors. The main difference lies in the structural makeup of the core. The structural material has a lesser effect on the neutron flux in the fueled region. Outside the fueled region, the structural material has a much greater effect on the flux. The presence of the parent isotope, (i.e., ^{59}Co) has little effect on the reaction rate per unit mass of that isotope, within the ranges that exist in reactors. This can be seen in the one-group cross sections described in Volumes 2 and 3. There is little change in them throughout the fuel region, even at the grid spacer locations. The effect becomes pronounced outside the fueled region. However, the absolute amount of the parent isotope does affect the amount of radionuclide (i.e., ^{60}Co) that is produced.

Volumes 2 and 3 provide a detailed description of how the neutronics calculations were performed. They document the input streams for the computer programs used in the neutronics analysis. Volumes 2 and 3 should be of particular interest to those individuals reviewing the calculations in detail. It requires that the reader have a background in nuclear engineering and be somewhat familiar with the computer codes involved.

4.3.2 Results

Table 4.1 gives the predicted core average concentrations of a number of activation products for all of the assemblies from which samples were available. The units are curies of radionuclide per initial gram of parent isotope. These are for the core average and must be multiplied by the appropriate scaling factors for a comparison with sample measurements. This is discussed in Section 5.0.

5.0 COMPARISON--EXPERIMENTAL VERSUS CALCULATION

5.1 DISCUSSION

Based on the ORIGEN2 calculations described in Section 4.0 and the ANISN calculations described in Volume 2, predicted activation levels were determined for the specific locations of the samples. The predicted levels were then compared with the measured values. Figures 5.1 through 5.14 show a comparison of the sample analysis with the predictive calculations.

In addition to the sample results described in Section 3.0, there were two additional sources of data available. These were the fuel assemblies identified at the beginning of Section 2.0. BCL published a report under ESEERCO, the Empire State Electrical Energy Research COrporation. Their report detailed the results of their laboratory analysis of a Westinghouse 14x14 standard fuel assembly from the Ginna plant, owned by Rochester Gas and Electric (ESEERCO 1987). Their report presented the results of both elemental and radionuclide analysis of the samples. These results are shown on Figures 5.15 through 5.19. Also shown on those figures are the results of predicted calculations that were done in a similar manner to those described for our work and a comparison of calculations and measurements. Of course the irradiation history was modified to reflect the actual history of their fuel. A similar though less extensive set of data was acquired from INEL for a Westinghouse 15x15 fuel assembly. The results of their analysis and a comparison to predictive calculations are given in Figures 5.20 through 5.24.

5.2 ANALYSIS

The overall comparison of the measurements to the calculations varies. The ^{60}Co comparisons are in reasonable agreement, though we had expected them to be closer, apriori. The two nickel isotopes, ^{59}Ni and ^{63}Ni, are quite a bit off. The comparison is quite good in the fueled region, but at the end fittings, the comparisons diverge. This was not unexpected, since the cross sections for the generation of ^{60}Co are better known than those for the generation of ^{59}Ni and ^{63}Ni. There are no ^{58}Ni(n,γ) or ^{62}Ni(n,γ) cross sections available, only natural nickel(n,γ). Accounting for the difference in the
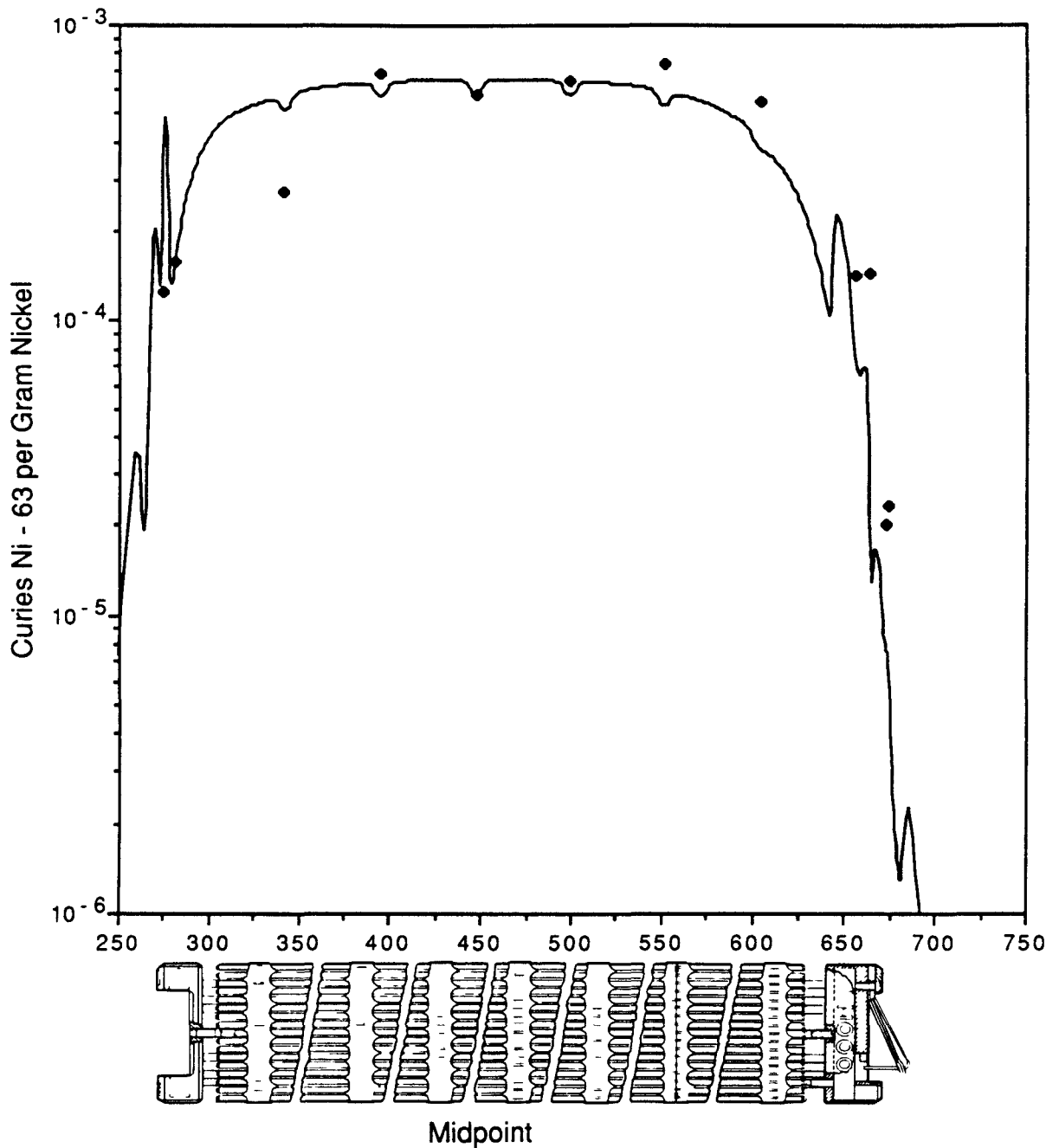
FIGURE 5.1. Westinghouse ⁶³Ni Measurements Versus Calculation

thermal cross section was thought to be enough and that differences in the epithermal and fast regions would be negligible. However, the magnitude of the difference between measurements and the calculations indicates otherwise.

The most likely source of the large differences between measured and calculated activations is the inability of the one-dimensional calculations

5.2
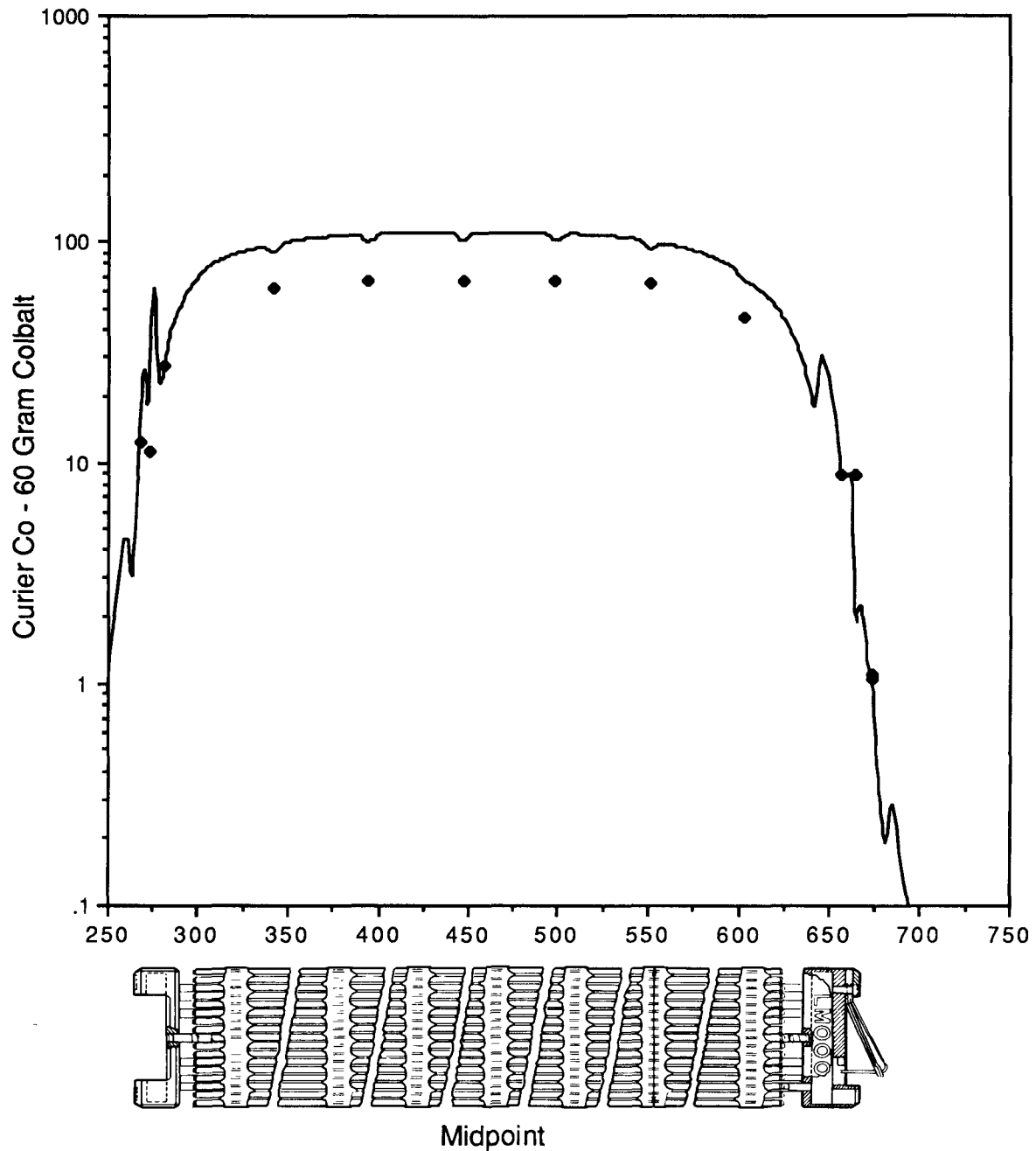
FIGURE 5.2. Westinghouse ^{60}Co Measurements Versus Calculation

to represent structural details in the x-y plane. The effects of neutron streaming up the gas plenum, and the influence on the detailed thermal flux shape caused by penetrations of the upper and lower end fittings by coolant channels are not represented by the one-dimensional ANISN calculation. The

5.3
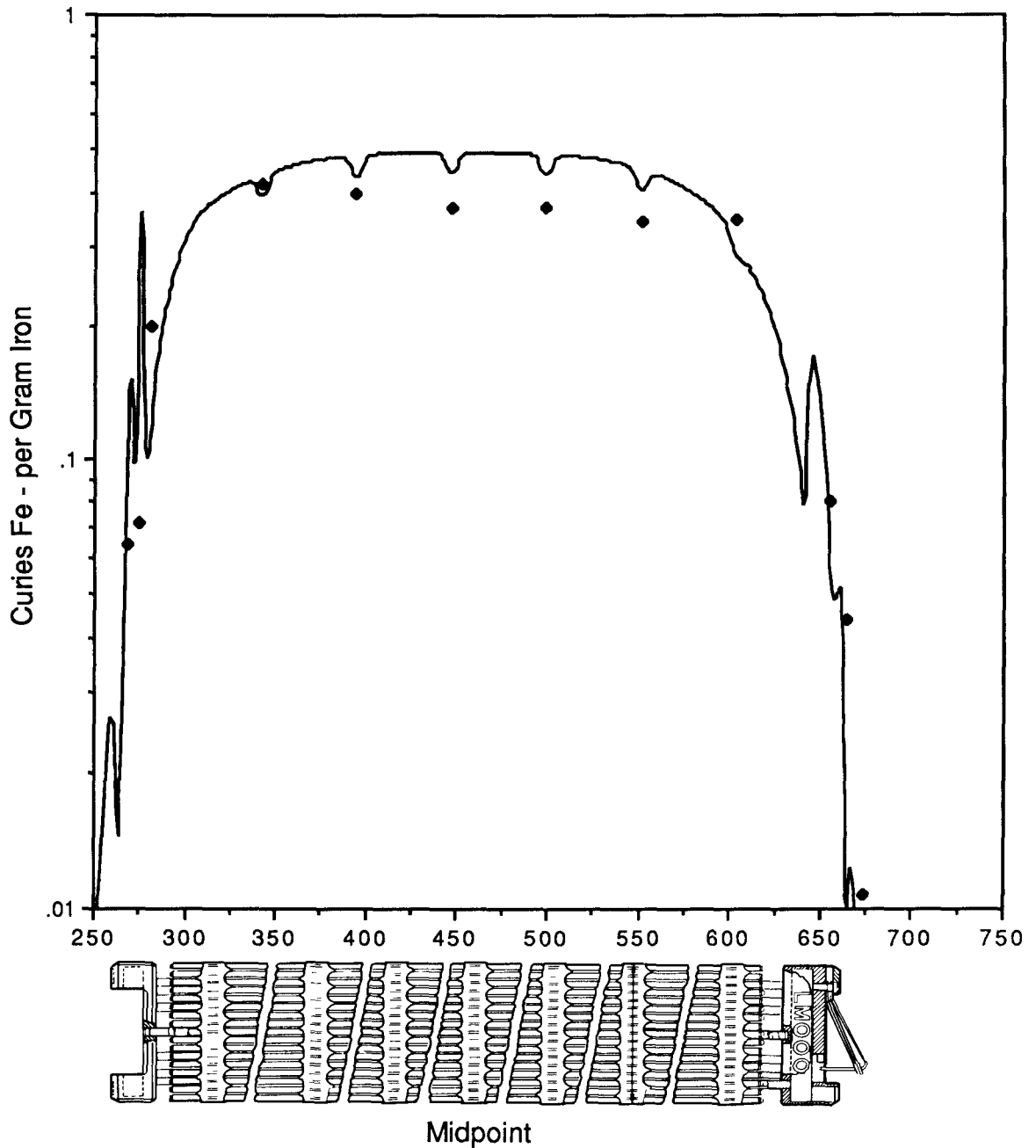
FIGURE 5.3. Westinghouse ^{55}Fe Measurements Versus Calculation

ANISN model homogenizes completely the discrete rods of B$_4$C control rod material above the fueled region. To investigate the effects of lost spatial detail, a series of three-dimensional Monte Carlo calculations were performed, and while there was some indication of streaming, the calculations were not conclusive. The differences between measure and calculated
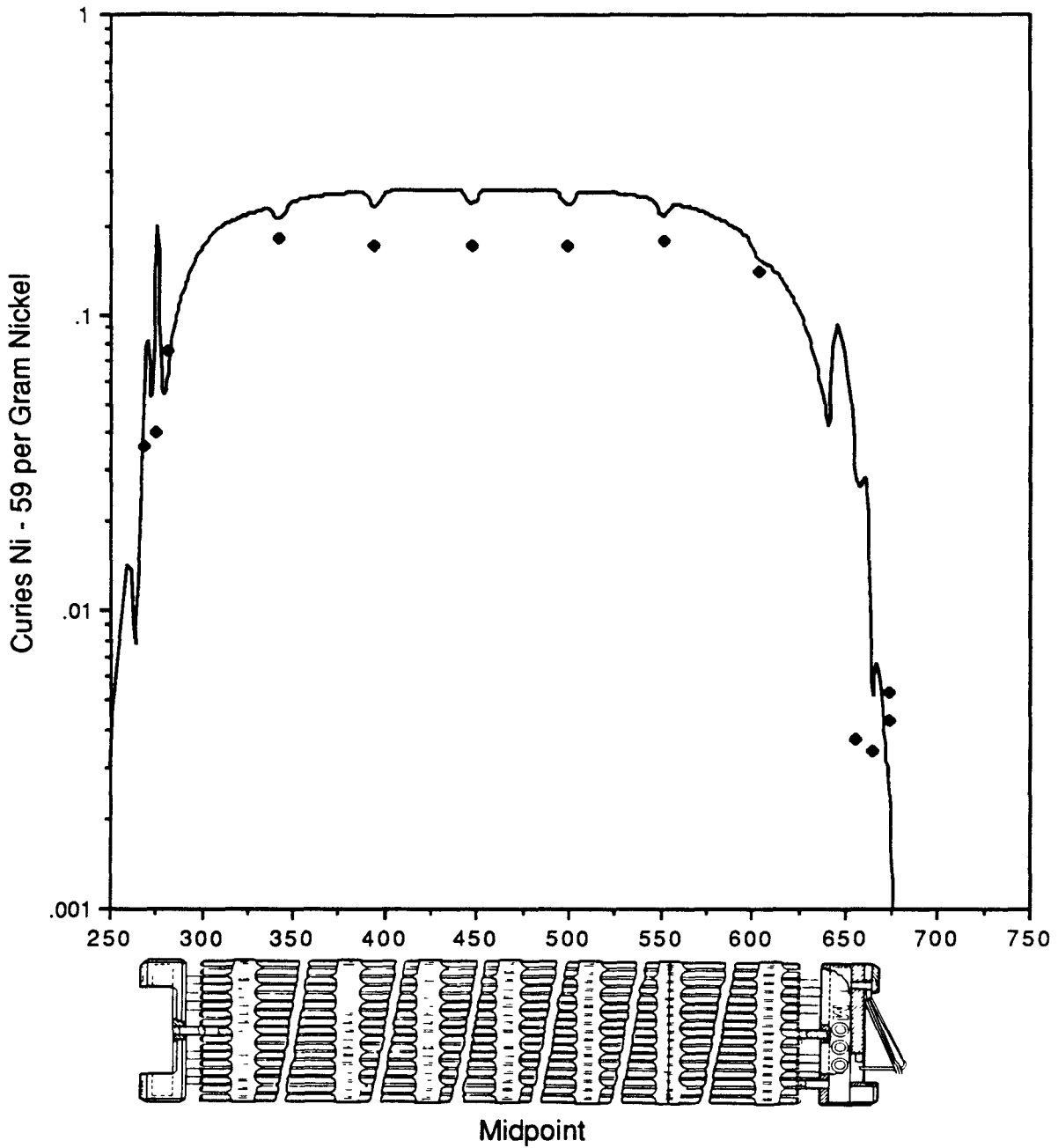
FIGURE 5.4. Westinghouse ^{59}Ni Measurements Versus Calculation

activations point directly to the need for including more spacial detail in calculations of the neutron flux above and below the fueled region of the core.

Curies Co-60 per g Cobalt		
Calculated	Measured	Measured/Calculated
8.780E-1	1.04E0	1.185E0
1.017E0	1.09E0	1.072E0
3.033E0	8.72E0	2.875E0
9.990E0	8.85E0	8.860E-1
6.642E1	4.57E1	6.880E-1
8.460E1	6.49E1	7.670E-1
1.008E1	6.73E1	6.680E-1
9.999E1	6.73E1	6.730E-1
9.036E1	6.18E1	6.840E-1
2.556E1	2.75E1	1.076E0
2.691E1	1.11E1	4.120E-1
1.737E1	1.24E1	7.140E-1
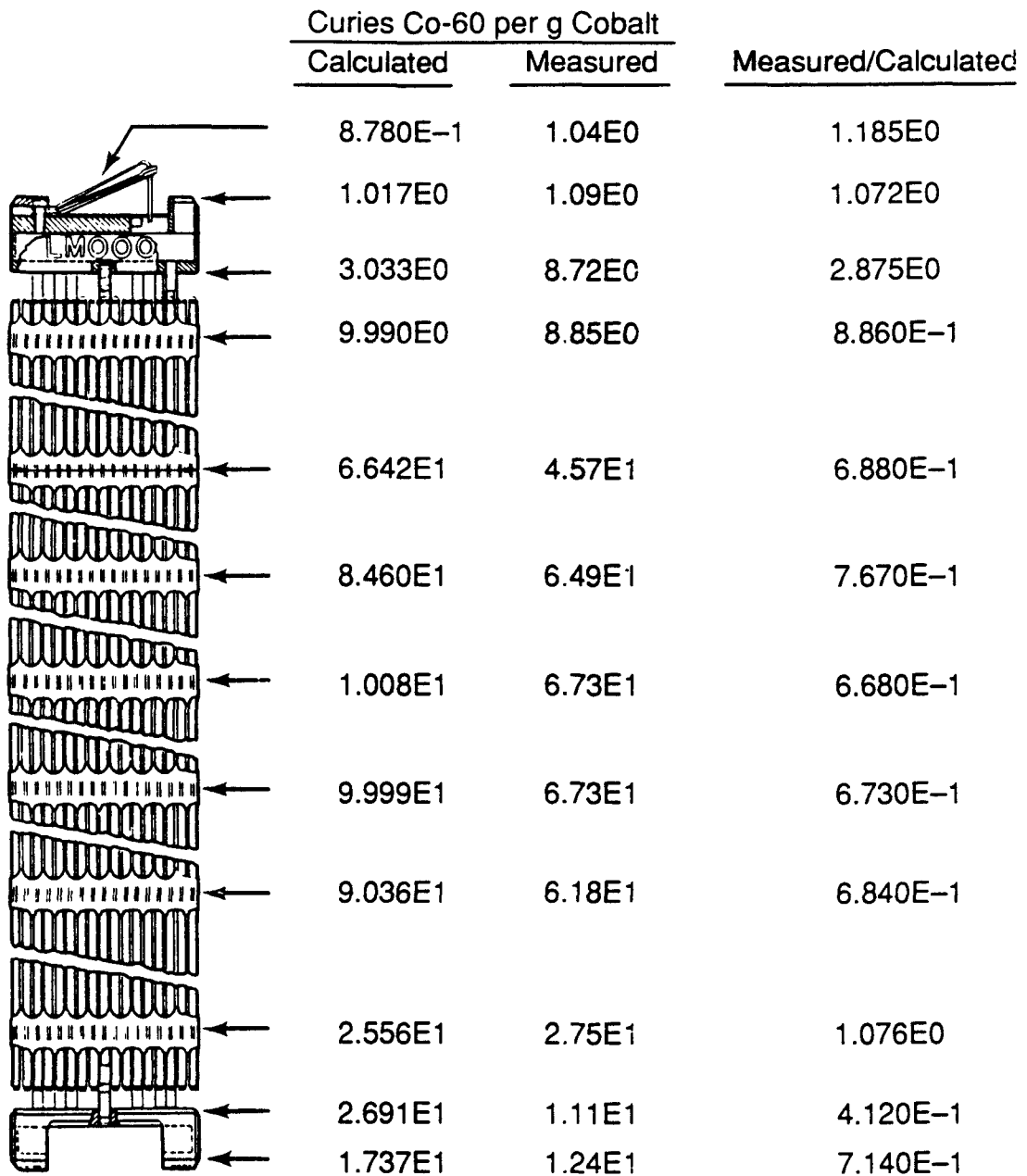
FIGURE 5.5. Westinghouse 14x14 (^{60}Co)

5.3 SCALING FACTORS

Because of the inability of the calculations to predict the measured activation it was decided to generate scaling factors based on the sample data alone. These factors are to be applied to ORIGEN2 calculations accounting for the differences in the neutron flux in the core compared to the outside of the core.

Curies Fe-55 per g Iron

Calculated	Measured	Measured/Calculated
4.93E-3	1.07E-2	2.170E0
5.69E-3	5.43E-3	9.540E-1
1.63E-2	4.41E-2	2.706E0
5.61E-2	8.06E-2	1.437E0
0.291	3.49E-1	1.199E0
0.41	3.46E-1	8.440E-1
0.443	3.69E-1	8.330E-1
0.439	3.98E-1	9.070E-1
0.397	4.19E-1	1.055E0
0.111	1.99E-1	1.793E0
0.147	7.25E-2	4.930E-1
0.101	6.48E-2	6.420E-1
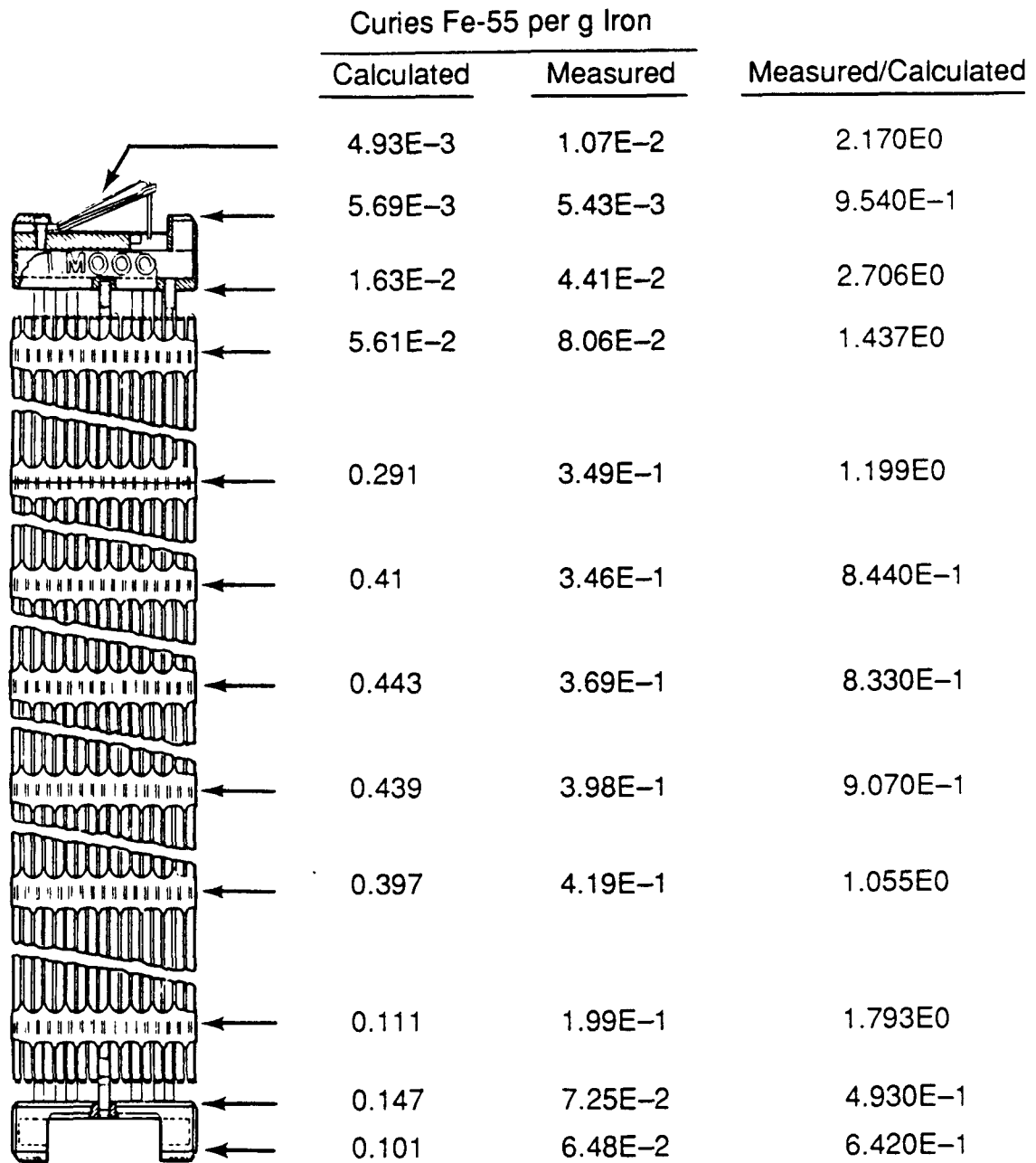
FIGURE 5.6. Westinghouse 14x14 (^{55}Fe)

Initially, we intended to develop separate scaling factors for each radionuclide. This turned out to be unsuccessful because the level of uncertainty in many of the measurements did not allow this detail with any great measure of confidence. Other concerns came up such as how to evaluate ^{60}Co. One set of data was available from the PNL sample analysis and another from

Curies Ni-59 per g Nickel		
Calculated	Measured	Measured/Calculated
2.16E−6	2.32E−5	1.074E1
2.50E−6	2.01E−5	8.040E0
8.77E−6	1.44E−4	1.642E1
2.36E−5	1.42E−4	6.017E0
4.12E−4	5.48E−4	1.330E0
5.74E−4	7.29E−4	1.270E0
6.21E−4	6.44E−4	1.037E0
6.16E−4	5.86E−4	9.510E−1
5.57E−4	6.81E −4	1.223E0
1.62E−4	2.74E−4	1.691E0
7.13E−5	1.58E−4	2.216E0
3.17E−5	1.26E−4	3.975E0
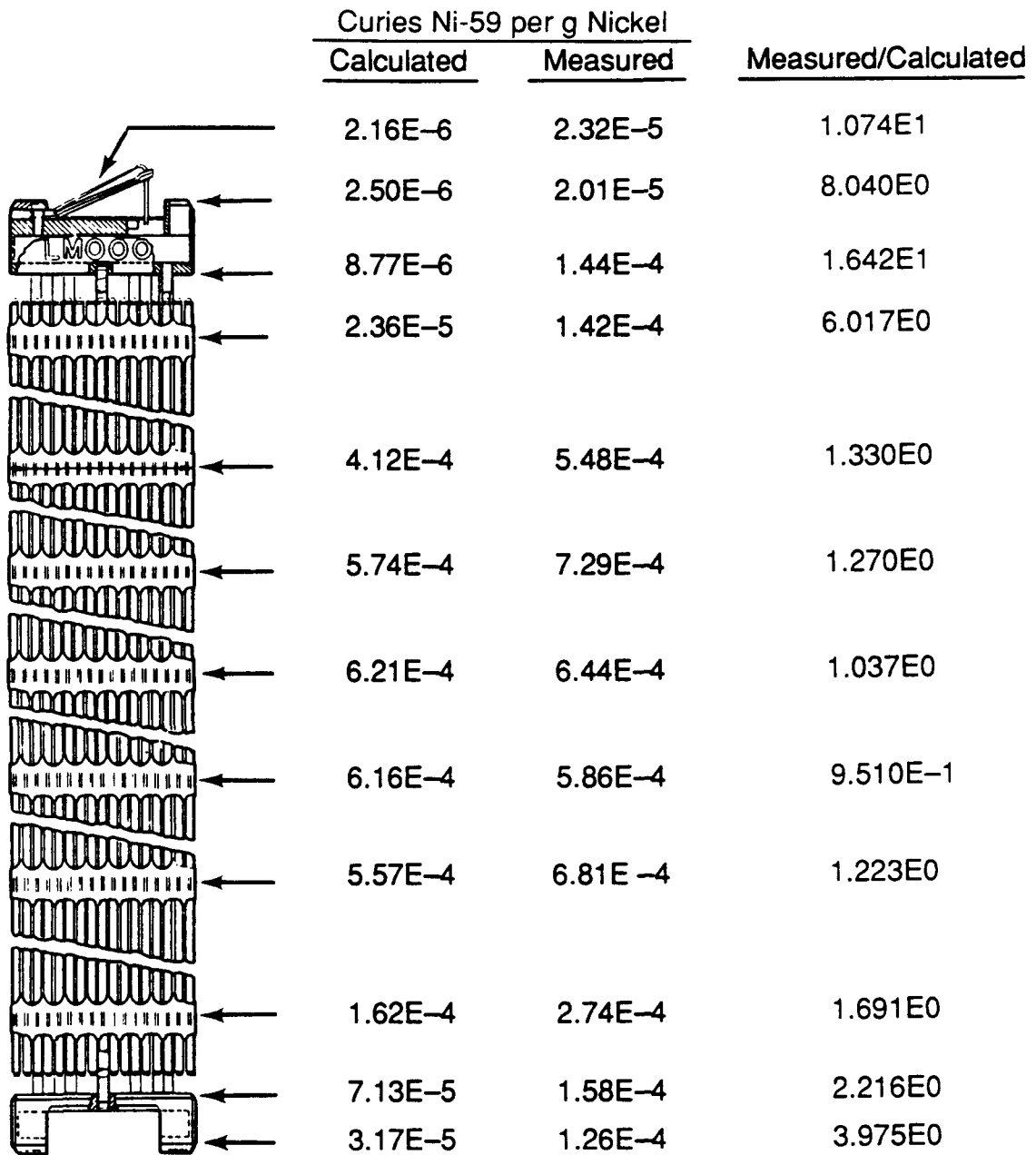
FIGURE 5.7. Westinghouse 14x14 (^{59}Ni)

BCL. The PNL data indicated that in the fueled region, ORIGEN2 was overpre-dicting the average reaction rate while the BCL data indicated the opposite. After looking at the data in a variety of ways, two patterns generally evolved. They were:

Curies Ni-63 per g Nickel		
Calculated	Measured	Measured/Calculated
2.92E–4	5.30E–3	1.815E1
3.37E–4	4.25E–3	1.261E1
1.18E–3	3.35E–2	2.839E1
3.19E–3	3.70E–2	1.160E1
5.56E–2	1.40E–1	2.518E0
7.75E–2	1.77E–1	2.284E0
8.38E–2	1.73E–1	2.064E0
8.31E–2	170E–1	2.046E0
7.52E–2	1.81E–1	2.407E0
2.18E–2	7.59E–2	3.4821E0
9.62E–3	4.01E–2	4.168E0
4.28E–3	3.59E–2	8.388E0
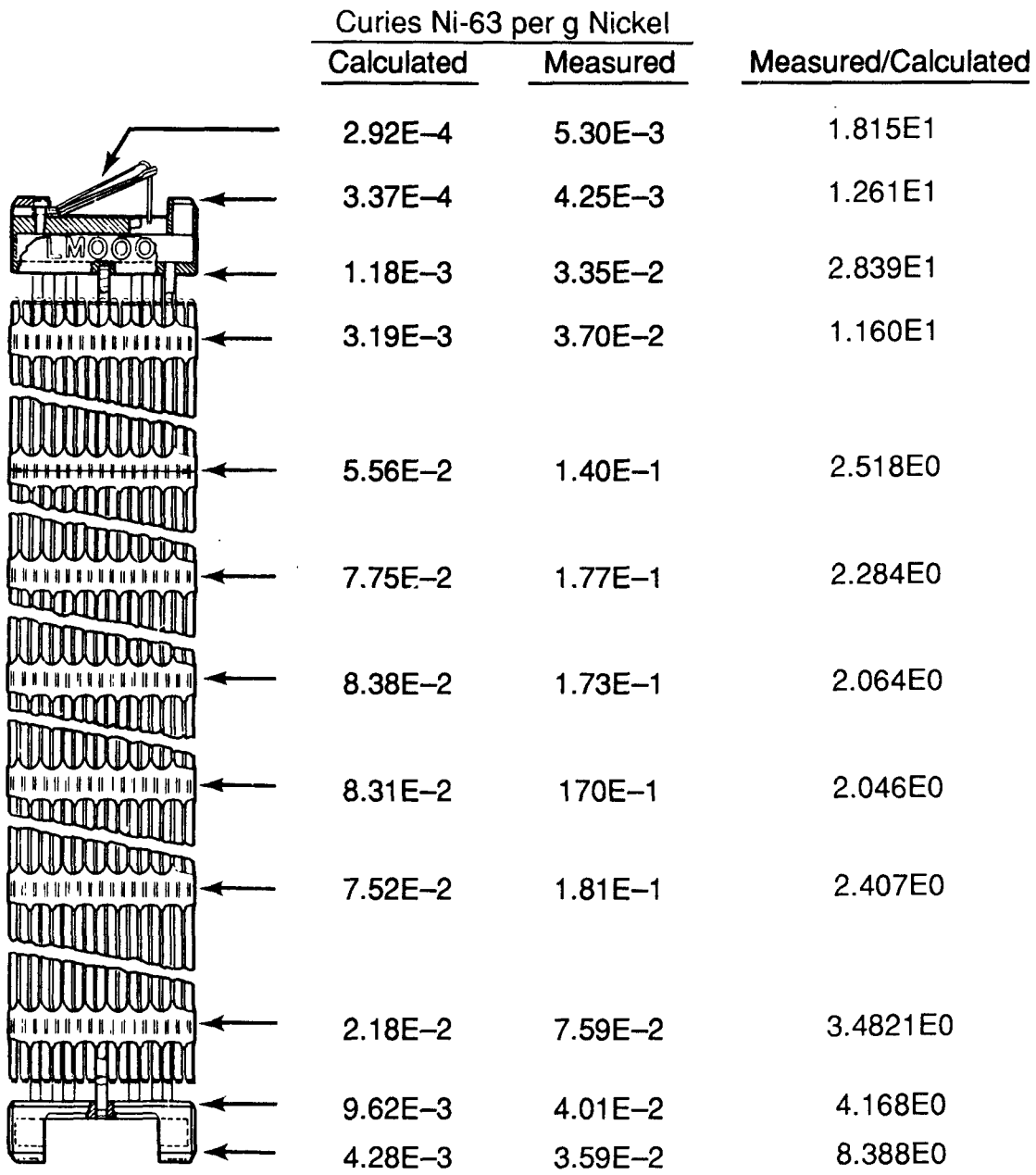
FIGURE 5.8. Westinghouse 14x14 (^{63}Ni)

- a consistency between the activation rates of many of the radionuclides at individual sample locations

- a similarity in the way the activation rates dropped off outside the fueled region.

The consistency of the activation rates can most readily be seen in Figures 5.25 through 5.36. These are plots of one radionuclide against another,

Curies Nb-94 per g Niobium		
Calculated[+]	Measured	Measured/Calculated
1.11E–5	1.64E–5	1.477E0
1.29E–5	1.24E–5	9.610E–1
4.19E–5	7.20E–5	1.718E0
1.43E–4	1.59E–4	1.112E0
1.37E–3	---	---
1.91E–3	---	---
2.06E–3	2.61E–3	1.267E0
2.05E–3	---	---
1.85E–3	---	---
5.28E–4	9.01E–4	1.706E0
3.57E–4	2.20E–5	6.200E–2
1.96E–4	1.32E–4	6.730E–1
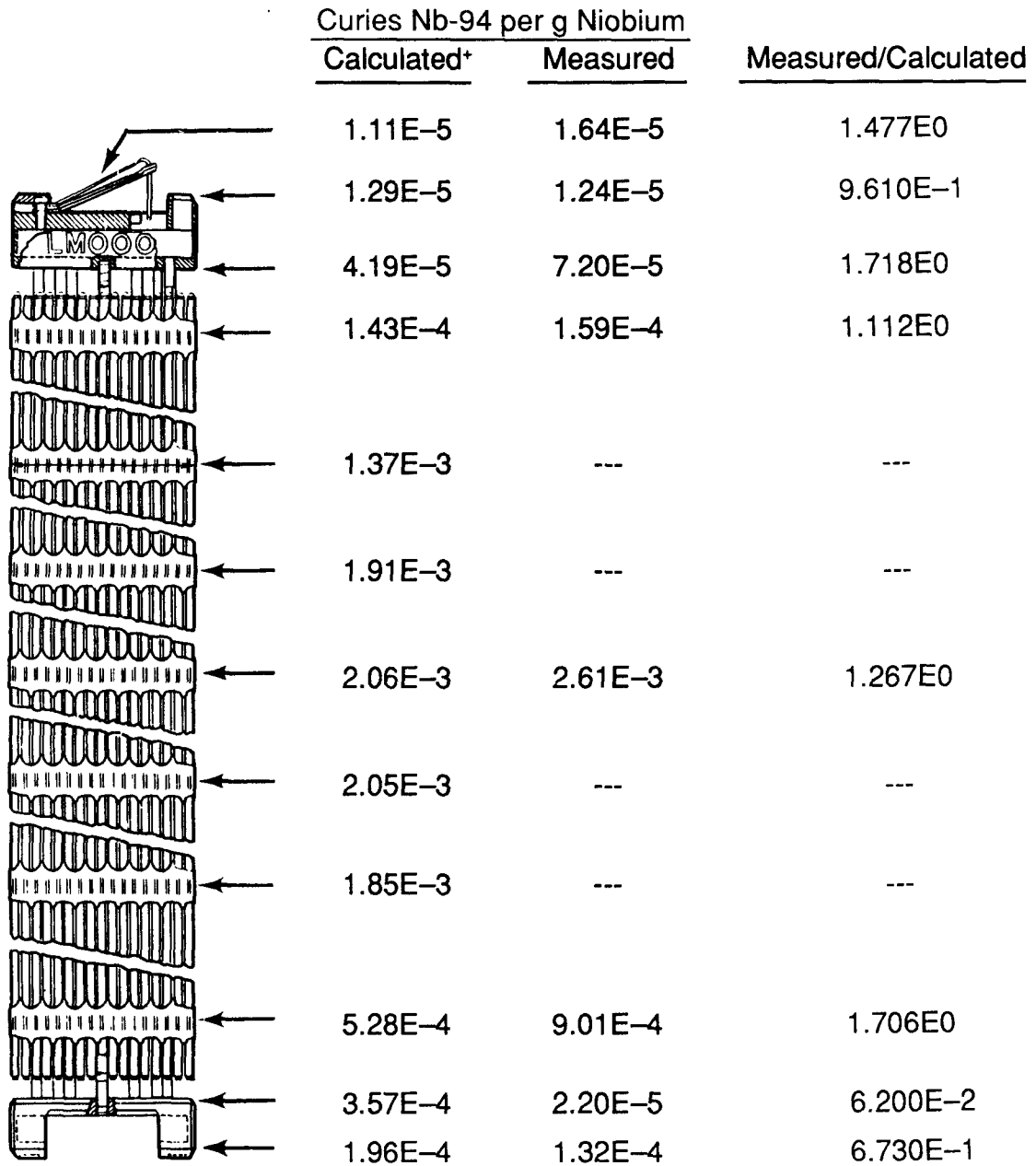
FIGURE 5.9. Westinghouse 14x14 (^{94}Nb)

in terms of curies per initial gram of parent element, in individual samples. What these plots simply show is that when the activation rate of radionuclide is high in a sample, other radionuclides are similarly high. This of course is a reflection of the absolute neutron flux. They show a clustering of the samples from the fueled region, and separate clusterings of the two end fittings. The samples from the gas plenum region fall in with bottom end

Curies Co-60 per g Cobalt		Measured/Calculated
Calculated	Measured	
8.32E–2	1.27E0	1.526E1
3.51E–1	2.78E0	7.920E0
8.93E–1	8.61E0	9.642E0
5.70E0	>4.90E0	N/A
5.03E1	>3.30E0	N/A
8.97E1	>3.90E0	N/A
1.14E2	>5.20E0	N/A
1.22E2	>4.00E0	N/A
1.45E2	>6.20E0	N/A
1.30E2	>4.40E0	N/A
9.08E1	>3.20E0	N/A
3.64E1	3.71E1	1.019
3.17E1	4.83E1	1.525E0
1.85E1	2.09E1	1.127E0
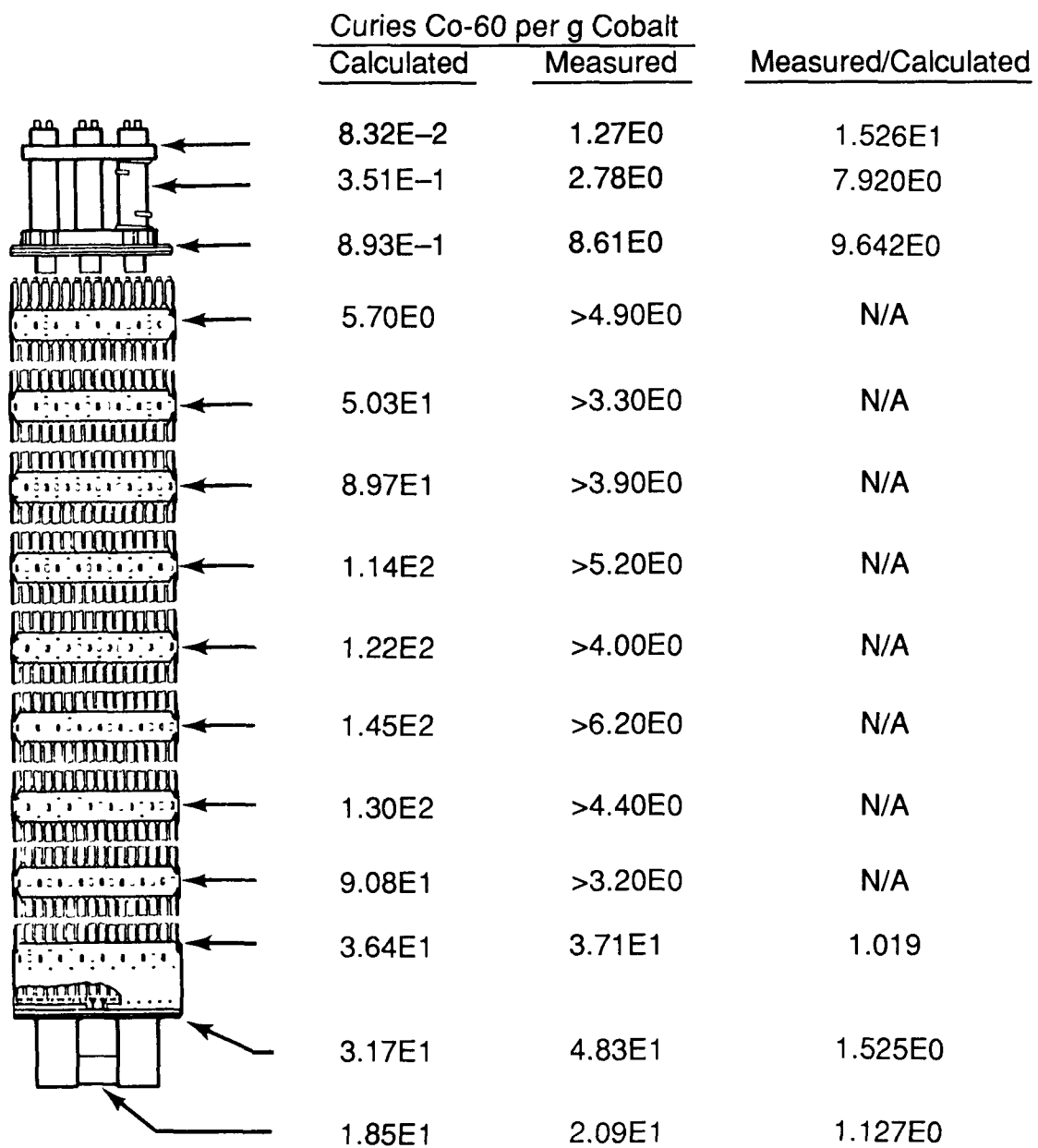
FIGURE 5.10. Combustion Engineering 14x14 (^{60}Co)

fitting. The slope of the drop-off is different for different comparisons, which is believed to be a reflection of the effect of the changing neutron spectrum on the individual reactions.

The similarity in the drop-off of the activation rate as plotted against their axial location in the fuel assembly is seen in Figure 5.37. Again,

Curies Fe-55 per g Iron		
Calculated	Measured	Measured/Calculated
4.89E–4	4.66E–3	9.530E0
2.06E–3	2.14E–2	1.039E1
4.93E–3	5.44E–2	1.103E1
3.30E–2	1.33E–1	4.030E0
2.16E–1	5.49E–1	2.542E0
3.96E–1	8.39E–1	2.119E0
5.05E–1	7.90E–1	1.564E0
5.40E–1	6.59E–1	1.220E0
6.51E–1	1.82E0	2.796E0
5.84E–1	8.35E–1	1.430E0
4.04E–1	6.37E–1	1.577E0
1.61E–1	4.18E–1	2.596E0
1.69E–1	2.97E–1	1.757E0
1.12E–1	1.52E–1	1.357E0
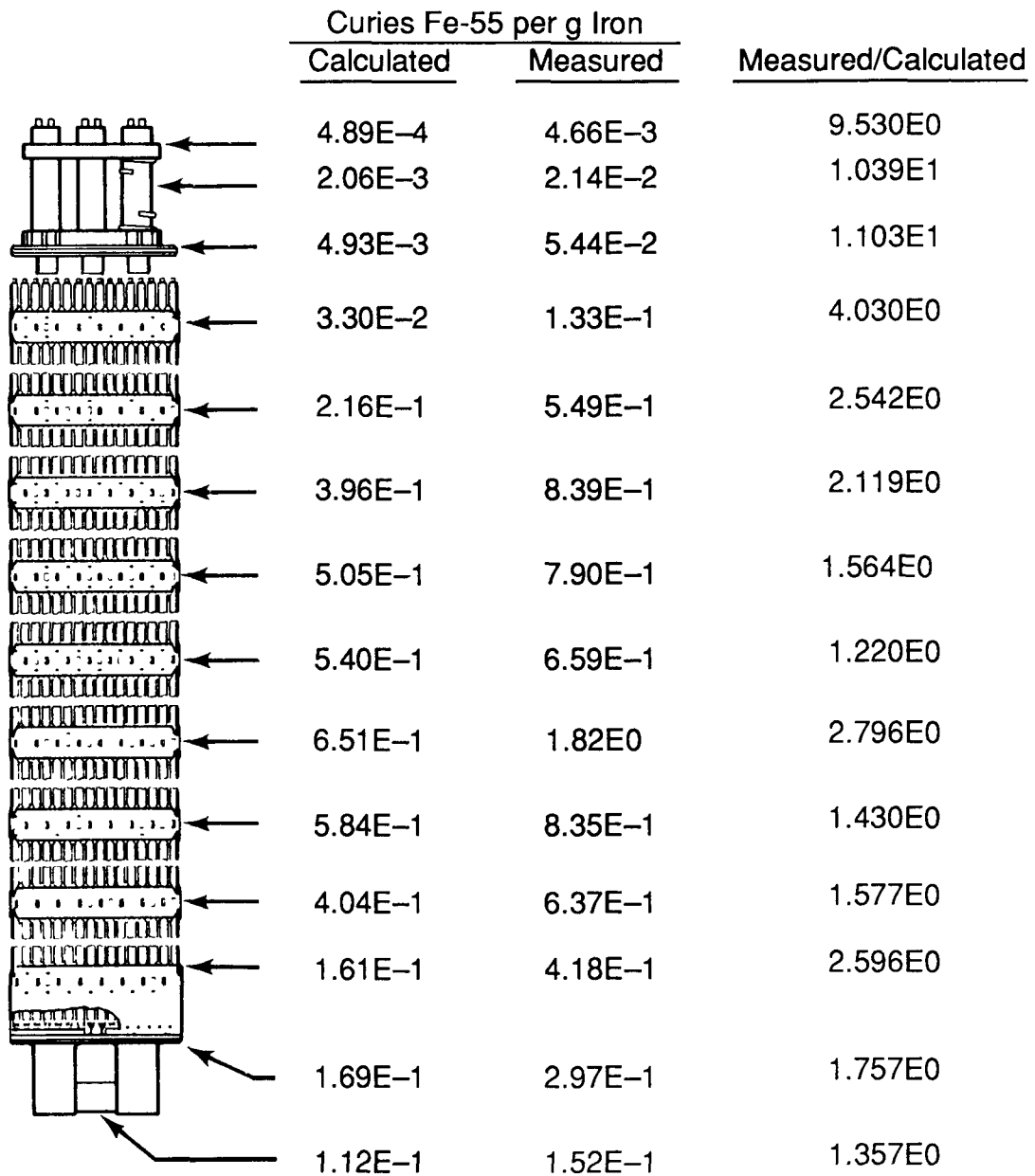
FIGURE 5.11. Combustion Engineering 14x14 (^{55}Fe)

there are differences between the various activation rates, but there is readily discernable a consistent pattern. In the case of the ^{94}Nb values, several of the nominal values were moved. For these points, the elemental measurement was reported as a "less than" value. The result of dividing the curies per gram of metal by a "less than" value for the parent element in the base metal is an upper limit for the curies per gram of initial parent

Curies Ni-59 per g Nickel		
Calculated	Measured	Measured/Calculated
2.36E-7	1.12E-5	4.746E1
6.75E-7	1.89E-5	2.800E1
2.17E-6	8.36E-5	1.617E1
1.11E-5	>4.80E-5	N/A
2.61E-4	>3.56E-4	N/A
4.38E-4	>2.70E-4	N/A
5.59E-4	>7.78E-4	N/A
5.96E-4	>2.46E-4	N/A
6.88E-4	>7.08E-4	N/A
6.18E-4	>3.54E-4	N/A
4.42E-4	>2.16E-4	N/A
1.79E-4	4.45E-4	2.486E0
8.58E-5	5.77E-4	6.725E0
2.76E-5	2.32E-4	8.406E0

FIGURE 5.12. Combustion Engineering 14x14 (^{59}Ni)

element. Thus, the nominal values were moved to be in line with the pattern being seen in the other radionuclides, while still within the range allowed for by the data.

The scaling factors presented in Section 1.0 (Table 1.1) were derived. Based on these two methods of evaluation, these were qualitatively derived

Curies Ni-63 per g Nickel		
Calculated	Measured	Measured/Calculated
3.77E-5	1.68E-3	4.456E1
1.08E-4	5.49E-3	5.083E1
3.46E-4	1.91E-2	5.520E1
1.77E-3	>1.4E-2	N/A
4.16E-2	>1.2E-1	N/A
6.99E-2	>9.0E-2	N/A
8.91E-2	>1.8E-1	N/A
9.50E-2	>7.2E-2	N/A
0.110	>1.7E-1	N/A
9.85E-2	>6.0E-2	N/A
7.05E-2	>4.5E-2	N/A
2.85E-2	1.35E-1	4.737
1.37E-2	1.66E-1	1.212E1
4.41E-3	6.44E-2	1.460E1
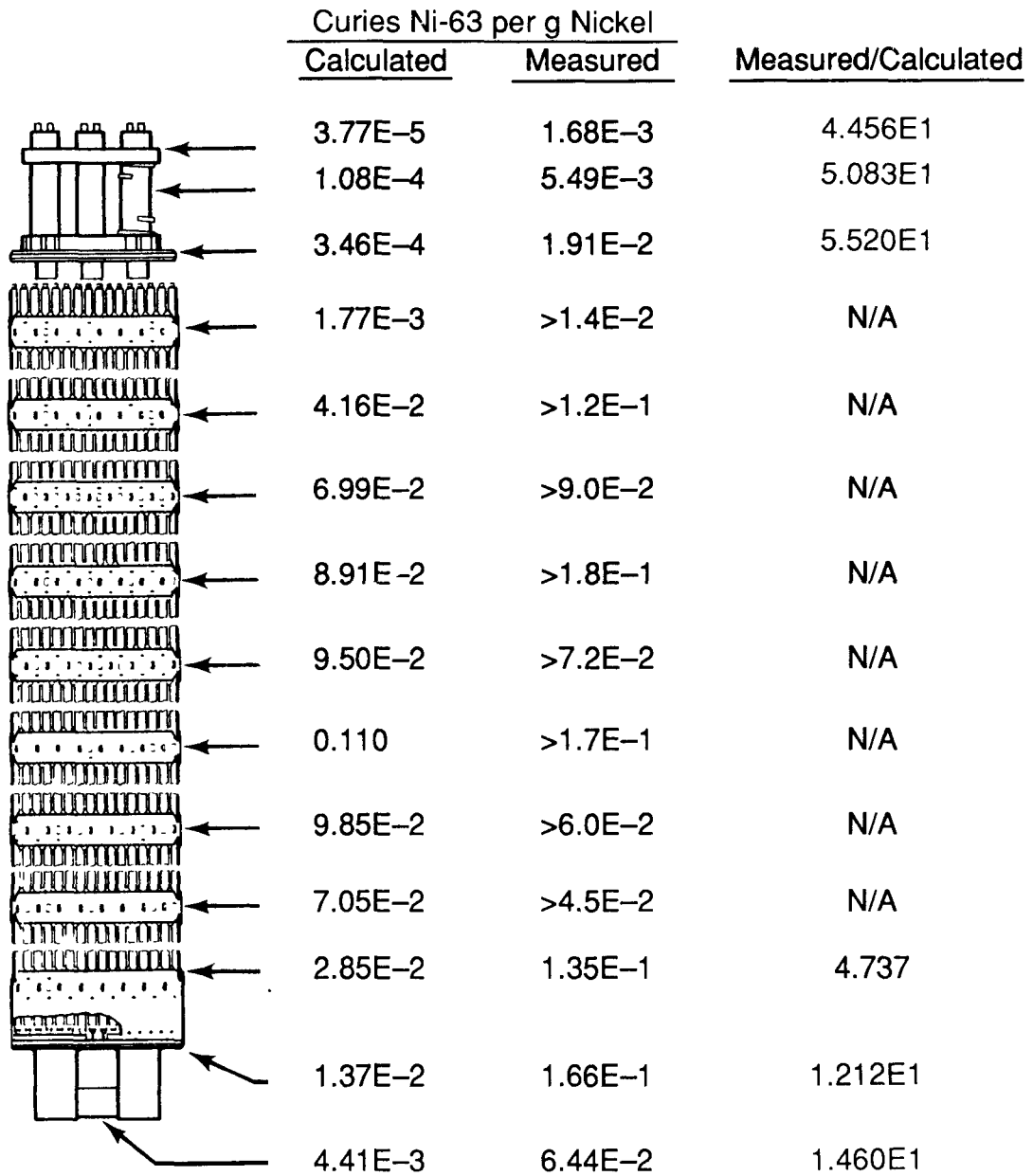
FIGURE 5.13. Combustion Engineering 14x14 (^{63}Ni)

and represent a "best estimate" based on the data available and the uncertainty in the data. They reflect how the generation of radionuclides varies in the spent fuel assembly on a macroscopic basis, while acknowledging the limitations that exist on the available data.

Curies Nb-94 per g Niobium

	Calculated	Measured	Measured/Calculated
	1.35E–6	>3.2E–5	N/A
	4.62E–6	1.27E–5	2.747E0
	3.82E–6	>2.9E–4	N/A
	7.81E–5	---	---
	1.18E–3	1.09E–4	9.200E–2
	2.02E–3	---	---
	2.57E–3	---	---
	2.75E–3	---	---
	3.19E–3	1.19E–4	3.700E–2
	2.86E–3	---	---
	2.02E–3	1.42E–4	7.000E–2
	8.11E–4	1.00E–3	1.233E0
	5.07E–4	>1.8E–4	N/A
	2.25E–4	>2.3E–5	N/A

FIGURE 5.14. Combustion Engineering 14x14 (^{94}Nb)

Curies Co-60 per g Cobalt		
Calculated	Measured	Measured/Calculated
7.70E−1	6.18E−1	8.030E−1
2.659E0	8.675E0	3.263E0
8.758E0	1.25E1	1.431E0
8.758E0	2.89E1	3.302E0
7.42E1	9.57E1	1.290E0
7.42E1	1.12E2	1.615E0
8.76E1	1.08E2	1.233E0
8.76E1	1.14E2	1.304E0
2.24E1	3.94E1	1.761E0
2.24E1	5.88E1	2.624E0
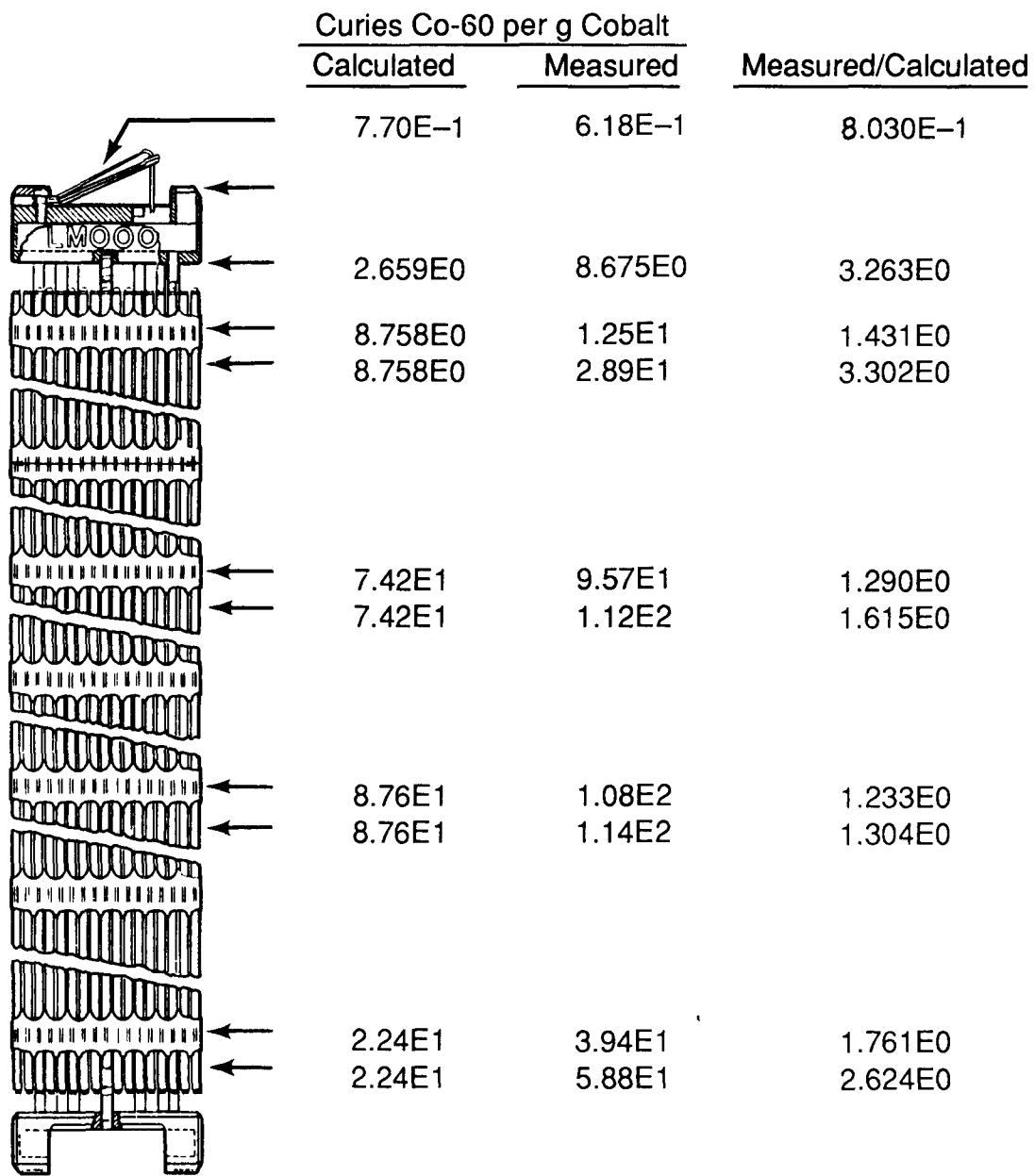
FIGURE 5.15. RG&E 14x14 (^{60}Co)

Curies Fe-55 per g Iron		
Calculated	Measured	Measured/Calculated
5.07E-3	5.74E-3	1.132E0
1.68E-2	5.34E-2	3.179E0
5.78E-2	1.12E-1	1.938E0
5.78E-2	1.49E-1	2.575E0
4.21E-1	6.54E-1	1.553E0
4.21E-1	5.79E-1	1.375E0
4.52E-1	8.63E-1	1.909E0
4.52E-1	4.93E-1	1.091E0
1.14E-1	3.53E-1	3.096E0
1.14E-1	2.43E-1	2.132E0
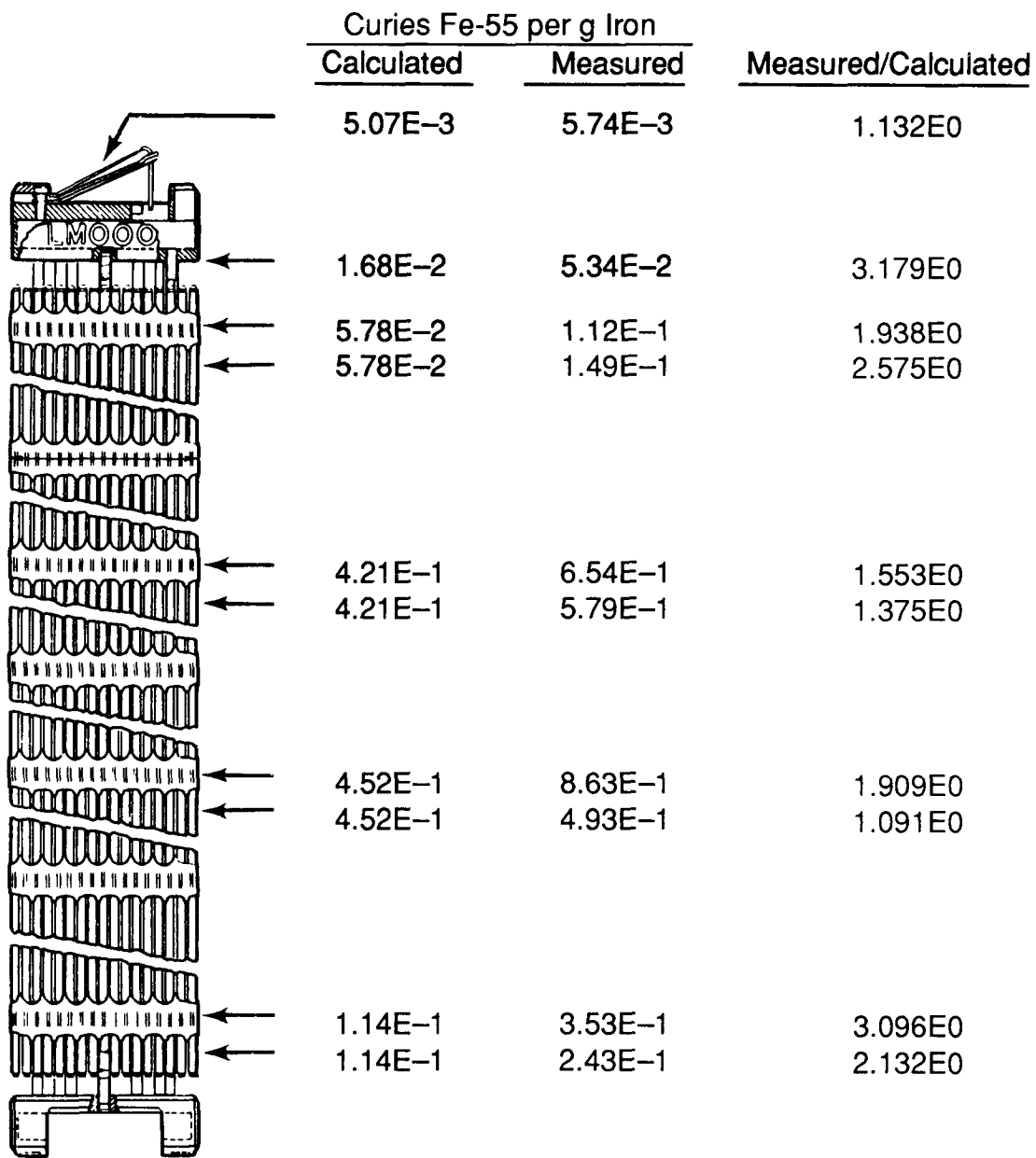
FIGURE 5.16. RG&E 14x14 (^{55}Fe)

| Curies Ni-59 per g Nickel | | |
Calculated	Measured	Measured/Calculated
1.59E–6	3.68E–6	2.314E0
6.45E–6	5.63E–5	8.730E–1
1.74E–5	7.75E–5	4.454E0
1.74E–5	1.53E–4	8.793E0
4.22E–4	3.83E–4	9.080E–1
4.22E–4	4.84E–4	1.147E0
4.53E–4	4.98E–4	1.099E0
4.53E–4	5.09E–4	1.124E0
1.19E–4	1.79E–4	1.504E0
1.19E–4	2.66E–4	2.235E0
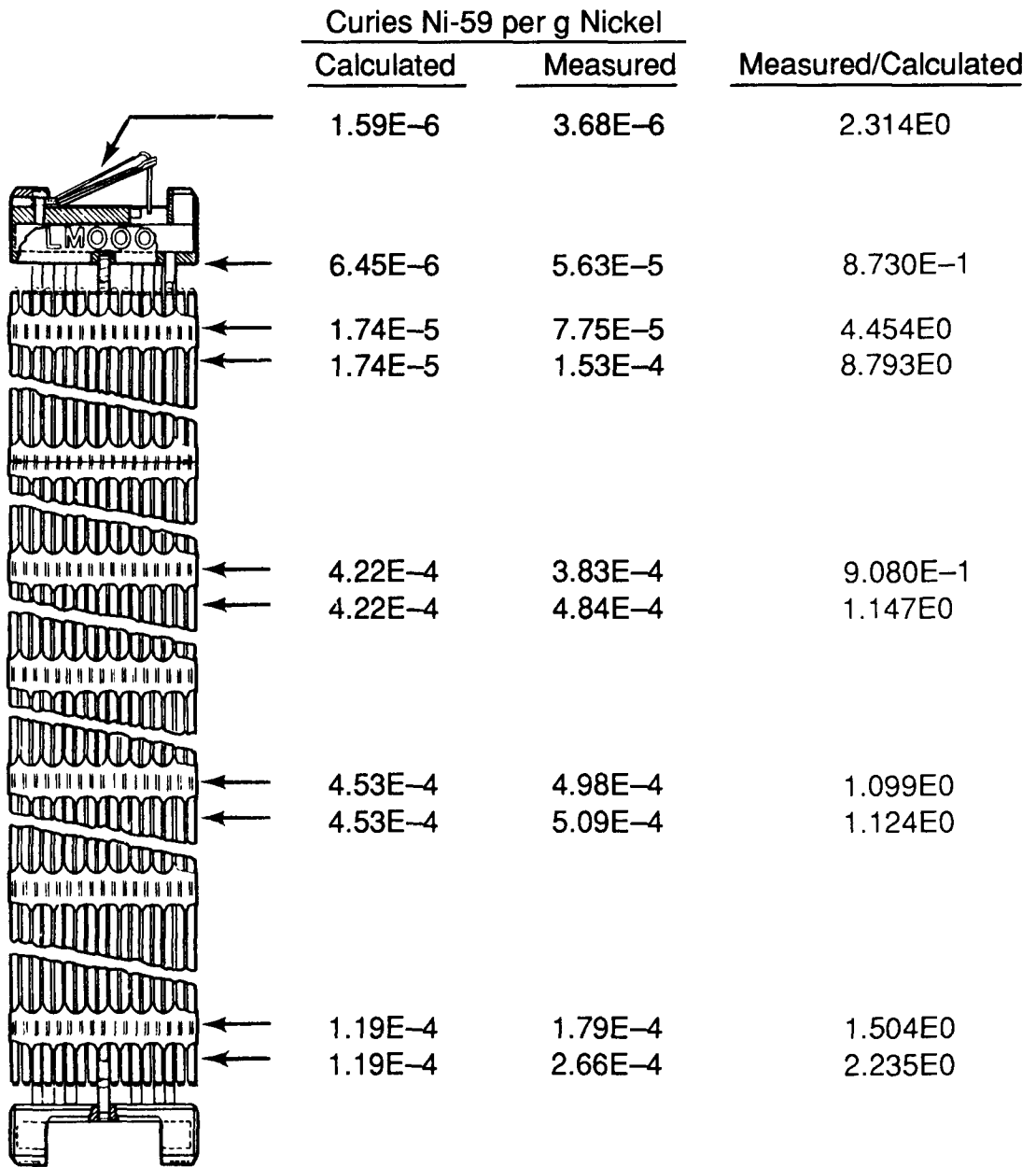
FIGURE 5.17. RG&E 14x14 (^{59}Ni)

Curies Ni-63 per g Nickel		
Calculated	Measured	Measured/Calculated
2.11E–4	1.077E–4	5.100E–1
8.54E–4	2.122E–3	2.485E0
2.30E–3	2.279E–3	9.910E–1
2.30E–3	4.401E–3	1.913E0
5.59E–2	1.173E–2	2.100E–1
5.59E–2	1.474E–2	2.640E–1
5.99E–2	1.508E–2	2.520E–1
5.99E–2	1.508E–2	2.520E–1
1.57E–2	5.619E–3	3.580E–1
1.57E–2	6.892E–3	4.390E–1
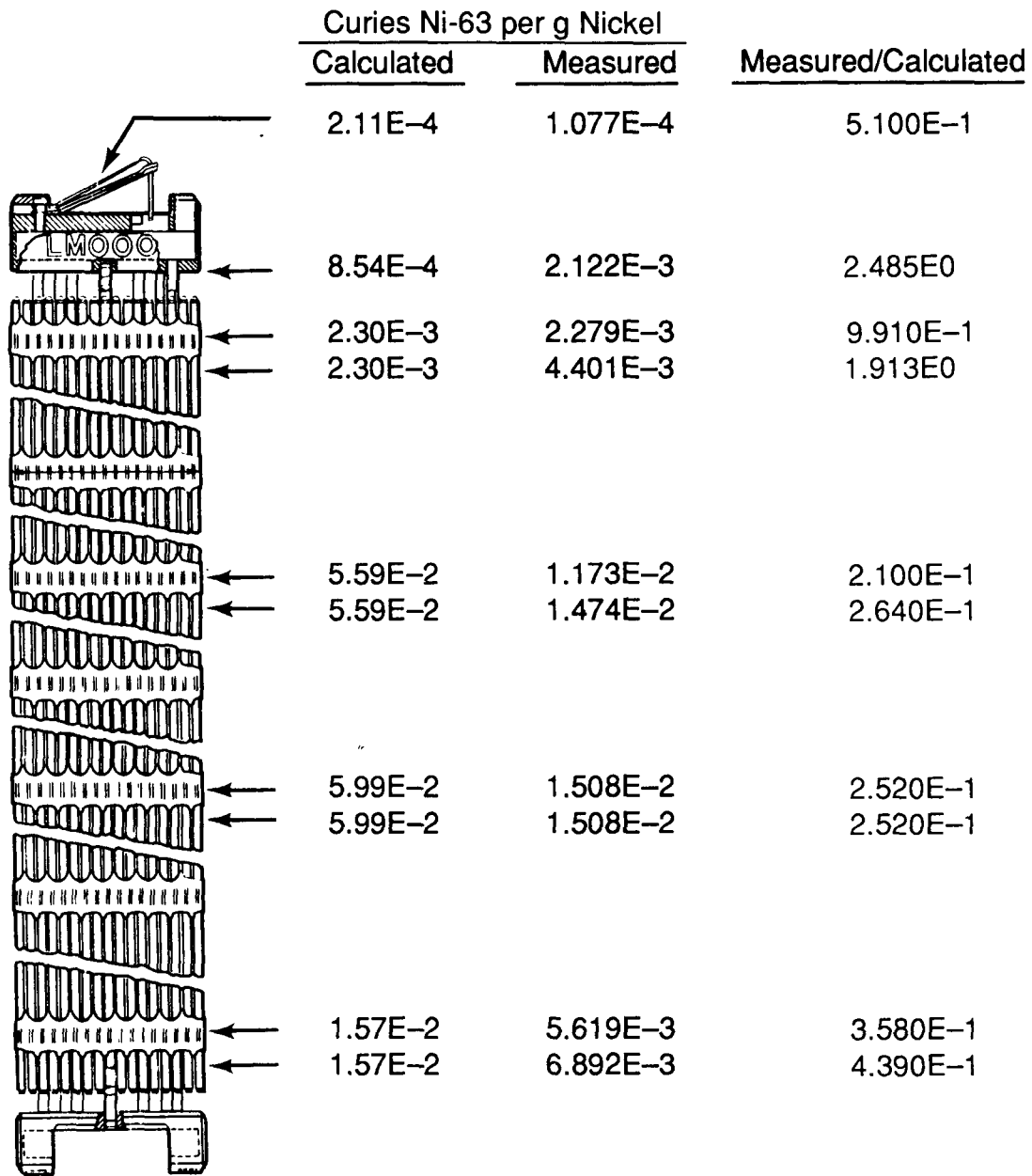
FIGURE 5.18. RG&E 14x14 (^{63}Ni)

5.19

Curies Nb-94 per g Niobium		
Calculated	Measured	Measured/Calculated
7.96E–6	5.15E–6	6.470E–1
3.00E–5	---	---
1.02E–4	4.43E–5	4.340E–1
1.02E–4	---	---
1.37E–3	4.43E–4	3.230E–1
1.37E–3	---	---
1.47E–3	5.46E–4	3.710E–1
1.47E–3	---	---
3.78E–4	1.76E–4	4.660E–1
3.78E–4	---	---
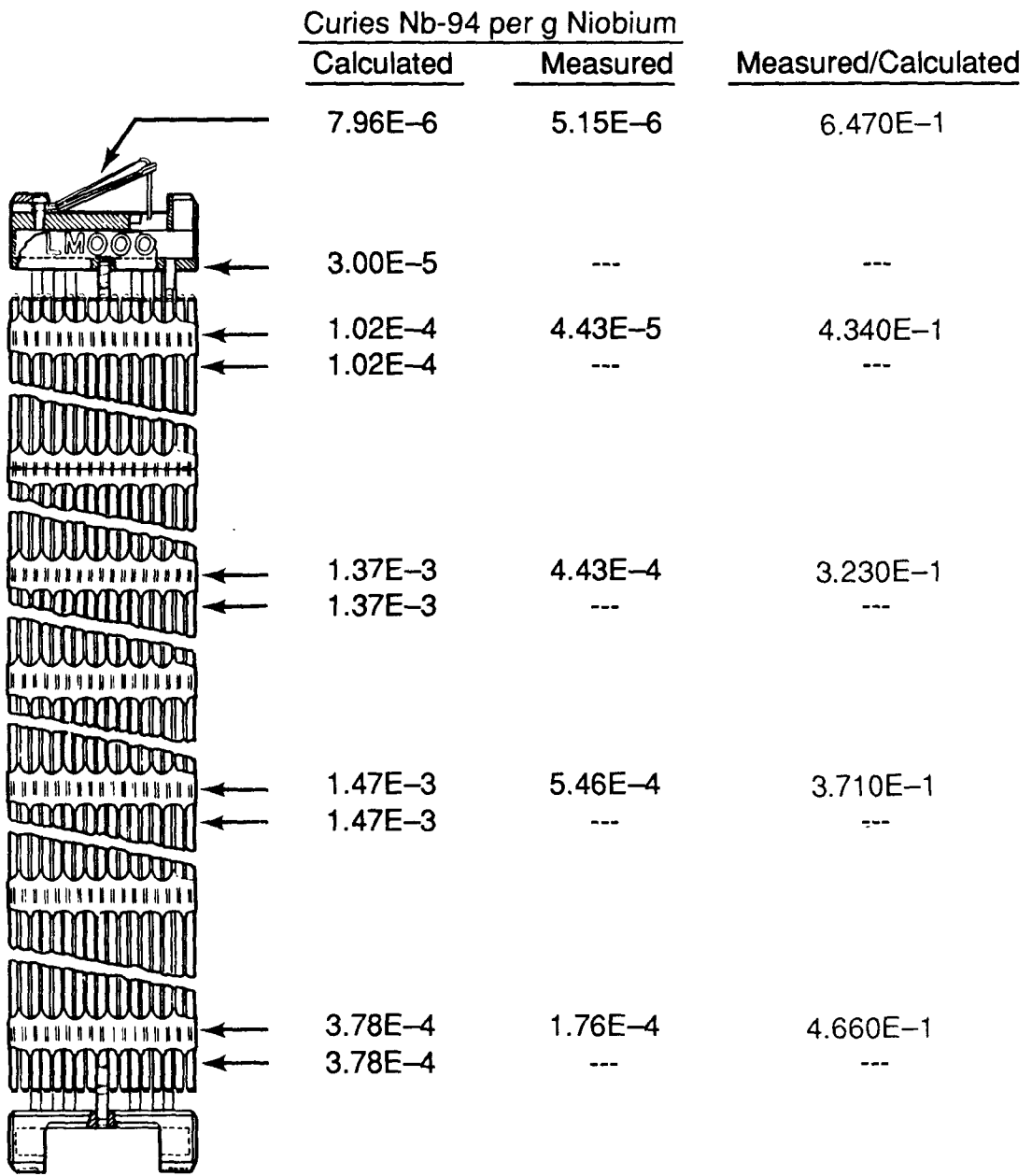
FIGURE 5.19.   RG&E 14x14 (^{94}Nb)

Curies Co-60 per g Cobalt		
Calculated	Measured	Measured/Calculated

1.43E2	1.89E2	1.323E0
1.43E2	>1.432E0	N/A
3.84E1	2.35E1	6.120E-1
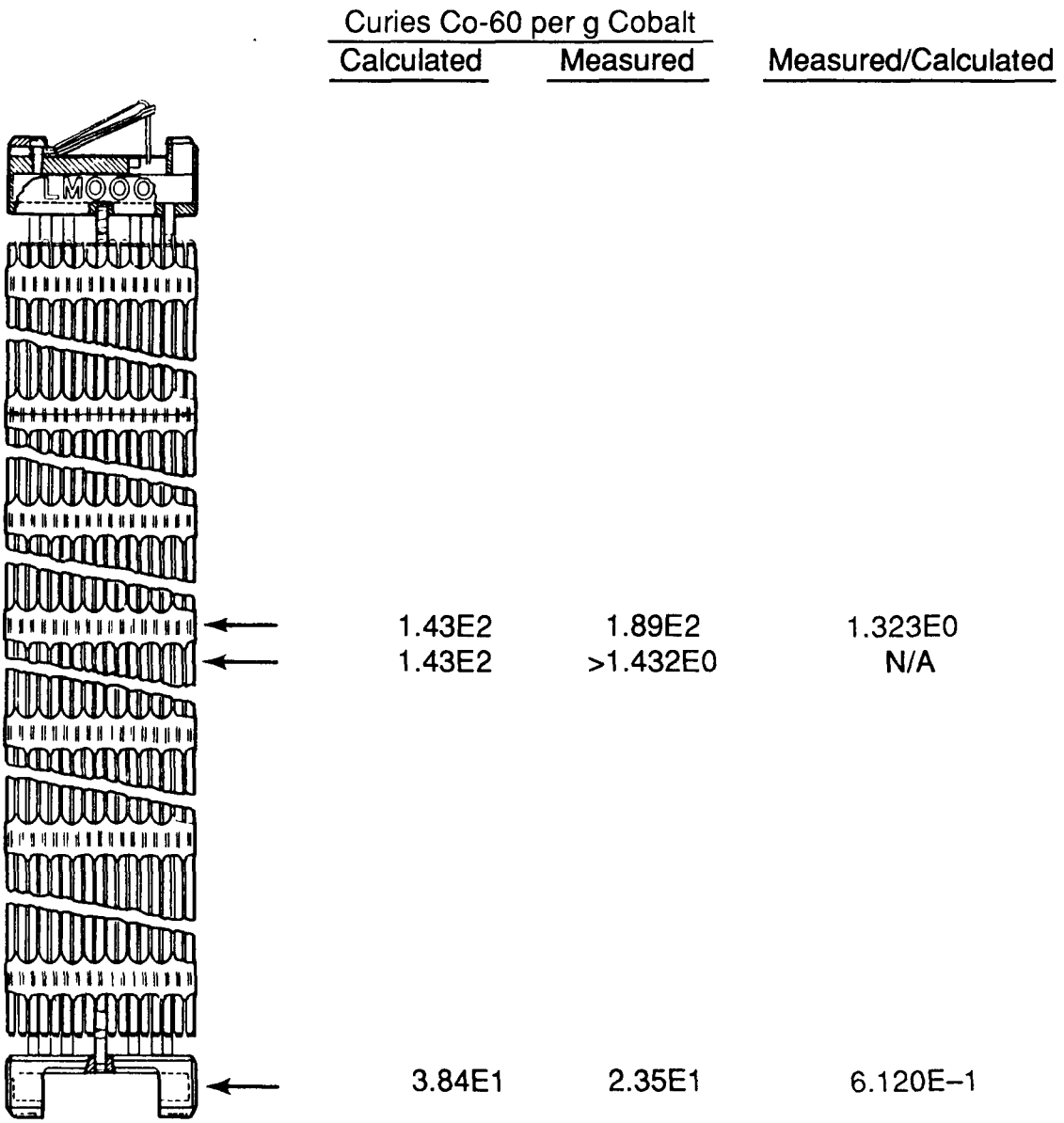
FIGURE 5.20. INEL 14x14 (^{60}Co)

5.21

Curies Fe-55 per g Iron		
Calculated	Measured	Measured/Calculated
7.17E−1	4.387E0	6.119E0
7.17E−1	6.41E−1	8.940E−1
1.95E−1	1.84E−1	9.440E−1
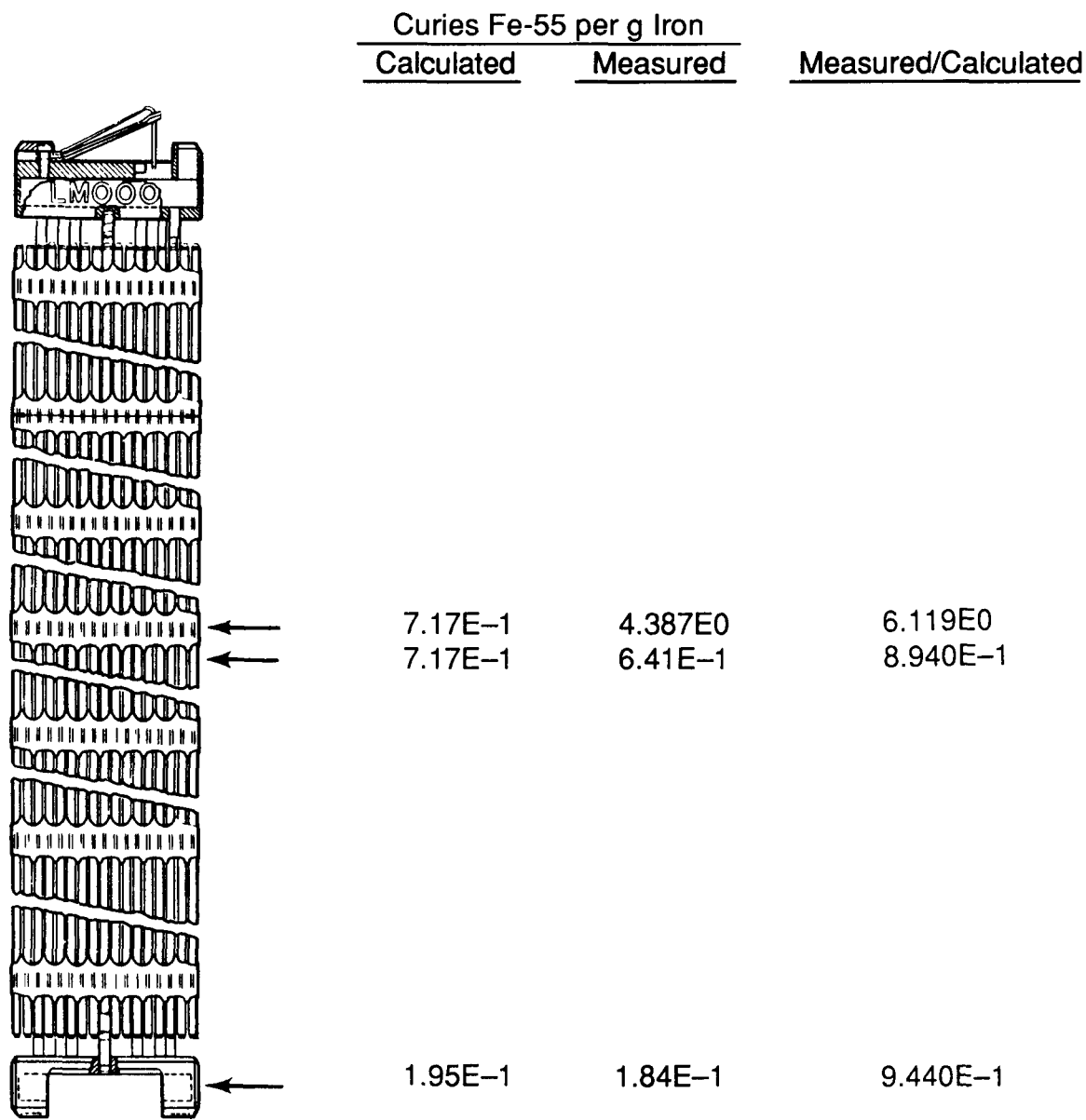
FIGURE 5.21. INEL 14x14 (^{55}Fe)

Curies Ni-59 per g Nickel		
Calculated	Measured	Measured/Calculated
7.5E-4	5.6E-4	7.470E-1
7.5E-4	2.2E-4	2.930E1
6.6E-5	3.5E-4	5.303E0
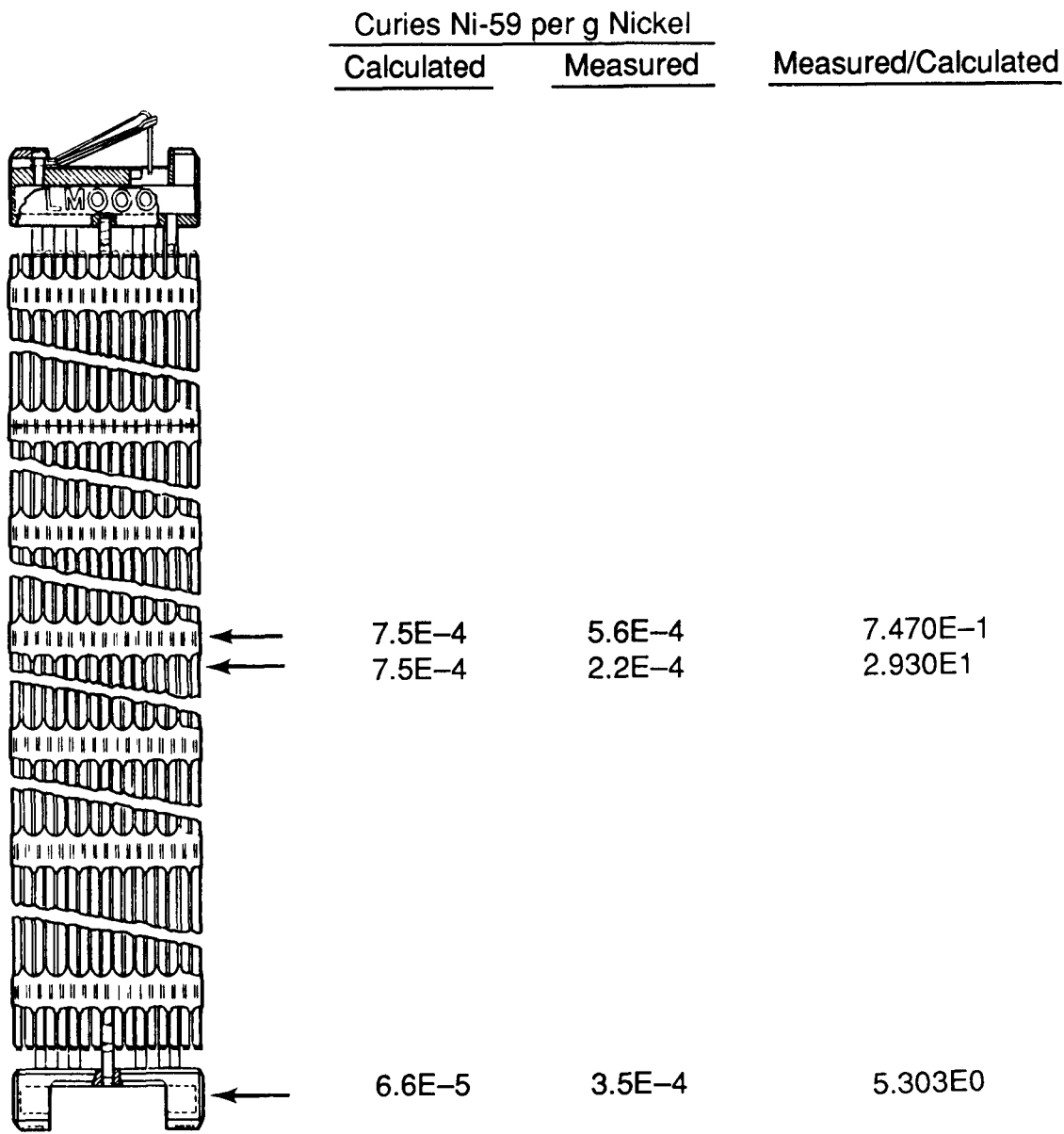
FIGURE 5.22. INEL 14x14 (^{59}Ni)

Curies Ni-63 per g Nickel		
Calculated	Measured	Measured/Calculated
1.06E–1	1.40E–1	1.320E0
1.06E–1	4.307E–2	4.060E–1
9.18E–3	4.061E–2	4.424E0
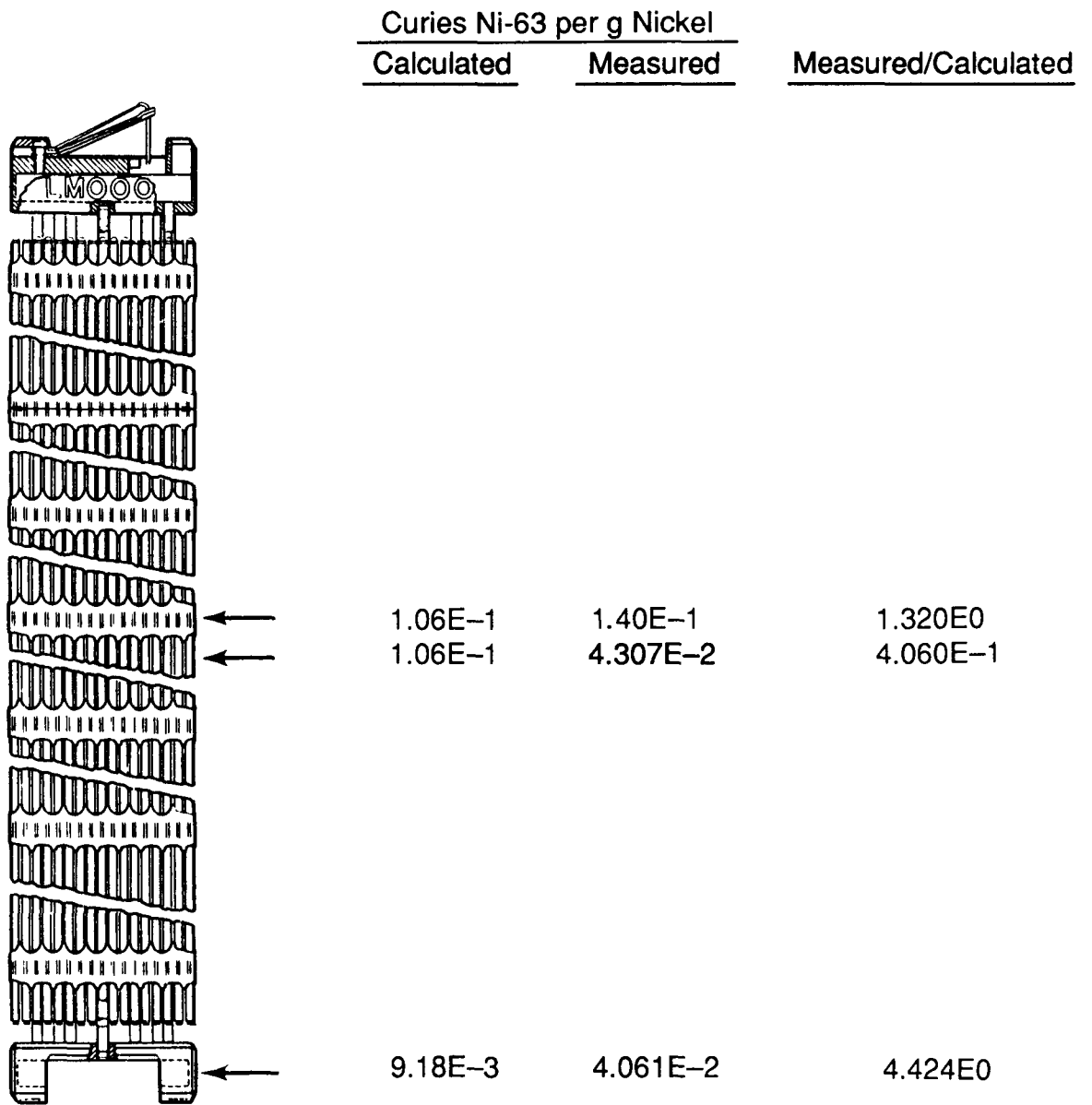
FIGURE 5.23.   INEL 14x14 (^{63}Ni)

Curies Nb-94 per g Niobium		
Calculated	Measured	Measured/Calculated
2.7E–3	2.6E–3	9.630E–1
2.7E–3	---	---
4.5E–4	---	---

FIGURE 5.24.   INEL 14x14 (^{94}Nb)

FIGURE 5.25. ⁵⁹Ni and ⁶³Ni in All Fuel Assembly Hardware
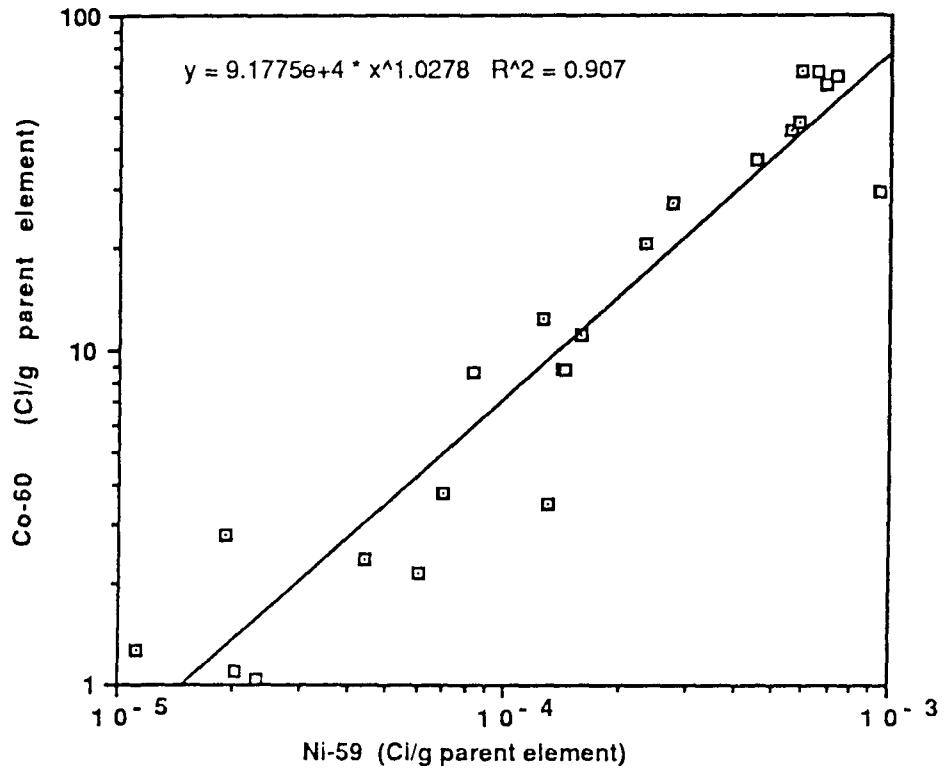
FIGURE 5.26. ⁶⁰Co and ⁵⁹Ni in All Fuel Assembly Hardware
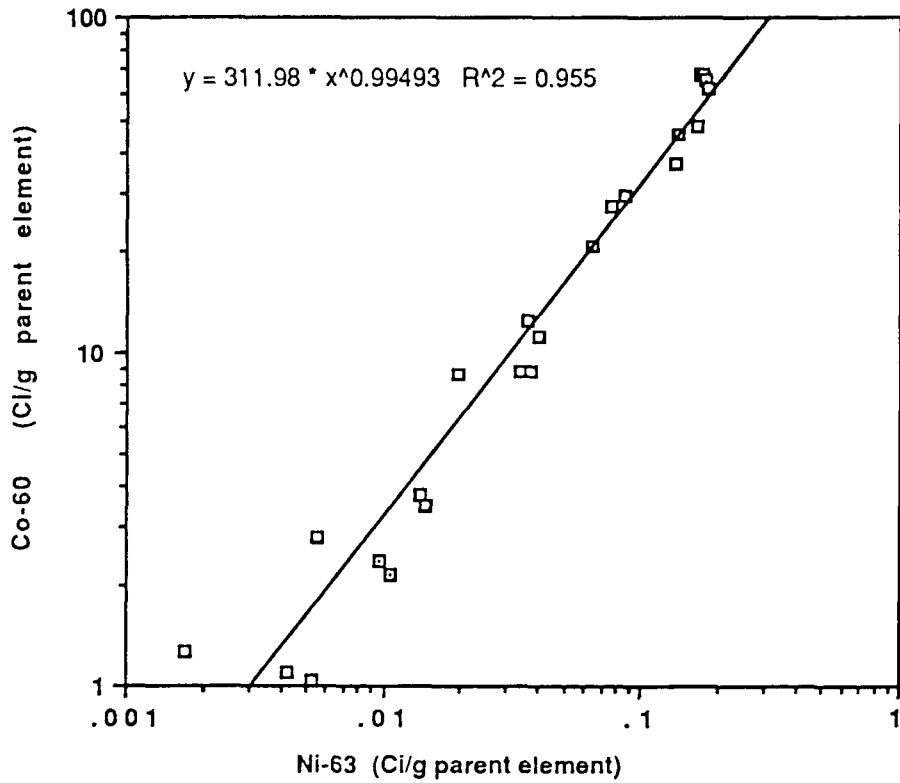
FIGURE 5.27. ^{60}Co and ^{63}Ni in All Fuel Assembly Hardware
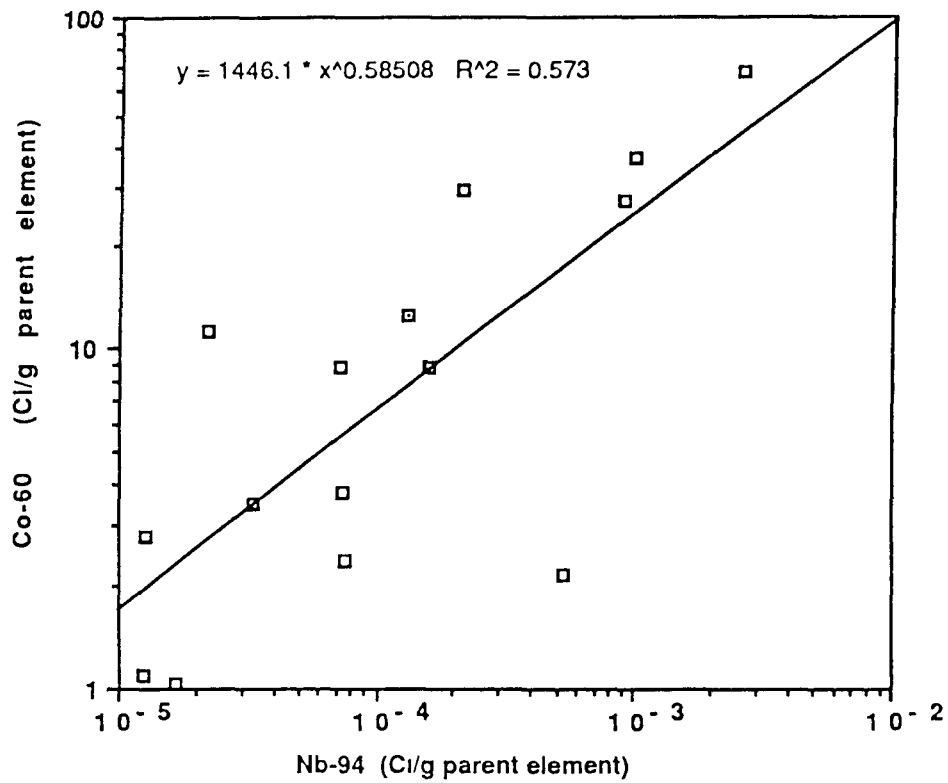
FIGURE 5.28. ^{60}Co and ^{94}Nb in All Fuel Assembly Hardware

$y = 388.64 * x^{1.0496}$ $R^2 = 0.997$

Ni-63 (Ci/g parent element)

Ni-59 (Ci/g parent element)
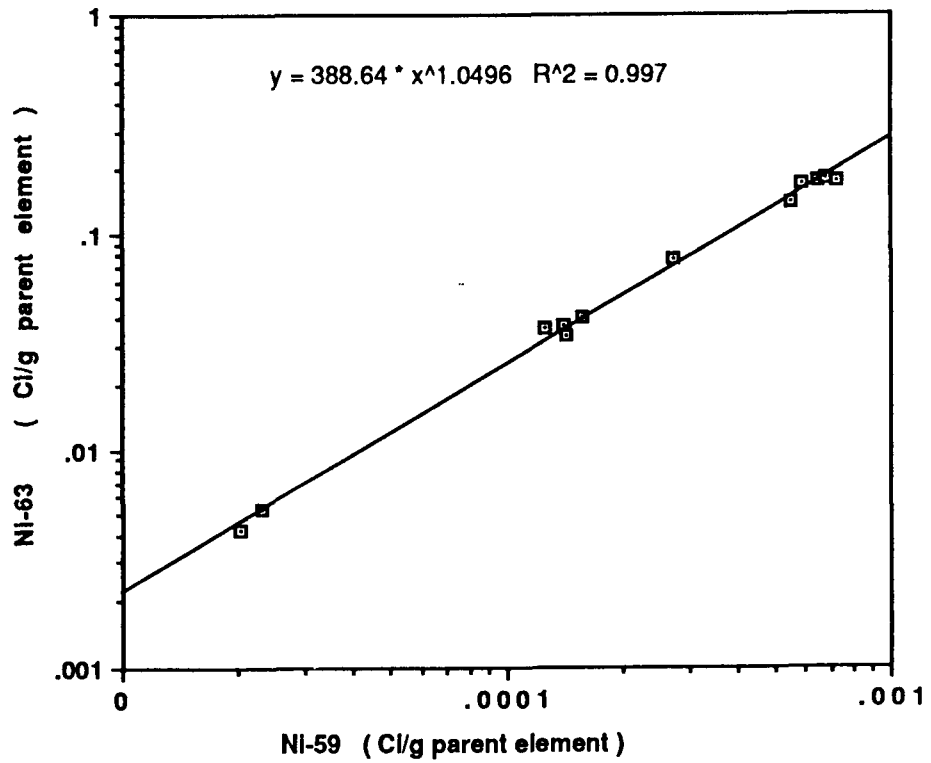
FIGURE 5.29. ^{59}Ni and ^{63}Ni in Spent Westinghouse Fuel Assembly Hardware

$y = 3652.2 * x^{0.66520}$ $R^2 = 0.786$

Greater than value. Arrow indicates where the point may actually be.

Co-60 (Ci/g parent element)

Nb-94 (Ci/g parent element)
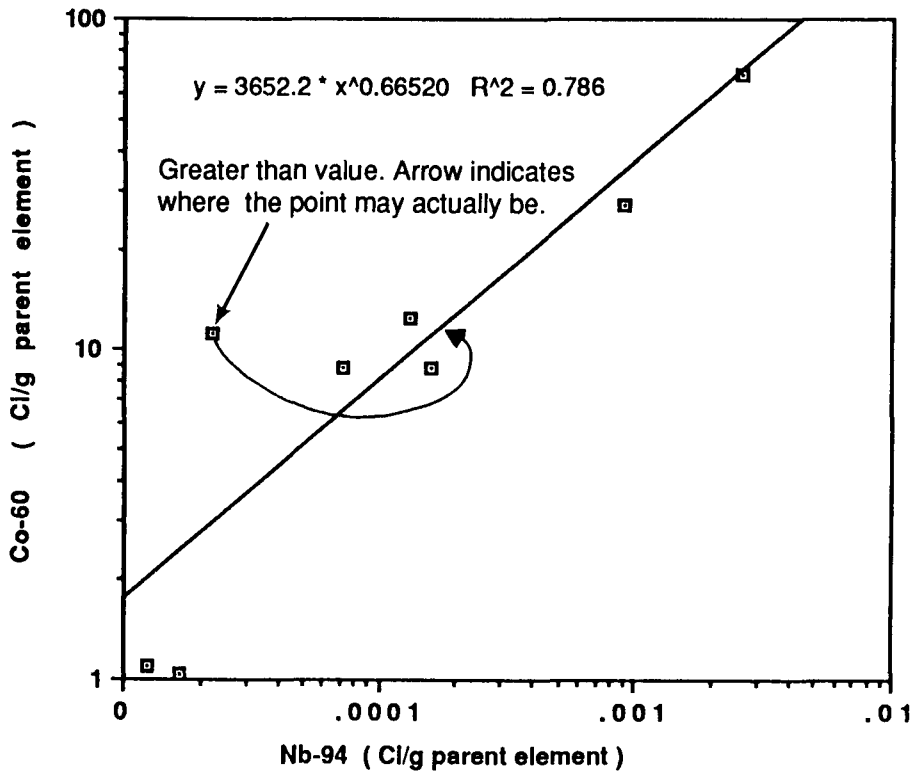
FIGURE 5.30. ^{94}Nb and ^{60}Co in Spent Westinghouse Fuel Assembly Hardware

5.28
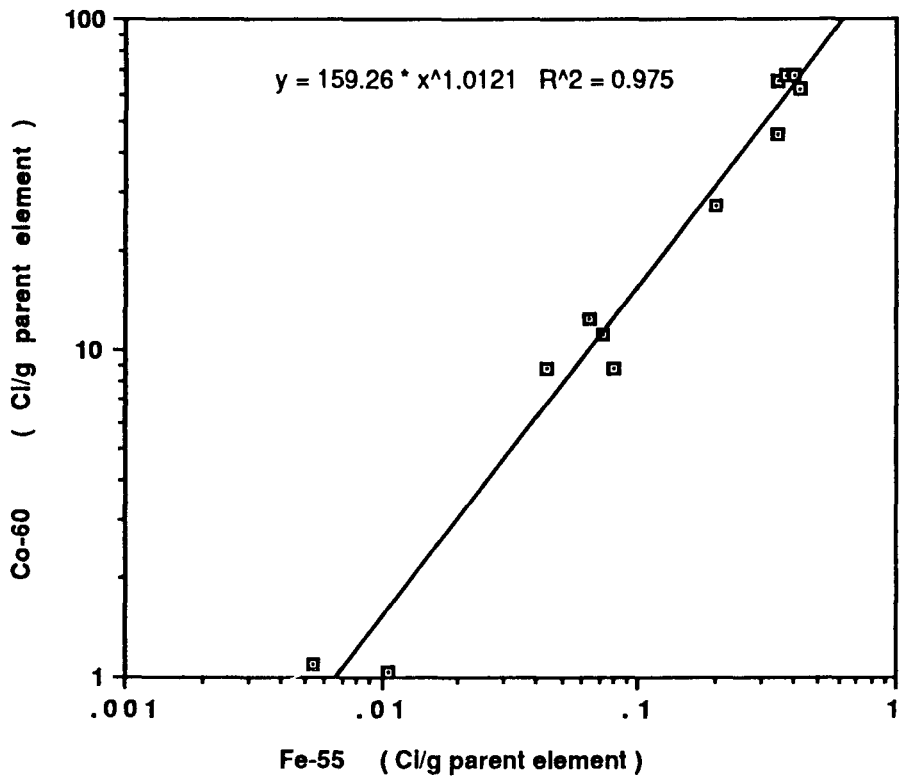
FIGURE 5.31. ^{55}Fe and ^{60}Co in Spent Westinghouse Fuel Assembly Hardware
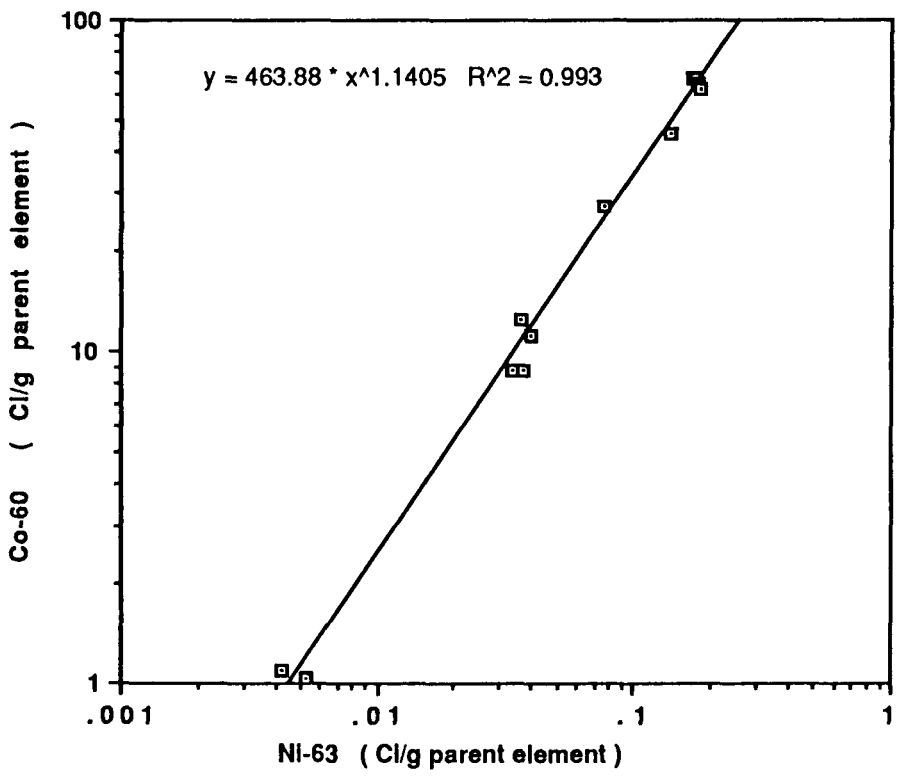
FIGURE 5.32. ^{63}Ni and ^{60}Co in Spent Westinghouse Fuel Assembly Hardware
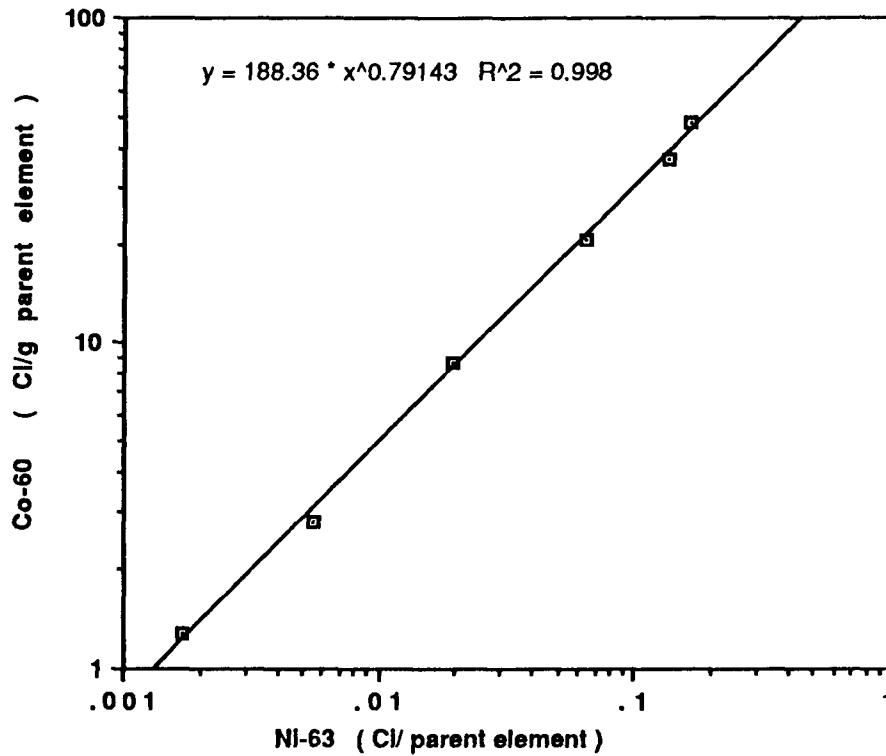
FIGURE 5.33. ^{60}Co and ^{63}Ni in Spent Combustion Engineering Fuel
Assembly Hardware
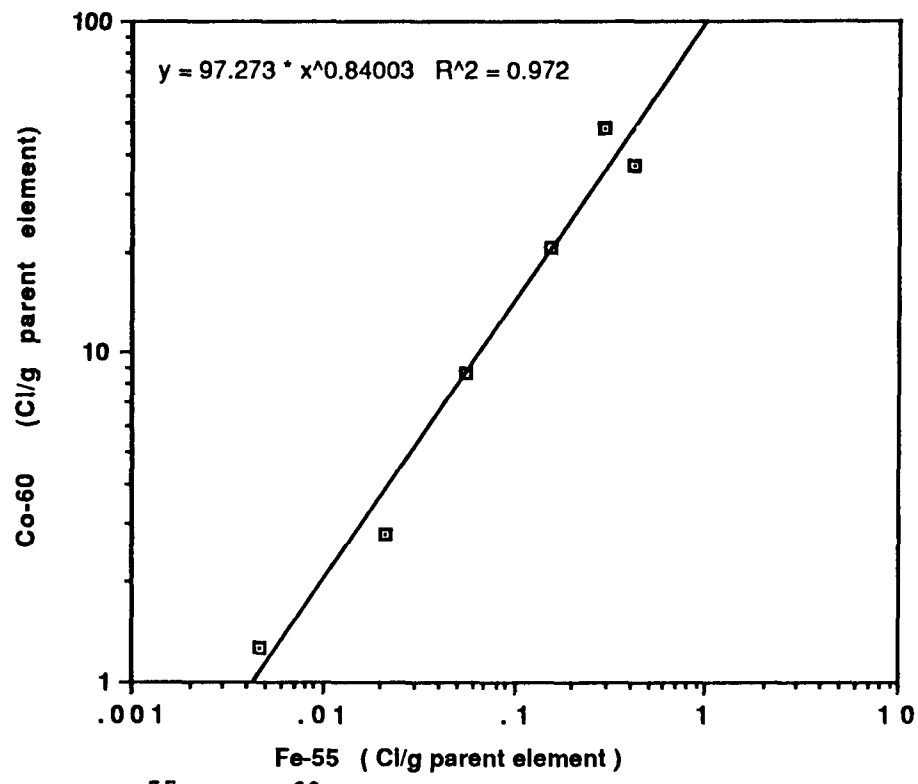
FIGURE 5.34. ^{55}Fe and ^{60}Co in Spent Combustion Engineering Fuel
Assembly Hardware
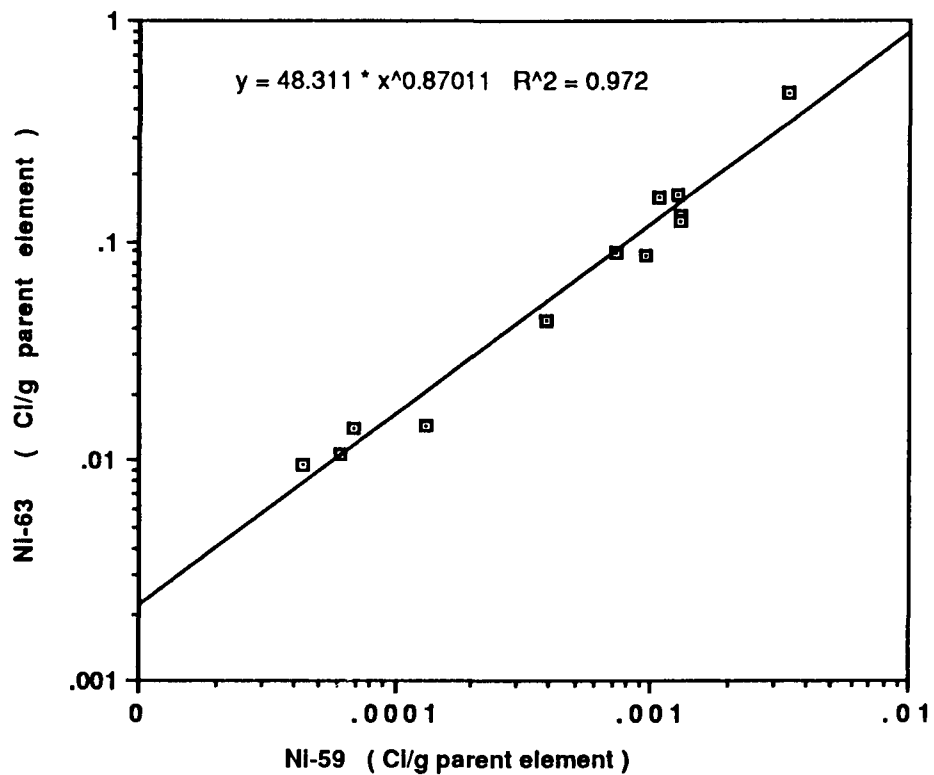
FIGURE 5.35. [59]Ni and [63]Ni in Spent General Electric Fuel Assembly Hardware
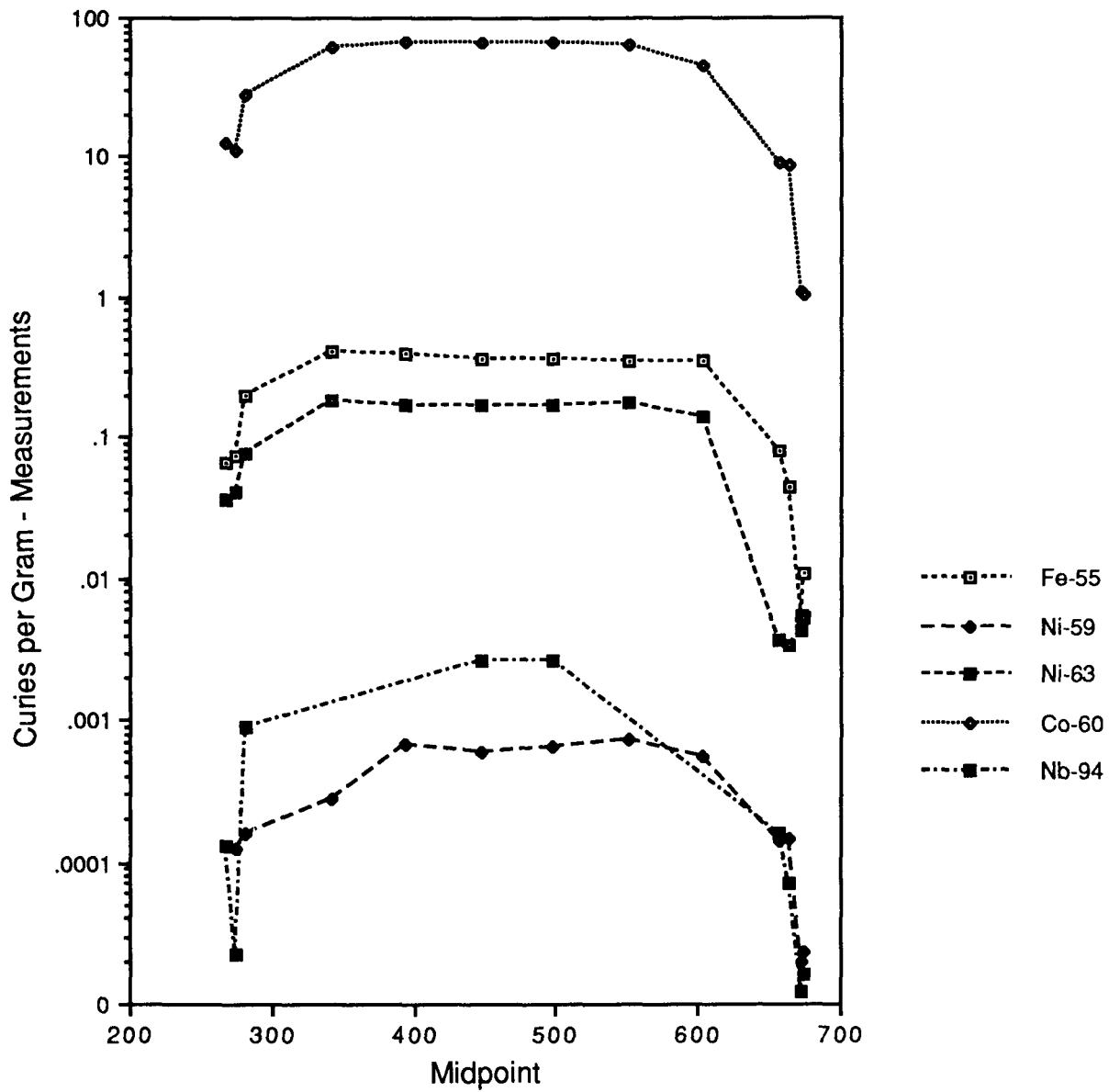
FIGURE 5.36. Activation Rate Versus Fuel Assembly Axial Location

6.0 10 CFR PART 61 CLASSIFICATION

The Nuclear Regulatory Commission (NRC) has established radiological limits for waste that can be disposed of in a shallow land burial site. These limits are specified in 10 CFR 61. The limits shown in Table 6.1 are extracted from 10 CFR 61. Low-level waste classified as Class A, B, or C, can be disposed of in a shallow land burial site, and it is the responsibility of the states to provide disposal sites. If the radionuclide inventory exceeds the Class C limits, it is referred to as greater than Class C (GTCC) and the responsibility for its disposal lies with the federal government. GTCC waste requires greater confinement than low-level waste. Currently, no disposal facilities exist for GTCC waste. The waste classification of fuel assembly hardware will affect the disposal options available and the cost of those options, for either the DOE or those utilities that may be considering fuel consolidation.

Other than those made of Zircaloy-4, all of the samples analyzed exceeded the Class C limits, with one exception, the holdown plate in the Combustion Engineering assembly (the upper-most sample). The Inconel samples exceed the limits for both ^{94}Nb and ^{63}Ni in all cases and ^{59}Ni for almost all cases. The stainless steel samples exceeded the limits for ^{63}Ni in many of the samples, but not ^{59}Ni and ^{94}Nb. These are still important since waste is classified as GTCC if the sum of the fractions is greater than 1.0. (If both ^{63}Ni and ^{94}Nb are at 0.55 of their individual limit, their sum of the fractions, 1.10, puts them above the limit.)

TABLE 6.1. 10 CFR 61 Class C Disposal Limits for Radionuclides of Interest in this Study

Radionuclide in Activated Metal	Class C Limit Ci/m^3
^{14}C	80.0
^{59}Ni	220.0
^{94}Nb	0.2
^{63}Ni	7000.0

Tables 6.2 through 6.4 gives the ratio of radionuclide inventory to 10 CFR 61 Class C limits for several isotopes. These ratios are based on the full density of the individual samples. Several factors have to be kept in mind if one is to apply these tables to actual disposal of activated metals. The first is that a piece, such as the top end fitting of the Westinghouse assembly, can have varying concentrations within it (W-12 & W-9 are two samples off the same piece). The ratio for a given piece as a whole is the average concentration in the piece, even though it may have hot spots.

TABLE 6.2. 10 CFR 61 Ratios for Westinghouse

ID	Material	Density g/cc	^{59}Ni	^{63}Ni	^{94}Nb	Ratio
W-10	INC	8.3	0.45	3.20	30.67	34.3
W-12	SS	8.0	0.06	0.40	0.02	0.5
W-9	SS	8.0	0.48	3.49	0.07	4.0
W-8	INC	8.2	2.80	22.96	286.18	311.9
W-7	INC	8.2	9.50	76.26	N/A	<85.8
W-6	INC	8.2	13.05	99.45	N/A	<112.5
W-5	INC	8.2	12.19	103.09	4920.00	5035.3
W-4	INC	8.2	10.29	93.60	N/A	<103.9
W-3	INC	8.2	12.49	104.14	N/A	<116.6
W-2	INC	8.2	5.03	43.81	1697.40	1746.2
W-11	SS	8.0	0.54	4.29	0.26	5.1
W-1	SS	8.0	0.36	3.27	0.83	4.5

TABLE 6.3. 10 CFR 61 Ratios for Combustion Engineering

ID	Material	Density g/cc	^{59}Ni	^{63}Ni	^{94}Nb	Ratio
CE-25	SS	8.0	0.04	0.19	0.02	0.2
CE-26	INC	8.2	0.51	4.69	11.69	16.9
CE-24	SS	8.0	0.26	1.86	0.17	2.3
CE-10	ZIRC	6.56	0.00	0.00	N/A	<0.0
CE-9	ZIRC	6.56	0.00	0.01	0.55	0.6
CE-8	ZIRC	6.56	0.00	0.00	N/A	<0.0
CE-7	ZIRC	6.56	0.00	0.01	N/A	<0.0
CE-6	ZIRC	6.56	0.00	0.00	N/A	<0.0
CE-5	ZIRC	6.56	0.00	0.01	0.97	1.0
CE-4	ZIRC	6.56	0.00	0.00	N/A	<0.0
CE-3	ZIRC	6.56	0.00	0.00	0.68	0.7
CE-2	INC	8.2	6.08	52.71	926.60	985.37
CE-14	SS	8.0	2.01	18.17	0.64	20.8
CE-1	SS	8.0	0.83	7.25	0.19	8.3

TABLE 6.4. 10 CFR 61 Ratios for General Electric

ID	Material	Density g/cc	^{59}Ni	^{63}Ni	^{94}Nb	Ratio
GE-19	SS	8.0	0.13	0.92	0.03	1.1
GE-18	SS	8.0	0.18	1.01	0.16	1.3
GE-17	INC	8.2	1.76	11.11	24.40	37.3
GE-15	ZIRC	6.56	0.01	0.03	0.17	0.2
GE-13	ZIRC	6.56	0.03	0.10	N/A	<0.1
GE-11	ZIRC	6.56	0.03	0.08	N/A	<0.1
GE-9	ZIRC	6.56	0.03	0.13	N/A	<0.2
GE-7	ZIRC	6.56	0.04	0.18	0.30	0.5
GE-5	ZIRC	6.56	0.02	0.07	N/A	<0.1
GE-3	ZIRC	6.56	0.01	0.02	0.32	0.4
GE-1	SS	8.0	2.96	8.62	3.19	14.8
GE-2	SS	8.0	0.42	1.46	0.24	2.1

A second factor is that the limits are based on the curies of a radio-nuclide per unit volume. In 10 CFR Part 61, the limits are stated in curies per cubic meter (Ci/M^3). The measurements are based on curies per gram of sample, which are then divided by the density of the materials in grams per cubic meter in order to make a comparison to the limits. This assumes that the waste is full-density. Based on discussions with the NRC, this is our understanding of how the regulation is to be interpreted. There are those who contend that actual volume of the waste, including void space, is to be used in determining the radionuclide concentration for purposes of waste classification. This is apparently an unresolved issue.

Another issue is to determine how the average concentration of several pieces in a single container is to be treated. Again, based on discussions with the NRC, the intention seems to be that similar pieces can be packaged and averaged together for the purposes of waste classification. This would allow for hot spots or items that by themselves would be over the limits, to be averaged out with less activated parts or components to result in waste that is acceptable for disposal. It is not acceptable to artificially dilute a waste package with nonradioactive, or very low material.

7.0 COMPARISON WITH PREVIOUS SCALING FACTORS

Two sets of previous estimates in this area have been documented. The first was based on work performed at Oak Ridge National Laboratory by Croff (1980) and the second based on work performed at Pacific Northwest Laboratory by Luksic (DOE 1987). The current work results in different scaling factors than either of the previous works. This is simply the result of more research and an improvement in the ability to analyze the problem.

Table 7.1 is a comparison of the scaling factors developed in this work to the previous efforts. For simplicity, only PWR data is presented. The current values have less precision associated with them than either of the two previous works. This is an acknowledgement of the complexity of the problem that was not fully appreciated in the past. Of note is that the current scaling factors result in significantly higher activation rates than the original work by Croff. In comparison to the previous work by Luksic though, the current results are higher at the top end fitting, about the same at the bottom end fitting, and lower in the gas plenum region. It is anticipated that additional work would increase the precision of the results, but further order of magnitude changes are not anticipated.

TABLE 7.1. PWR Scaling Factors

Component	Element	ORNL-6051 (1978)	DOE/RW-0184 (1987)	PNL-6906 (1989)
Top	Ni	0.011	0.051	0.10
End	Nb	0.011	0.018	0.10
Fitting	Co	0.0074	0.034	0.10
Plenum	Ni	0.042	0.556	0.20
Spring	Nb	0.042	0.174	0.20
Region	Co	0.028	0.365	0.20
Bottom	Ni	0.011	0.290	0.20
End	Nb	0.011	0.107	0.20
Fitting	Co	0.0074	0.202	0.20

8.0 REFERENCES

Croff, A. G., M. A. Bjerke, G. W. Morrison, and L. M. Petrie. 1978. _Revised Uranium-Plutonium Cycle PWR and BWR Models for the ORIGEN Computer Code_. ORNL/TM-6051, Oak Ridge National Laboratory, Oak Ridge, Tennessee.

Croff, A. G. 1980. _A Users Manual for the ORIGEN2 Computer Code_. ORNL/TM-7175, Oak Ridge National Laboratory, Oak Ridge, Tennessee.

Empire State Electric Energy Research Corporation (ESEERCO). 1987. _Spent Fuel Consolidation and Characterization: Activity Determination and Classification of Assembly Skeletons_. EP85-4, prepared by Battelle Columbus Laboratories, Columbus, Ohio.

Luksic, A. T., R. W. McKee, P. M. Daling, G. J. Konzek, J. D. Ludwick, and W. L. Purcell. 1986. _Spent Fuel Disassembly Hardware and Other Non-Fuel Bearing Components: Characterization, Disposal Cost Estimates, and Proposed Repository Acceptance Requirements_. PNL-6046, Pacific Northwest Laboratory, Richland, Washington.

U.S. Department of Energy (DOE). 1987. _Characteristics of Spent Fuel, High-Level Waste, and Other Radioactive Wastes Which May Require Long-Term Isolation_. DOE/RW-0184, Office of Civilian Radioactive Waste Management, Washington, D.C.

DISTRIBUTION

No. of
Copies

No. of
Copies

OFFSITE

19 Department of Energy
    Office of Civilian Radioactive
      Waste Management
    Washington, DC 20545
    Attn: G. Appel
           J. C. Bresee
           A. B. Brownstein
           W. J. Danker
           J. B. Easterling
           M. Frei
           H. J. Hale
           C. Head
           V. King
           C. Kouts
           N. Moon
           G. Parker
           M. L. Payton
           J. D. Saltzman
           S. Singal
           R. Stein
           W. Stringfield
           E. Svenson
           J. Williams

 2 Department of Energy
    Albuquerque Operations Office
    P.O. Box 5400
    Albuquerque, NM 87115
    Attn: K. Golliher
           D. M. Lund

 4 Department of Energy
    Idaho Operations Office
    785 DOE Place
    Idaho Falls, ID 83402
    Attn: M. Fisher
           S. T. Hinschberger
           J. L. Lyle
           J. E. Solecki

    W. W. Bixby
    Department of Energy
    Idaho Operations West Valley
      Project Office
    P.O. Box 191
    West Valley, NY 14171-0191

 5 Department of Energy
    Nevada Operations Office
    P.O. Box 14100
    Las Vegas, NV 89114
    Attn: C. Gertz
           J. Robson
           L. Skousen
           M. Valentine
           E. Wilmont

    M. Heiskell
    Department of Energy
    Oak Ridge Operations Office
    P.O. Box E
    Oak Ridge, TN 37831

    P. M. Lang, NE-4
    Department of Energy
    Office of Nuclear Energy
    Washington, DC 20545

    W. Walker
    Department of Energy
    WIPP Project Office
    P.O. Box 3090
    Carlsbad, NM 88220

    J. D. Floyd
    Advanced Nuclear Fuels Corporation
    P.O. Box 90777
    Bellevue, WA 98009

 3 Advanced Nuclear Fuels Corporation
    2101 Horn Rapids Road
    Richland, WA 99352
    Attn: D. Adams
           G. Busselman
           T. Lotz

4　Argonne National Laboratory
　9700 South Cass Avenue
　Argonne, IL　60439
　Attn:　S. Y. Chen
　　　　　J. Peterson
　　　　　M. J. Steindler
　　　　　Y. C. Yuan

　J. R. Siegel
　Atomic Industrial Forum
　7101 Wisconsin Avenue
　Bethesda, MD　20814-4805

2　Babcock & Wilcox
　P.O. Box 10935
　Lynchburg, VA　24506
　Attn:　J. Matheson
　　　　　L. Walton

2　Battelle, Chicago Office
　7000 South Adams
　Willowbrook, IL　60521
　Attn:　H. Avci
　　　　　A. A. Bauer

6　Battelle, Columbus Laboratories
　505 King Avenue
　Columbus, OH　43201
　Attn:　J. A. Carr
　　　　　M. Failey
　　　　　R. S. Kingsley
　　　　　J. Taylor
　　　　　J. Waddell
　　　　　Technical Library

2　Bechtel National, Inc.
　P.O. Box 3965
　San Francisco, CA　94119
　Attn:　L. Jardine
　　　　　N. Norman

5　Brookhaven National Laboratory
　Upton, NY　11973
　Attn:　B. Barletta
　　　　　R. Fullwood
　　　　　V. Salor
　　　　　C. Sastre
　　　　　R. Youngblood

B. Snyder
Brown Boveri Nuclear Service, Inc.
9190 Red Branch Road
Columbia, MD　21045

F. Patti
Burn & Roe
550 Kinderkamack Road
Oradell, NY　07469

R. Wilde
Carolina Power & Light Co.
Rt. 1
P.O. Box 327
New Hill, NC　27562

V. J. Barnhart
Chem-Nuclear Systems Inc.
135 Darling Drive
Avon, CT　06001

2　Combustion Engineering
　1000 Prospect Hill Road
　P.O. Box 500
　Windsor, CT　06095-0500
　Attn:　W. Burns
　　　　　D. Hayduk

D. Andress
David Andress Associates, Inc.
11008 Harriett Lane
Kensington, MD　20895

S. Kraft
Edison Electric Institute
1111 - 19th Street NW
Washington, DC　20036

2　Fluor Technologies, Inc.
　3333 Nicholsen Drive
　Irvine, CA　92730
　Attn:　T. O. Mallonee
　　　　　V. Pierce

J. R. Fitch
Fluor Technologies, Inc.
505 King Avenue
Columbus, OH　43201

2   General Electric Nuclear Energy
175 Curtner Avenue
San Jose, CA 95125
Attn: B. Judson
       R. E. Spicka

11 EG&G Idaho, Inc.
P.O. Box 1625
Idaho Falls, ID 83415
Attn: B. Hill
       M. A. Knecht
       R. Piscatella
       W. Watters
       W. W. Hickman
       H. Worle (6)

4   Electric Power Research Institute
P.O. Box 10412
Palo Alto, CA 94303
Attn: R. W. Lambert
       P. J. Robinson
       J. Santucci
       R. Williams

J. Burger
Empire State Electric Energy
  Research Corporation
1155 Avenue of the Americas
New York, NY 10036

W. R. Rhyne
H & R Technical Associates
575 Oak Ridge Turnpike
Oak Ridge, TN 37830

3   E. R. Johnson Associates, Inc.
11702 Bowman Green Dr.
Reston, VA 22090
Attn: B. M. Cole
       E. R. Johnson
       N. B. McLeod

H. Isakari
Kaiser Engineering
P.O. Box 23210
Oakland, CA 94623

2   Lawrence Livermore National
    Laboratory
P.O. Box 808
Livermore, CA 94550
Attn: R. Van Konynenberg
       H. Shaw

E. Stergakos
Long Island Lighting Company
175 East Old Country Road
Hicksville, NY 11801

3   Los Alamos National Laboratory
P.O. Box 1663
Los Alamos, NM 87545
Attn: D. T. Oakley
       K. S. Pillay
       J. L. Warren

2   Northeast Utilities
P.O. Box 270
Hartford, CT 06101
Attn: G. Betancourt
       B. Isakson

5   Nuclear Assurance Corporation
5720 Peachtree Lane
Norcross, GA 30092
Attn: D. Collier
       J. V. Houston
       W. J. Lee
       M. Smith
       J. Stobes

4   NUS Corporation
910 Clopper Road
Gaithersburg, MD 20878
Attn: H. Eckert
       F. G. Gallo
       C. Heath
       Y. S. Kim

N. W. Edwards
Nutech Engineers
14 S. Martinvale Lane
San Jose, CA 95119

J. D. Rollins
Nutech Engineers
340 Six Branches Court
Roswell, GA 30076

11 Oak Ridge National Laboratory
P.O. Box 2008
Oak Ridge, TN 37831
Attn: A. G. Croff
       C. W. Forsberg
       H. W. Godbee
       D. S. Joy
       J. A. Klein
       W. C. McClain
       K. J. Notz
       J. W. Roddy
       R. Salmon
       S. N. Storch
       T. D. Welch

G. McCabe
Office of Technology Assessment
Ocean & Environmental Programs
600 Pennsylvania Avenue, S.E.
Washington, DC 20003

D. L. Phung
PAI Corporation
P.O. Box 1135
Oak Ridge, TN 37830

E. L. Helminski
Radioactive Exchange
P.O. Box 9528
Washington, DC 20016

G. W. Kendall
REECO
P.O. Box 14400
Las Vegas, NV 89114

S. Petney
RE/SPEC Inc.
P.O. Box 14984
Albuquerque, NM 87191

T. Fuierer
Rochester Gas & Electric Corp.
89 East Avenue
Rochester, NY 14649

6 Sandia National Laboratory
P.O. Box 5800
Albuquerque, NM 87185
Attn: G. Allen
       A. W. Dennis
       T. Hunter
       P. O'Brien
       C. Mansure
       J. Stiegler

J. Schemel
Sandvik Specialty Metals Corp.
P.O. Box 6027
Chemical Drive
Kennewick, WA 99336

2 Science Applications International
     Corporation
101 Convention Center Drive
Las Vegas, NV 89109
Attn: W. MacNabb
       R. Morrisette

C. Smith
Science Applications International
  Corporation
3015 Hopyard Road
Suite M
Pleasanton, CA 94556

S. Marshall
State of Nevada
Division of Health
505 East King Street
Carson City, NV 89710

E. L. Gronemeyer
State of Washington
Department of Social and
  Health Services
Olympia, WA 98504

2 Stone & Webster
   3 Executive Campus
   P.O. Box 5200
   Cherry Hill, NY 08034-5200
   Attn: M. Gennaro, 3-Y
       T. J. Luksic

   E. Kuhn
   Stone & Webster
   One Penn Plaza
   New York, NY 10119

   W. R. Teer
   Transnuclear, Inc.
   One North Broadway
   White Plains, NY 10601

4 U.S. Nuclear Regulatory Commission
   Division of Waste Management
   Washington, DC 20555
   Attn: J. T. Buckley
       T. Johnson
       G. Roles
       W. Prichard

2 University of Arizona
   Department of Nuclear and
    Energy Engineering
   Tucson, AZ 85721
   Attn: R. G. Post
       M. E. Wacks

   C. M. Malbrain
   WasteChem
   One Kalissa Way
   Paramus, NY 07652

   P. Tuite
   Waste Management Group
   P.O. Box 579
   Crompond, NY 10517

   L. R. Eisenstatt
   West Valley Nuclear Services Co.
   P.O. Box 191
   West Valley, NY 14171-0191

2 Westinghouse Electric Corporation
   P.O. Box 3912
   Pittsburgh, PA 15663
   Attn: B. R. Nair
       N. Savin

   C. C. Little
   Westinghouse Electric Corporation
    Nuclear Waste Department
   P.O. Box 3912
   Pittsburgh, PA 15230

   H. M. Batchelder
   Westinghouse Electric Corporation
    WIPP Project
   P.O. Box 2078
   Carlsbad, NM 88220

2 Westinghouse Idaho Nuclear Company
   P.O. Box 4000
   Idaho Falls, ID 83404
   Attn: J. R. Berreth
       D. A. Knecht

8 Weston
   955 L'Enfant Plaza, SW
   Eight Floor
   Washington, DC 20024
   Attn: E. F. Benz
       M. Conroy
       J. DiNunno
       J. Lilly
       R. R. Macdonald
       M. Rahimi
       D. Siefken
       W. Wowak

2 Battelle, Pacific Northwest
    Laboratories
   Washington Office
   370 L'Enfant Promenade
   Suite 900
   901 D. Street SW
   Washington, DC 20024-2115
   Attn: S. Short
       T. Wood

No. of
Copies

10 DOE Office of Scientific and
     Technical Information

<u>ONSITE</u>

 2 <u>DOE Richland Operations Office</u>

    C. E. Collantes
    E. C. Norman

 3 <u>Westinghouse Hanford Operations</u>

    C. S. Clark
    R. A. Watrous
    R. T. Wilde

55 <u>Pacific Northwest Laboratory</u>

    G. H. Beeman
    H. C. Burkholder
    J. Creer
    J. L. Daniel
    L. R. Dodd

No. of
Copies

    A. Doherty
    S. W. Heaberlin
    C. M. Heeb
    M. Kreiter
    U. P. Jenquin
    R. A. Libby
    A. T. Luksic (25)
    J. McElroy
    R. W. McKee
    G. Mellinger
    J. Mendel
    R. Rhoads
    D. E. Robertson
    W. Ross
    M. Schutz
    M. R. Shay
    B. D. Shipp
    R. I. Smith
    R. W. Walling
    M. White
    Publishing Coordination MH
    Technical Report Files (5)